Anomalous Valency States of some Lanthanide Elements, Produced by Neutron Irradiation

Thesis

Michael Taylor, M.A.,

Anomalous Valency States of some Lanthanide Elements, Produced by Neutron Irradiation

Submitted for the Degree of Ph.D.

(Chemistry)

1984

Date of submission: 29.8.84

Date of award: 19.1.85

CONTENTS

INDEX

Acknowledgements

I am pleased to acknowledge the help I have received from many sources. My thanks are especially due to

Dr. D.A. Johnson and
Dr. A.G. Maddock for their encouragement and expert help over a long period of time;

Professor D. Apers for his advice on electrophoresis;

The Master and Fellows of St. Catharine's College, Cambridge and The Governors of Worcester College of Higher Education for financial help;

Mr. B. Witcombe and Mr. W. Squires, for their technical help;

Dr. A. Rotheray, for discussions on computer modelling;

Dr. P. Fowles, The Radiation Centre, Birmingham University;

The Staff of the Universities Research Reactor, Risley;

Mrs. S. Foster, for her help with the manuscript;

and not least, my wife and daughters, for their patience.

Abstract

This study examines changes in the charge state of some lanthanide elements contained in ionic lattices, bombarded by small fluxes of fast and thermal neutrons accompanied by a minimal gamma flux.

Reduction from Ln^{3+} to Ln^{2+} is shown to have taken place by precipitating the latter from aqueous solution onto barium sulphate and examining the beta activity of the precipitate; and independently by measuring the reducing action of the divalent ion on aqueous methylene blue. The extent of the change is shown to be greater than might be expected from the number of neutron-lanthanide interactions. The reduction (demonstrated with neutrons from two independent sources) arises largely from the effects of the fast neutron flux rather than an (n, γ) reaction with thermal neutrons. The divalent state survives in aqueous solution for an appreciable time in the absence of rapidly oxidising species.

The study is principally concerned with the reactions of dysprosium and europium; it is suggested that the method of inducing reaction can be extended to other elements in the series with a good chance of success.

List of Figures

List of Tables

CHAPTER ONE

Introduction

1.1 Since Chadwick's discovery of the neutron in 1932 [1], many workers have taken advantage of its lack of electrical charge to study interactions between neutrons and atomic nuclei. Because of their lack of charge, neutrons are distinguished for not producing much ionisation in the material they traverse; but they may induce such changes if sufficient transfer of kinetic energy can take place. In media composed of heavy atoms ionisation should be uncommon because a neutral atom must acquire a velocity comparable with the notional velocity of the valence shell orbital electrons for ionisation to take place. In ionic lattices, although the same principles apply, the situation is less clearly defined. This study is concerned with changes in the ionisation state of some neutron irradiated lattices.

One of the most striking sets of observations was made by Pleasanton and Snell [2], who concluded that very high positive charges (+22) were observable as results of internal conversion processes, followed by Auger cascades, in ^{131}Xe; they drew attention to the fact that charges as high as +7 had previously been observed by Tate and Smith [3] in 1934, as a result of the impact of single electrons with caesium ions, and that in 1928, J.J.Thomson [4] noted mercury ions carrying charges of +8 in his parabola experiments.

If such high charges are induced in a condensed phase, the fate of the liberated electrons will determine the final

distribution of charge states. There is no reason to suppose that after a sufficient elapsed time, the original states will not be approached, but equally it is probable that electron loss, electron capture at anionic, cationic or interstitial sites, and the limited mobility of negative ions through condensed phases at ambient temperatures, will introduce some rather long-lived alterations. Atoms initially neutral (i.e., those in molecular combination) may thus achieve positive (or in rarer cases, negative) charge states, whilst those initially carrying positive charges should provide ions with both higher and lower positive charges than were present in the original matrix. Because the higher oxidation states are likely to be especially unstable, and hence decay, it is likely that atoms initially in a high formal oxidation state may be expected to appear in reduced states rather than enhance their oxidation number.

The possibility of changes such as these depends on the availability of the necessary activation and reaction energies. There are two principal mechanisms through which the energy may be obtained from bombardment; scattering and absorption. I shall first consider the mechanism of energy transfer, and then the mechanisms of electron loss and their consequences.

Transfer of energy during the collision between the incoming neutron and the target atom or ion may be elastic (meaning that kinetic energy is conserved) or inelastic (meaning that it is not). The interaction may be with the atomic nucleus or, very rarely, with extra-nuclear electrons, the mode and

consequences of collision being dependent on the energy of the incoming neutron and the atomic number of target atom. But if the incoming neutron becomes bound by the target nucleus, then the corresponding bonding energy will excite the product nucleus; in addition there will be added the kinetic energy of the incoming neutron. The excitation is dissipated by photon emission, which in turn produces some recoil. The kinetic energy acquired in the recoil may lead to ionisation. The manner in which the energy is dissipated again varies with its magnitude and may well be split between recoil and ionisation effects; radioactive decay of the compound nucleus may give rise to further ionisation.

1.2 Elastic collision

Consider an elastic collision between a neutron of initial velocity v_1 and mass m_1 and a stationary nucleus of mass A. (See Figure 1.1). For the special case in which the mass of the moving particle is unity, and setting the initial velocity also to unity, we may show that when $\theta = 180^{\circ}$

$$v_2 = \frac{(A-1)}{(A+1)} \qquad \ldots\ldots\ldots (1.1)$$

from which it is clear that v_2 and hence the final kinetic energy of the neutron, can only be zero if A = 1; i.e., if the target nucleus is either a neutron or a proton. Furthermore, the fraction of the energy transferred is governed only by the mass of the target nucleus and not by the energy of the incident particle.

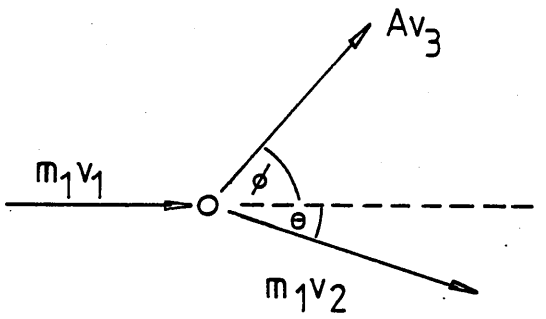

Figure 1.1

Collision of a neutron with a stationary target of mass A

For the average collision (as distinct from one in which the maximum energy transfer takes place), if the initial and final energies are E_1 and E_2 respectively we may say

let $X = \ln\left(\frac{E_1}{E_2}\right)$

let E_t be the fraction of energy transferred; then

$$E_t = 1 - e^{-X} \qquad \text{.....(1.2)}$$

It is upon this effect that the moderation of fast neutrons (that is to say, the gradual reduction of their kinetic energy) is based. The expression is readily evaluated and shows that with other than light target nuclei the fraction E_t is small. None the less, if the initial energy is sufficiently large, the energy transfer may be large in absolute terms; for a nucleus of mass 160 and an initial neutron energy of 5MeV, the transferred energy amounts to over 63 keV per collision, or about 6×10^3 MJ mol^{-1}. In chemical terms this is substantial; but it is less than the excitation energy which may be acquired by neutron absorption.

1.3 Inelastic collision

When a neutron is absorbed into a static nucleus, there is a release of energy - the binding energy of the neutron. Over a wide range of target masses this energy is nearly constant and amounts to about 8 MeV per neutron, or 7.7×10^5 MJ mol^{-1}. In addition to this excitation, the compound nucleus acquires much of the kinetic energy of

the neutron. The additional excitation of the compound nucleus arising in this way is

$$E = \frac{E_n m_a}{m_n + m_a} \qquad \text{.....(1.3)}$$

where E_n is the excitation energy transferred

m_a is the mass of the target

m_n is the mass of the neutron

Taking as before, a target of mass 160 as an example, the additional energy on absorption of a 5 MeV neutron would be 4.97 MeV, plus the 8 MeV binding energy, or nearly 13 MeV; this amounts to some 1.25×10^6 MJ mol^{-1}. Although energies of this magnitude could be expected to produce unusual chemical effects, not all collisions result in absorption. It is important to realise that this energy will be dissipated by photon emission, and only the recoil energy from this process will be available to cause chemical effects within the matrix.

1.4 Probability of neutron capture

To assess the chance of a neutron suffering any interaction with target nuclei, we may use the 'reaction cross-section'. Consider a beam of n particles cm^{-3} passing through a volume of target containing N targets cm^{-3}. Suppose that the targets do not shadow each other. Let the particles move with velocity v cm s^{-1}. Let the current density be j particles $cm^{-2}s^{-1}$; then

$$j = nv \qquad \text{.....(1.4)}$$

If each target has an area of σ cm^2 as seen by the incoming particles, then in unit volume there is a total apparent target area of $N\sigma$ cm^2. (Apparent, because we are considering σ as measuring the real chance of collision rather than the geometric area of the nucleus).

If the reaction rate per unit volume is R interactions s^{-1}, then

$$R = jN\sigma \qquad \text{.....(1.5)}$$

The product $N\sigma$ is commonly written Σ, whence

$$R = j\Sigma \qquad \text{.....(1.6)}$$

In this context it is usual to express σ as the sum of cross-sections for various interactions:

$$\sigma = \sigma_s + \sigma_a$$

and the assessment of reaction rate becomes a matter of establishing values for these factors. To assess particle attenuation in a medium having a substantial value for Σ we note that at any depth z,

$$dj = -j\ \Sigma\ dz$$

whence

$$j = j_o e^{-\ \Sigma\ z}$$

By analogy with the decay law we can then define the half-thickness of the absorber as that material thickness which reduces the initial current density by a factor of two:

$$z_{\frac{1}{2}} = \frac{0.693}{\Sigma} \qquad \ldots\ldots\ldots (1.7)$$

and if the mean distance between collisions be L

$$L = \frac{1}{\Sigma} \qquad \ldots\ldots\ldots (1.8)$$

1.5 Magnitude of cross-sections

The magnitude of neutron cross-sections for various processes depends not only on the nature of the target, but on the incident neutron energy. We may consider three energy ranges:-

(a)	'Fast'	15 MeV - 0.1 MeV
(b)	'Resonance'	0.1 MeV - 0.2 eV
(c)	'Slow'	0.2 eV - zero

In the fast range, capture generally takes place to a small extent, and so

$$\sigma_{total} \simeq \sigma_{scatter}$$

It can be shown that

$$\sigma_{total} = 2\pi \left(R + \frac{\hbar}{\sqrt{2mE}} \right)^2 \qquad \ldots\ldots\ldots (1.9)$$

where R is the target radius

m is the neutron mass

h is $\frac{\hbar}{2\pi}$ (6.5817×10^{-16} eV s)

E is the neutron energy

In this expression the factor 2 is a consequence of 'shadow scattering', equal in magnitude to the geometrical scatter. The expression reduces to

$$\sigma_{total} = 2\pi\left(R + \frac{N}{\sqrt{E}}\right)^2$$

where N is a constant equal to 1.53×10^{-20}

and R, the target radius, is given by

$$R = CA^{\frac{1}{3}}$$

where C is a constant equal to 1.4×10^{-13} cm. Thus R is of the order of 1×10^{-12} cm; this means that without appreciable loss of accuracy we may write

$$\sigma_{total} = 2\pi R^2 \qquad \ldots\ldots\ldots (1.10)$$

Scatter cross-sections therefore vary but little with neutron energy in the fast range. This is illustrated in Figure 1.2. The value of the absorption cross-section here is dependent on a variety of factors including the size and completeness of the largest nucleon shell. For many elements (as shown for hydrogen in Figure 1.2) [5] the total cross-section varies between 5×10^{-24} cm^2 and 20×10^{-24} cm^2; for lanthanide elements the value is approximately 6×10^{-24} cm^2. The scatter cross-section calculated from equation 1.10 would be 3.7×10^{-24} cm^2, indicating that at these neutron energies, absorption and scattering compete on roughly equal terms.

The amount of energy required by the target will differ according to the mode of de-excitation. There will be a recoil as the neutron enters the target; to this will be added either the rather small recoil following emission of a gamma ray, or the larger recoil following the re-emission of the neutron. This latter, vectorially added to the recoil following the initial absorption, may make a contribution not far removed from that of the elastic scattering case.

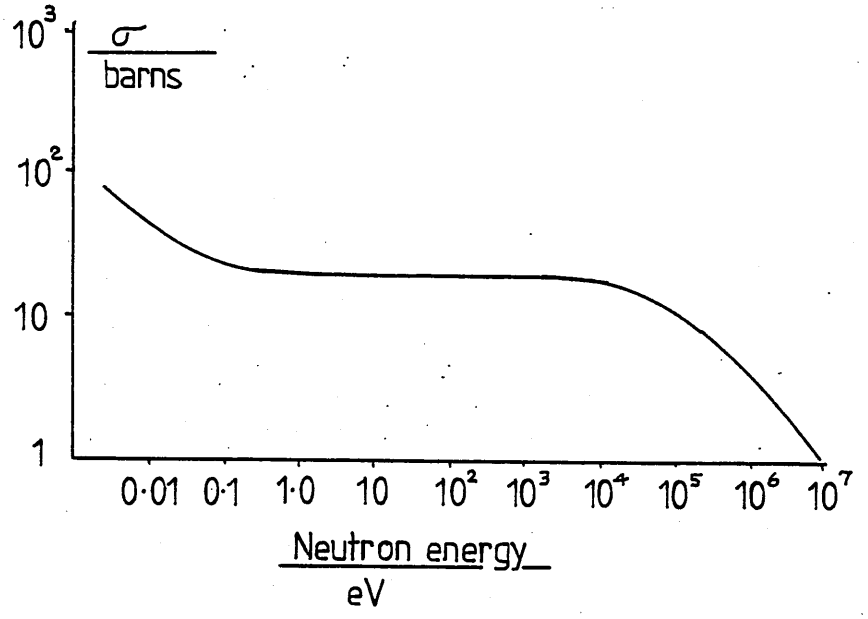

Figure 1.2

Scattering cross-section for hydrogen

(Murray, Nuclear Energy, p48)

In the resonance or intermediate range, the possibility exists that the energy of the neutron may correspond to the excitation energy to a particular nuclear level. When this happens it leads to intense absorption and very high values for the absorption cross-section. The resonances are, however, narrow and somewhat widely spaced. This observation leads (by application of Heisenberg's principle) to the conclusion that the compound nucleus, if formed, has a lifetime of some 10^{-14} to 10^{-15} seconds. This is long by comparison with the time needed for a neutron in flight to traverse the nucleus (about 10^{-18} seconds), and so justifies the concept of a quasi-stationary state for the compound nucleus formed by absorption.

In the slow range, the excitation energy of any compound nucleus formed is equal to the binding energy of the incoming neutron. This energy will be distributed amongst the various particles of which the nucleus is composed, and the probability of random fluctuation allowing it all to be concentrated in one particle is small. Again, emission of a particle will be unlikely, and de-excitation is likely to come about through the emission of gamma rays. The way in which the absorption cross-section varies in the slow region is illustrated by Figure 1.3, based on data for the nuclide ^{109}Ag. From this we see that

(a) the value of the cross section is significantly higher than was the case for high-energy scattering;

(b) near each resonance, the value of the cross-section increases sharply;

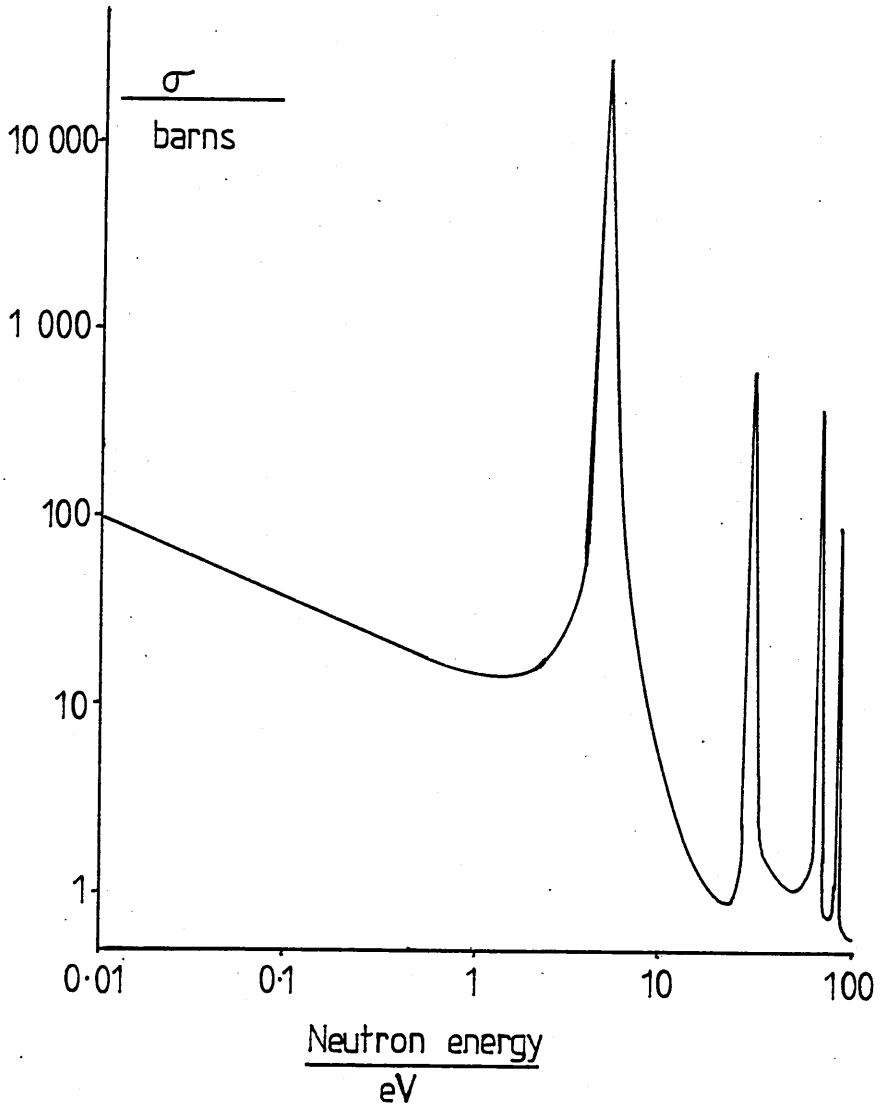

Figure 1.3

Variation in capture cross-section with neutron energy for ^{109}Ag.

(c) away from a resonance, the cross-section varies roughly inversely with the velocity of the neutron.

Summary

1) For fast neutrons, scattering and absorption have similar, low, probabilities; the probability of such reactions does not vary greatly with neutron energy.
2) In the resonance region scattering is important but absorption becomes highly probable in some very narrow energy ranges.
3) For slow neutrons, and in the region of resonance absorptions, capture cross-sections can be very large.
4) Capture cross-sections for slow neutrons may outweigh scattering cross-sections for fast neutrons, but for a small target, fast neutron scattering provides more kinetic energy to produce chemical change.
5) Both fast and slow neutron capture are followed by photon emission and its associated recoil, but only a fraction of the γ-ray energy will be dissipated in the target.
6) Inelastic fast neutron scatter may deposit significant recoil energies in the target.

1.6 De-excitation processes

If upon collision of a neutron with a target the original nuclei or particles remain and no compound nucleus is formed, then the process is that which I have called scattering. If new nuclei or elementary particles are produced, then the process is called nuclear reaction. Such reactions may conveniently be thought of as proceeding through an intermediate compound nucleus of greater or lesser stability. In both cases the excited nucleus will

sooner or later decay to its ground state, and the manner in which the excess energy is lost will influence the macroscopic effects which we observe. Nuclei in the condensed phase excited by elastic scattering will lose excess energy by collision with near neighbours; compound nuclei formed by inelastic scattering will decay either by radiation, or by the emission of material particles. During any such emission the parent nucleus must recoil to conserve linear momentum. The momenta involved (remembering the relativistic effect of mass-energy interchange) are, for the emitted particle,

$$P = mv \quad ; \quad E = \tfrac{1}{2}mv^2 \qquad \text{whence} \quad P = \sqrt{2Em}$$

$$P = mc \quad ; \quad E = mc^2 \qquad \text{whence} \quad P = \frac{E}{c}$$

Adding, we obtain

$$P_{total} = \sqrt{2\,Em + \frac{E^2}{c^2}} \qquad \text{.....(1.11)}$$

In the emission of protons, neutrons, or alpha particles the term $\frac{E^2}{c^2}$ is vanishingly small. In the case of gamma (or neutrino) emission, the term 2em reduces to zero. If an electron is emitted, as in beta decay, then both terms must be considered.

The effects observed as a result of de-excitation may depend on whether investigation is limited to nuclear properties or whether the chemical state and environment of the decaying atom is considered.

1.7 The effects of recoil in excited or compound nuclei

If the recoiling nucleus is part of a molecule in the gas phase, then it can be shown that the recoil energy is distributed amongst the kinetic energy and the internal energy of the molecule according to the expression

$$\frac{\text{internal energy}}{\text{kinetic energy}} = \frac{M}{m}$$

where M is the mass of the rest of the molecule containing the directly affected atom

m is the mass of the directly affected nucleus

As an example, consider an HI molecule in which the iodine atom emits a γ-ray; in this case, the disparity between M and m is maximised. Only $\frac{1}{129}$ of the recoil energy would be internal and hence available to cause bond rupture. It is observed that most HI molecules survive the recoil intact. In most other molecular cases so far investigated, bond rupture does occur in consequence of the higher $\frac{M}{m}$ ratio.

For the emission of a single gamma ray, we may compute the recoil energy thus:-

Let the gamma ray momentum be P_γ

$$P_\gamma = \frac{E}{c}\gamma$$

If the recoiling fragment has mass m

$$mv = \frac{E_\gamma}{c}$$

$$v = \frac{E_\gamma}{cm}$$

So the recoil energy ($\frac{1}{2}mv^2$) is given by

$$E_r = \frac{m}{2}\left(\frac{E_\gamma}{cm}\right)^2$$

$$E_r = \frac{E_\gamma^{\ 2}}{2c^2 m}$$

Putting m in atomic mass units and E_γ in MeV we obtain

$$E_r = \frac{CE^2}{m} \quad \text{eV}$$

where C is a constant equal to 537.

The enumeration of this expression is shown, for various recoiling masses and gamma ray energies, in Table 1.1. If covalent chemical bond energies are taken on the average to be [7] of the order of 5×10^5 J mol^{-1}, then this translates roughly to 5 eV per particle. In most practical cases the ratio $\frac{M}{m}$ is greater than one. Provided that the energy is not dissipated by a cascade of gamma rays emitted in different directions, whose momenta might therefore cancel each other, and allowing for the fact that we should properly consider only the component of the gamma momentum lying in the direction of the axis of any bond, the figures of Table 1.1 indicate that bond rupture is, at worst, highly probable.

In the condensed phase the situation is not so clear. To a first approximation the mass of the system other than the

Mass of recoiling fragment (m)	Energy imparted (eV)		
	E_γ = 2MeV	4MeV	6MeV
50	43	172	387
100	21	86	193
150	14	57	129
200	11	43	97

Table 1.1

Energies in electron volts imparted by gamma ray recoil to various fragment masses. [6]

directly affected atom can be thought of as infinite, implying that all the recoil energy is available for electron-exciting (as opposed to mass-exciting) effects. Effects such as these were first observed by Brooks in 1904 [8], and the chemistry of the recoil species was investigated by Szilard and Chalmers in 1934 [9]; the effect bears their names.

The subsequent fate of the affected atom may therefore be settled in chemical environments different from that in which the recoiling nucleus began, if recoil has originated in a discrete molecule. In the condensed phase, the recoil may contribute to electron perturbing effects.

1.8 The decay of compound nuclei

The decay of a compound nucleus may follow three major routes:

1) gamma emission
2) emission of nucleons or small nucleon clusters
3) fission.

If in any of these substantial electron displacement is caused, distortion of 'normal' valency states will result and may persist for observable times. This is normally the result of gamma emission occurring alone or in concert with other effects as part of a decay scheme. Five effects may be distinguished.

1) Isomeric transition

This effect is found when a nucleus exists in an excited state from which decay is partially forbidden. The result is that the lifetime of the upper energy state becomes measurable. The species is symbolised by the superscript ^{m}, indicating 'metastability'. Such states commonly decay by gamma emission.

2) Internal conversion

During gamma emission, extranuclear electrons may simultaneously be displaced. To explain this it may be said that the initial gamma ray gives up a part of its energy equal to the ionisation energy of an electron in the K- or L- shell, thereby liberating that electron with kinetic energy equal to the gamma energy less the building energy of the electron concerned. This is an oversimplification; the processes of gamma emission and electron emission go on simultaneously, the decay being partitioned between the two. The relative contribution of each is expressed in the conversion coefficient, which ranges from zero to unity. Although the available energy normally permits the loss of K- or L- shell electrons, this is not always the case. Sometimes (eg in ^{99m}Tc) the energy can only be converted in the M- or N- shell, whilst in others (eg ^{235m}U) only P- and Q- electrons are lost.

The deeper the shell from which the elctrons are lost, the greater the consequent disturbance to the whole electron environment of the nucleus; reference has already been made to the striking observations of Pleasanton and Snell.

3) Whiplash ionisation

If the recoil velocity of an atom or ion approaches the 'velocity' of an electron in an outer orbital, then that electron may be lost. Regarding the electron as a particle existing in a Bohr- approximation orbit we may say

let the ionisation energy be E_i; then

$$E_i = \tfrac{1}{2} m_e v_e^2$$

let the recoil velocity of the atom be v_r; for ionisation

$$v_r = v_e$$

$$E_i = \frac{m_e E_r}{M} \qquad \text{.....(1.12)}$$

where M is the mass of the atom concerned.

Using this expression, and assuming that the ionisation energies of about 100 kJ mol^{-1} are involved, one may calculate that whiplash ionisation will begin at a recoil energy of about 3 MeV. This energy, as has been shown, is attainable in a variety of ways.

4) Electron shake-off

Any sudden change in the electron distribution surrounding a nucleus will cause a change in the effective nuclear charge visible to the outer electrons. Usually, the effect has as its cause a change in the atomic number, caused for example by β-decay or electron capture. In most cases, the electron cloud will expand or contract adiabatically to meet the new situation. In a certain proportion of decays, however, the atom becomes sufficiently locally excited to lose further

electrons, increasing its overall charge state. A crude estimate of the energy adjustment has been suggested to be [10]

$$E = CZ^{0.4}n \text{ eV} \qquad \ldots\ldots\ldots(1.13)$$

where Z is the nuclear charge

n is the increase in charge thus caused

C is a constant equal to 22.8

Again, very substantial charges may be generated by this process; Carlson [11] found species such as Na^{6+} and Rb^{10+} following the decay of noble gas atoms.

5) The Auger effect

When a vacancy is created in an inner shell by any of the foregoing processes, the hole is usually filled by an electron dropping down from a higher level. In the process, an amount of energy equal to the difference of the energy level of the hole and the level from which it is filled, is released. This energy can itself cause further ionisation, (i.e. be internally converted), and so for every electron drop two (at least) vacancies may be created. The effect is self perpetuating; it is analogous to an internal conversion of the X-ray energy equivalent to the inter-shell movement of the electrons. Electrons liberated in this way are known as Auger electrons. The process may be summarised:

1) the excited nucleus decays to a ground state nucleus
2) emission of a K- electron accompanies transition
3) the nucleus is now in ground state but the atom is still excited
4) an L- electron fills a K- hole leaving an L- hole

5) the energy of the L-K transition appears as an X-ray

6) the X-ray is internally converted to leave second L-hole.

The charges generated may be very high. Figure 1.4 reproduces results obtained by Pleasanton and Snell (loc.cit.) following the decay of ^{131m}Xe.

The effect is generally known as the production of a 'vacancy cascade' and its existence makes clear that at least transiently, very high charge states must be expected in any ionic lattice following an ionisation event. The subsequent distribution and persistence of high charges, and their detection, are controlled by other factors.

Internal conversion and fluorescent emission are always in competition in the Auger process. The proportion of fluorescent emission rises with increasing nuclear charge, but the proportion of internal conversion rises as we move towards the outer orbitals. Auger electrons are generally of low energy except for the first of any cascade.

1.9 Results of de-excitation

I have argued that both elastic and inelastic collisions provide mechanisms through which a target nucleus may acquire a substantial excess of energy over the ground state, and that this energy is lost through ways which are likely to produce, at least in the first instance, more or less highly charged positive ions accompanied by a shower of free electrons. Reference has already been made to the fate of such particles; the routes by which

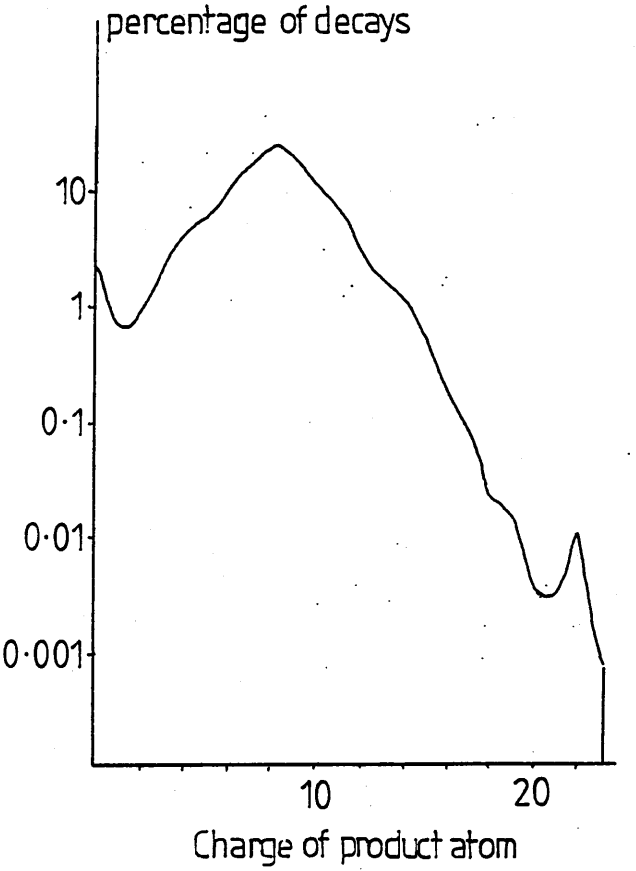

Figure 1.4

Charge spectrum following isomeric transition in ^{131m}Xe (Pleasanton and Snell, loc.cit.)

the final states are achieved must arise from the properties of the 'hot zone' surrounding each event, the leakage of energy by radiation, kinetic contact and electron movement, the limited mobility of the highly charged massive fragments within the ionic lattice, and the higher mobility of the excited electrons (albeit they are likely to be trapped in a number of ways). The relaxation time for such charged species has been shown by Stratton [12] to be governed by the dielectric constant of the medium and its electrical conductivity:

$$t = \frac{e}{s}$$

where t is the relaxation time

e is the dielectric constant

s is the conductivity

Using this expression we find that in a metal, $t = 10^{-19}$ seconds; in an aqueous solution, 10^{-10} seconds; but in an insulating crystal the disturbed charge region may be almost indefinitely stable.

The electrons emitted from an Auger event, however, must end somewhere. Even if some remain uncombined in the crystal, as has been shown to happen in some circumstances [13], they will react with something as soon as the crystal is dissolved for analysis. In an ionic lattice the most obvious electron traps are the neighbouring positive ions. After a time interval no longer than a few lattice vibrations following an ionising event, the hot zone may well have cooled leaving one central ion of higher than normal positive charge, surrounded by an atmosphere of positive ions carrying

lower charges than before the event took place. The spatial extent of this zone may be extensive since not all the energies are at once converted; hence interaction may occur between emitted gamma rays or conversion electrons and the orbital electrons of relatively distant nuclei. In this study I have tried to identify some at least of the altered charge states referred to above, through aqueous chemistry. Their stability in these circumstances requires some comment.

If the original oxidation state is designated M, the oxidised state M_+ and the reduced state M_-, then when the solid is dissolved in water both M_+ and M_- may be thermodynamically unstable with respect to reduction and oxidation by the solvent medium. However, if these reactions happen at different rates, the more slowly reacting species may be detectable. The possibilities are that:

(a) both M_+ and M_- react rapidly upon solution
(b) M_+ reacts more slowly than M_-
(c) M_- reacts more slowly than M_+

The first of these would lead to entirely negative results. In searching for differences in probability between (b) and (c), we may initially have recourse to the relative thermodynamic stabilities of the two states in aqueous solution. These are determined

(a) for M_+ by the quantity

$$E = E^{\ominus}(M_+/M) - 1.23 \text{ volts}$$

the latter figure being the standard potential of the oxygen electrode;

(b) for M_- by the quantity

$$E = 0.0 - E^{\ominus}(M/M_-)$$

the former figure being the standard potential of the hydrogen electrode.

If one of these figures is significantly greater than the other then the assumption may be made that the reaction will be thermodynamically, and perhaps kinetically, favoured. However, I argue that although there is no theoretical connection between thermodynamic and kinetic stability for the type of reaction involved in my systems a good correlation may be expected between the observed rates of reaction and the values of $\Delta G_m^{\ominus}$, and that these in turn are mirrored by the values of the appropriate ionisation energies. This being the case, the ionisation energies, considered with the appropriate nuclear parameters, may be used to indicate those elements for which the investigation raises hopes of success.

1.10 Selection of elements for study

I have suggested that neutron irradiation may lead to ions with either increased or decreased positive charge compared with that which they initially carried in the original lattices. Such changes will be most easily detected in

elements which have only one valency state which is stable to both oxidation and reduction. The lanthanide elements accord with this criterion, as is shown in Table 1.2. From this we see that oxidation states other than +3 have been produced in these elements, albeit with difficulty, and this offers hope of success. To make a specific choice both the probability of interaction between neutron and target, and the likely kinetic stability of the products, must be taken into account.

1.11 Nuclear parameters

There are 54 stable lanthanide nuclides. All have very similar geometrical nuclear radii, and hence nearly identical scattering cross-sections for fast neutrons. Their absorption cross-sections for thermal neutrons vary widely; if only those with values greater than 100 barns are considered, the number of choices is reduced to seven. Because one possible mode of analysis involves measurement of the beta-decay of compound nuclei, four of the seven are excluded because their products of reaction with incoming thermal neutrons are themselves radiochemically stable. On chemical grounds, however, it is interesting to include the nuclide ^{165}Ho, which would otherwise be excluded.

The nuclides still remaining are ^{151}Eu, ^{164}Dy, ^{165}Ho, and ^{168}Yb. Important nuclear parameters for these are shown in Table 1.2. From the table we may conclude that using only natural isotopic mixtures, the maximum probability of interaction with slow neutrons is with europium and

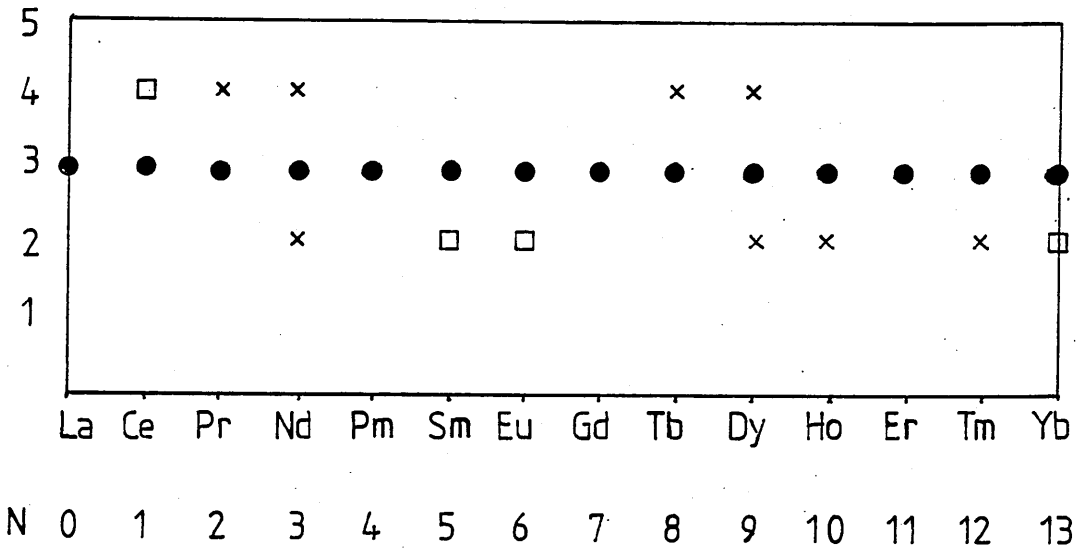

● most stable state

⊡ some stability in aqueous solution

× unstable in aqueous solution

N number of f electrons in the ion Ln^{3+}

Figure 1.5

Known oxidation states of the lanthanide elements

(From Open University unit S304-27)

		^{151}Eu	^{164}Dy	^{165}Ho	^{168}Yb
Nuclear radius	(cm)	7.47×10^{-13}	7.66×10^{-13}	7.68×10^{-13}	7.72×10^{-13}
Isotopic abundance	(%)	47.8	28.1	100	0.14
Reaction cross-section	(fast) (cm^2)	3.51×10^{-24}	3.69×10^{-24}	3.71×10^{-24}	3.74×10^{-24}
	(thermal) (cm^2)	8.4×10^{-21}	2.7×10^{-21}	6.5×10^{-23}	1.1×10^{-20}
Fractional energy loss in scatter		0.0136	0.0123	0.0123	0.0120
No. of collisions, 5 Met-thermal		1449	1574	1583	1612
Σ for MCl_3	(fast)	0.014	0.008	0.03	4×10^{-5}
(specified isotopes)	(thermal)	34.3	6.19	0.53	0.12
Half thickness	(cm) (fast)	34.7	86.6	23.1	16.985
	(cm) (thermal)	0.02	0.11	1.31	5.8
Fraction of neutrons having collided					
in 1 mm MCl_3	(fast)	1.4×10^{-3}	8×10^{-4}	3×10^{-3}	4×10^{-6}
	(thermal)	0.968	0.46	0.05	0.012

Table 1.2 Nuclear parameters for selected lanthanide nuclides.

dysprosium; ytterbium was at first rejected on the grounds that interaction with slow neutrons would be very small. In the event, since the reaction occurs with fast neutrons, this consideration is ill-founded.

1.12 Thermodynamic stability of lanthanide ions

Both +2 and +4 states are known for a number of lanthanides. This study is concerned with the stability of the +2 state, and in particular with the stability of that state in aqueous solution, where it is susceptible to oxidation via the reaction

$$M^{2+}(aq) + H^{+}(aq) \rightarrow M^{3+}(aq) + \tfrac{1}{2}H_2(g) \quad \ldots\ldots\ldots (1.14)$$

Thus the thermodynamics of this reaction are of critical importance. Variations in $\Delta G_m^{\ominus}$ for the reaction can be investigated by using the appropriate Born-Haber cycle:

$$\begin{array}{ccc} Ln^{2+}(g) + H^{+}(aq) & \longrightarrow & Ln^{3+}(g) + \tfrac{1}{2}H_2(g) \\ \uparrow & & \downarrow \\ Ln^{2+}(aq) + H^{+}(aq) & \xrightarrow{\Delta H_m^{\ominus}} & Ln^{3+}(aq) + \tfrac{1}{2}H_2(g) \end{array}$$

Writing $\Delta H_m^{\ominus}$ for $H^{+}(aq) + e(g) \rightarrow \tfrac{1}{2}H_2(g)$ as a constant C

the standard enthalpy of hydration of Ln^{2+} as $\Delta H_h(Ln^{2+})$

the standard enthalpy of hydration of Ln^{3+} as $\Delta H_h(Ln^{3+})$

the third ionisation energy for $Ln^{2+} \rightarrow Ln^{3+}$ as I_3,

we may say that

$$\Delta H_m^{\ominus} = \Delta H_h^{\ominus}(Ln^{3+},g) - \Delta H_h^{\ominus}(Ln^{2+},g) + I_3 + C \quad \ldots\ldots\ldots (1.15)$$

The change in the standard Gibbs function is therefore

$$\Delta G_m^{\ominus} = \Delta H_h^{\ominus}(Ln^{3+},g) - \Delta H_h^{\ominus}(Ln^{2+},g) + I_3 + C - T\Delta S_m^{\ominus} \quad ...(1.16)$$

In analysing variations in $\Delta G_m^{\ominus}$ we may first note that the value of $T\Delta S_m^{\ominus}$ will be nearly constant across the series, since reactions of exactly the same type are involved. Secondly, we note that variations in both $\Delta H_h^{\ominus}(Ln^{2+},g)$ and $\Delta H_h^{\ominus}(Ln^{3+},g)$ will be smooth; these quantities are controlled by the solvated ionic radii whose variations find their origins firstly in the increase in nuclear charge throughout the series, and secondly in the degree of penetration of the electron core by the f electrons. In the lanthanide series this penetration increases rapidly as the charge on the ion increases, which in turn results in a comparative absence of ligand field effects; hence there is little to disturb the smooth reduction in radius from one ion to the next - the well known 'lanthanide contraction'. The penetration effect, as viewed by the outermost electrons, is measured by the difference between the effective nuclear charge experienced by the electron and the total charge on the ion formed when that electron is removed. Variations in this quantity are shown in Figure 1.6, with values for the first transition series as a comparison. The difference $\Delta H_h^{\ominus}(Ln^{3+},g) - \Delta H_h^{\ominus}(Ln^{2+},g)$ may change across the series, but it will do so in a smooth and undramatic way; the change in radius from one ion to the next being only some 3%. Corrections due to changes in hydration number are even smaller by comparison. [14]

This means that irregularities in the variation of $\Delta G_m^{\ominus}$ can only be due to like changes in the remaining factor of equation (1.16) namely I_3. Examination of Figure 1.7, in which values of I_3 are plotted against atomic number, reveals a pronounced saw-tooth pattern.

The origins of the irregularities are these. As the series is traversed there is a regular increase in the electron population of the 4f shell in Ln^{2+} ions:

4f electrons	$0/5d^1$	2	3	4	5	6	7	$7/5d^1$	9	10	11	12	13
Ion Ln^{2+}	La	Ce	Pr	Nd	Pm	Sm	Eu	Gd	Tb	Dy	Ho	Er	Tm

The energy of the 4f shell may be separated into three components. The first is due to the coulombic attraction of the positively charged core for these electrons. The second is due to the coulombic repulsion between the electrons. The third (which has no classical analogue) is called the exchange energy; this exerts a stabilising effect on the ion. It is very roughly proportional to the number of parallel spin interactions, so that on ionisation the exchange energy loss is proportional to the number of such interactions which are destroyed.

In the range $Ce^{2+} \rightarrow Eu^{2+}$ the electrons will, following the aufbauprinzip, occupy separate 4f orbitals (i.e. they will follow Hund's first rule). Hence they will all have parallel spins. The overall increase in the ionisation energy reflects the increasing nuclear charge. Between europium and gadolinium, the discontinuity is a consequence of the $4f^8$ configuration of the latter, which for the first time in the series, allows removal of an electron without any interference

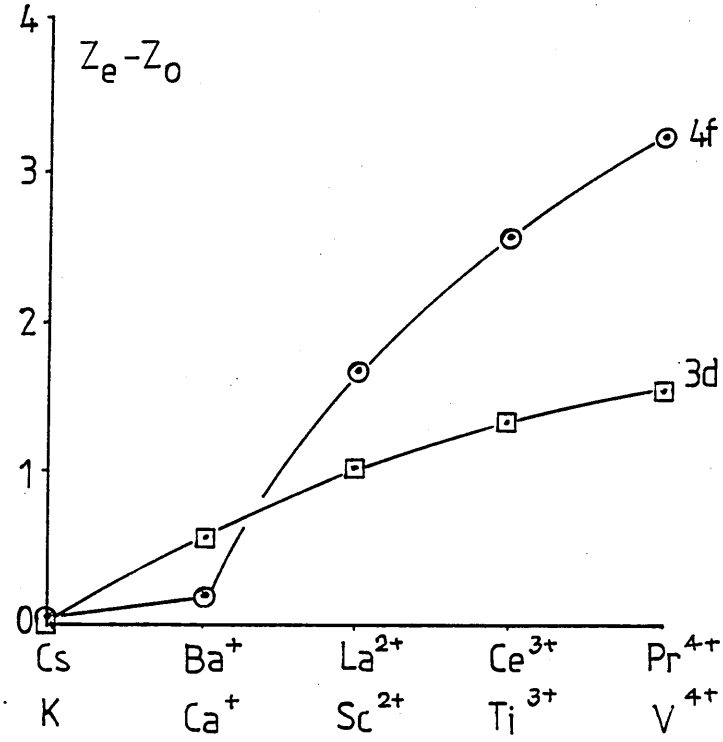

Figure 1.6

Values for the difference between effective nuclear charge and total net nuclear charge for $[Xe]4f^1$ and $[Ar]3d^1$ systems.

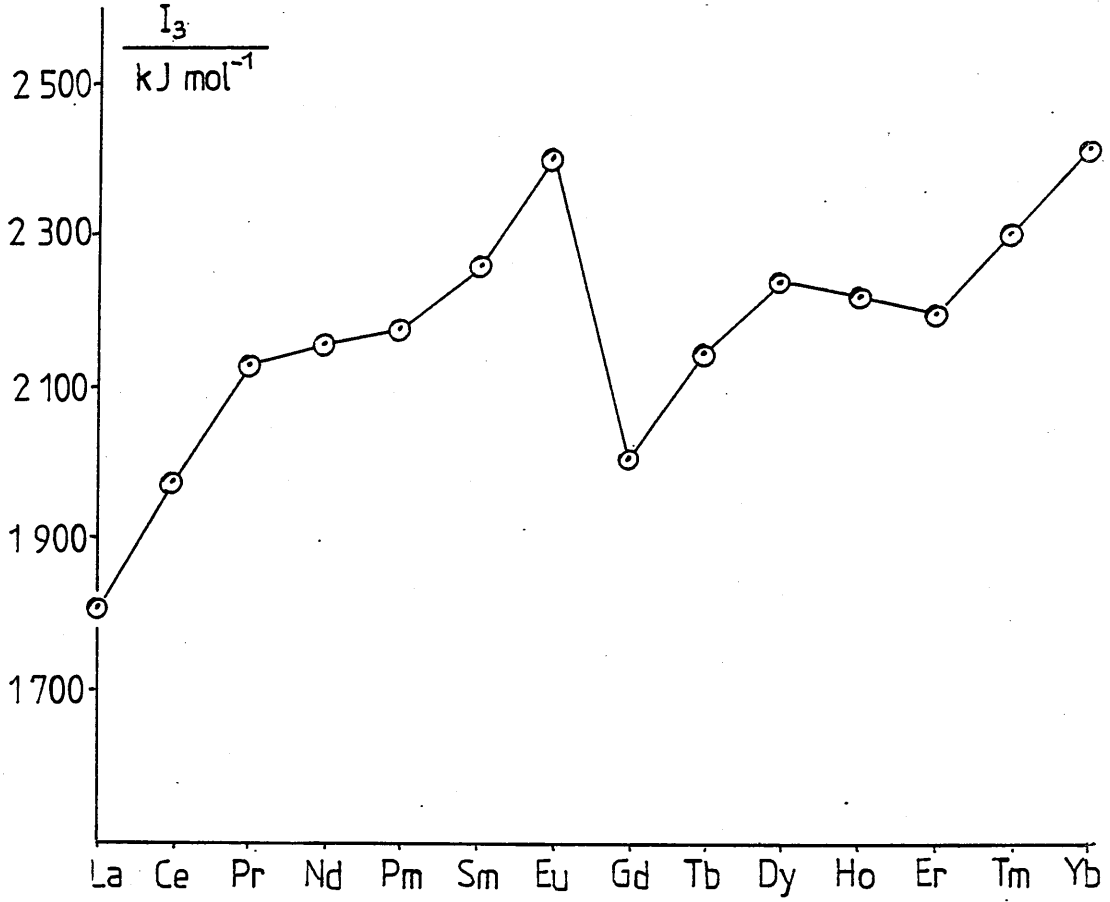

Figure 1.7

Variations in the third ionisation energy of Ln^{2+} ions with $[Xe]4f^n$ configurations.

with the total number of parallel spin interactions. It is therefore at gadolinium that the maximum stabilising influence of the exchange energy is manifested and the value of I_3 is lowered. At the same time, the repulsion suffered by the electron whose removal converts Gd^{2+} into Gd^{3+} is greater than the corresponding repulsion in europium. The sum of these two effects produces the 'gadolinium break'. (J.F. Gadolin, in 1794, prepared a mixed sample of rare earths from the then recently discovered mineral, Gadolinite.)

There are also important breaks in the trend of I_3 at praeseodymium and at dysprosium, giving the 'quarter shell' and 'three quarter shell' effects; the latter is the more pronounced. These can be explained by considering interactions between the angular momenta of the f electrons; those which rotate in the same sense about a given axis repel each other less strongly than those whose angular momenta are opposed. The f electrons are those whose subsidiary quantum number is 3 and which can therefore exist in M_l states -3 through zero to +3. A table of occupancy of these states may be drawn up and part is shown as Table 1.3. If it is assumed that the repulsion energy contributed by a non-rotating pair has a constant value R and that this is lessened in like-rotating pairs by the same increment δ by which it is increased in unlike-rotating pairs, then we may calculate the change in repulsion energy produced by each ionisation $Ln^{2+} \rightarrow Ln^{3+}$. The values are shown in Table 1.4. From this table we see that the ionisation $f^4 \rightarrow f^3$ (corresponding to $Nd^{2+} \rightarrow Nd^{3+}$) has a higher repulsion energy than might be expected from

ion	f^n	M	Ln^{2+}			Ln^{3+}		
		-3 -2 -1 0 +1 +2 +3	a	b	c	a	b	c
La^{2+}	1	↑	0	0	0	0	0	0
Ce^{2+}	2	↑ ↑	1	0	0	0	0	0
Pr^{2+}	3	↑ ↑ ↑	3	0	0	1	0	0
Nd^{2+}	4	↑ ↑ ↑ ↑	3	0	3	3	0	0
Pm^{2+}	5	↑ ↑ ↑ ↑ ↑	3	3	4	3	0	3
Sm^{2+}	6	↑ ↑ ↑ ↑ ↑ ↑	4	6	5	3	3	4
Eu^{2+}	7	↑ ↑ ↑ ↑ ↑ ↑ ↑	6	9	6	4	6	5

a - number of pairs of like rotation

b - number of pairs of unlike rotation

c - other pairs

Table 1.3

Occupancy of M states in various lanthanide ions

f^1	0
f^2	$+R-6\delta$
f^3	$+2R-3\delta$
f^4	$+3R$
f^5	$+4R+3\delta$
f^6	$+5R+2\delta$
f^7	$+6R+\delta$

Table 1.4

Changes in exchange energy consequent upon interactions between electron angular momenta for ionisations $f^n \rightarrow f^{n-1}$ in the lanthanide series.

the trend, and hence a lower ionisation energy. This effect is maximised at f^5 but then reduces again at f^6, mirroring the upward break in the I_3 curve at samarium.

The same sequence of changes takes place after the gadolinium break, producing similar discontinuities at dysprosium and erbium. In practice, the changes in the third ionisation energy are not of equal magnitude to each other, which reflects both the improbability of the equivalence of δ in upward and downward adjustments of the exchange energy, and also the improbability of its constancy across the whole series.

We may therefore conclude that I_3, and hence $\Delta G_m^{\ominus}$, should exhibit a general increase as the series is traversed, broken by a substantial reduction at gadolinium and smaller reductions at neodymium and dysprosium. This entirely bears out the observed results shown in Figure 1.7. This leads to the expectation that the thermodynamic stability of the aqueous Ln^{2+} ions will vary in the order

$$La < Ce < Pr < Nd < Pm < Sm < Eu >> Gd < Tb < Dy > Ho > Er < Tm < Yb$$

and nothing in the argument has been specific to any one reaction. Johnson [15] has proposed that a similar variation in $\Delta G_m^{\ominus}$ should be observed for any reaction in this series in which the number of 4f electrons decreases by one. Another example would be the reaction

$$MCl_2(s) = \tfrac{1}{3}M(s) + \tfrac{2}{3}MCl_3(s) \qquad \text{.....(1.17)}$$

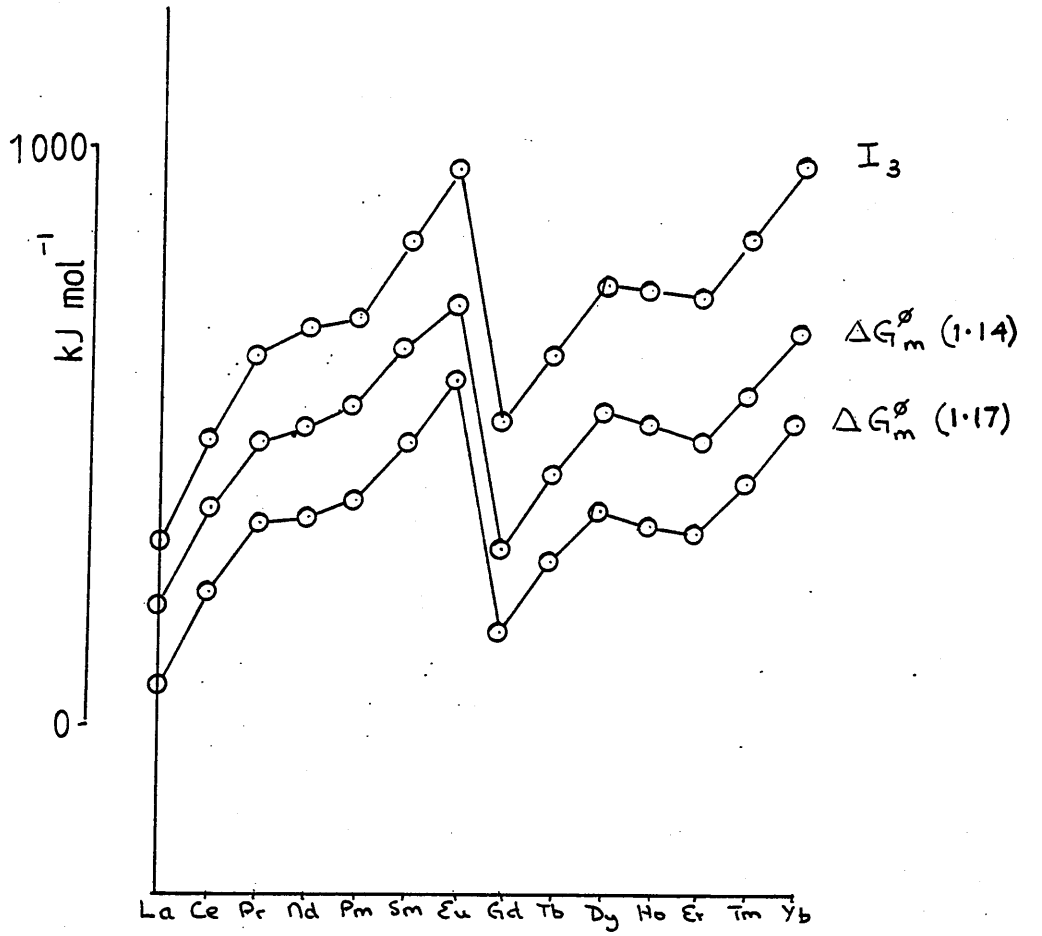

Figure 1.8

Variations in the energies of some lanthanide processes.

whose values of $\Delta G_m^{\ominus}$ are a measure of the thermodynamic stability of the solid dichlorides towards disproportionation. All these predictions are borne out in practice; Figure 1.8 shows the correspondence in trends in I_3 and in $\Delta G_m^{\ominus}$ for reactions (1.14) and (1.17).

The variations in $\Delta G_m^{\ominus}$ shown in Figure 1.8 account for the known dipositive states of the elements shown in Figure 1.5. Such states exist where $\Delta G_m^{\ominus}$ is relatively high; the preparable dichlorides are those of neodymium, possibly promethium, samarium, europium, dysprosium, thulium and ytterbium. Well characterised aqueous ions exist only for samarium, europium, and ytterbium.

Using Figure 1.8 as a basis for prediction, we might say that the least unstable dichlorides would be those of samarium, europium, thulium, and ytterbium. Of those, $SmCl_2$ was prepared by Matignon and Cazes [16] in 1906; $EuCl_2$ by Urbain and Bourion [17] in 1911; and $YbCl_2$ by Klemm and Schuth [18] in 1929. After this, no further dihalides were prepared until 1959 when $NdCl_2$ was made by Drudig and Corbett [19], whose method was extended to make $DyCl_2$ in 1966 by Corbett and McCollum [20] and to $TmCl_2$ in 1960, by Asprey and Kruse [21]. These elements lie in the next 'layer of instability' as predicted by Figure 1.8. The ion Ho^{2+} was reported by de Block in 1971 [22].

The values of $\Delta G_m^{\ominus}$ for reaction (1.14) are, without exception, negative. Thus in the absence of any kinetic hindrance, no aqueous dipositive ions of these elements would be known.

What is more striking is the apparent relationship between the thermodynamic instability of the various ions, their ease of preparation, and their rate of oxidation. This correspondence between thermodynamics and kinetics has no theoretical basis but is frequently invoked as a 'rule of thumb', and in reactions under consideration operates with pronounced success. Such a correlation has been invoked by Latimer [23] and applied by him to the oxidation of monatomic aqueous ions; he used values of E as criteria of likely reaction rate. The idea has not found favour with other authors.

1.13 Dysprosium and europium as the elements chosen

Using these chemical criteria to reinforce the choice made on nuclear grounds from the parameters of Table 1.12, it is clear that since Eu^{2+} has already been prepared, ^{151}Eu offers good chance of successful identification of any reduced species produced. Ytterbium would be chemically just as suitable, but the low isotopic abundance of ^{168}Yb makes it unlikely that any effects based in neutron capture could be observed. Dysprosium, the remaining nuclear candidate, would seem blessed with only small chances of success on chemical grounds. However, Apers and his co-workers, speaking of bivalent holmium [24], say 'it is reasonably stable when proper precautions are taken to avoid the presence of any fast oxidising species. It is slowly oxidised by oxygen, hardly by water, as is expected when no direct electron transfer can take place.' The half life of the species in oxygen saturated water was found by these authors to be about ten minutes, and in

nitrogen saturated water, about 55 minutes. Bivalent dysprosium should be comparable in its stability, and these times are more than enough to complete aqueous analyses. On these grounds, europium and dysprosium were chosen as the elements to be investigated.

A more cogent difficulty lies in the choice of compound to be used. The oxides of the lanthanides are made by calcining the hydroxides at high temperature. This process renders the oxide progressively more difficult to dissolve in acid, the longer it is continued. Any measures designed to dissolve the oxide quickly (increasing the concentration of the acid, heating the solution) are just those which will promote oxidation of the bivalent species. The anhydrous chlorides are readily soluble in dilute acid and are easily prepared; but it has been observed [13] that in NaCl crystals, irradiation with X-rays produces free chlorine atoms. This in turn suggests that if reduced lanthanide species are found and identified by their reducing action, the reduction may in reality be due to free electrons. It would be expected, though, that any such reduction would be exactly cancelled by the oxidising action of the residual chlorine atom. In X-ray irradiated sodium chloride containing equal numbers of 'F' and 'V' type centres, solution in dilute acid gives hydrogen in equivalent amount to the 'F' centres whilst solution in aqueous potassium iodide gives iodine equivalent to the 'V' centres. The amounts of these two products are found to be equal.

X-rays will arise within the crystal lattice as a result of the incomplete conversion of Auger showers and the capture of γ-photons will also produce such centres; on the other hand, dysprosium is not one of those elements known to form compounds containing Ln^{3+} ions with electrons in the conductance band.

Finally, it is necessary to investigate whether the production and yield of reduced species is affected by the neutron energy, and to make some assessment of the energy balance of any reaction found.

1.14 Pattern of investigation

1. Both dysprosium and europium have unusually large capture cross sections for thermal neutrons. The nuclides ^{151}Eu and ^{164}Dy form not only the ground states of ^{152}Eu and ^{165}Dy, but also isomeric states of these. The activation and decay schemes are shown as Figures 1.9 and 1.10. From these it will be seen that ^{165}Dy is formed in large measure by the isomeric transition from $^{165ml}Dy$, but that most ^{152}Eu is formed directly. The latter, however, decays substantially by electron capture from the K-shell. In both elements the possibility of vacancy cascades is present since the isomeric transition of dysprosium is strongly internally converted.

The irradiated lattices may thus contain:-

(i) in the case of dysprosium, highly positively charged dysprosium ions possibly surrounded by an envelope of Dy^{2+} ions or trapped electrons.

(ii) in the case of europium, highly positively charged samarium ions surrounded by an envelope of Eu^{2+}.

2. It is equally possible that sufficient energy may be deposited in the lattice by direct collision between nuclei and fast neutrons, to cause redistribution of electrons amongst the various ions. The probability of such interactions does not vary greatly with the nuclear species involved.

3. The investigation is first carried out with a mixed neutron flux. The effect found is then investigated using only fast neutrons to discover whether it may be solely attributed to these fast neutrons, solely to thermal neutrons, or to a mixture of both.

4. Finally the experiments are repeated using fast neutrons generated in a different way, to provide confirmation of the results found in stage 3.

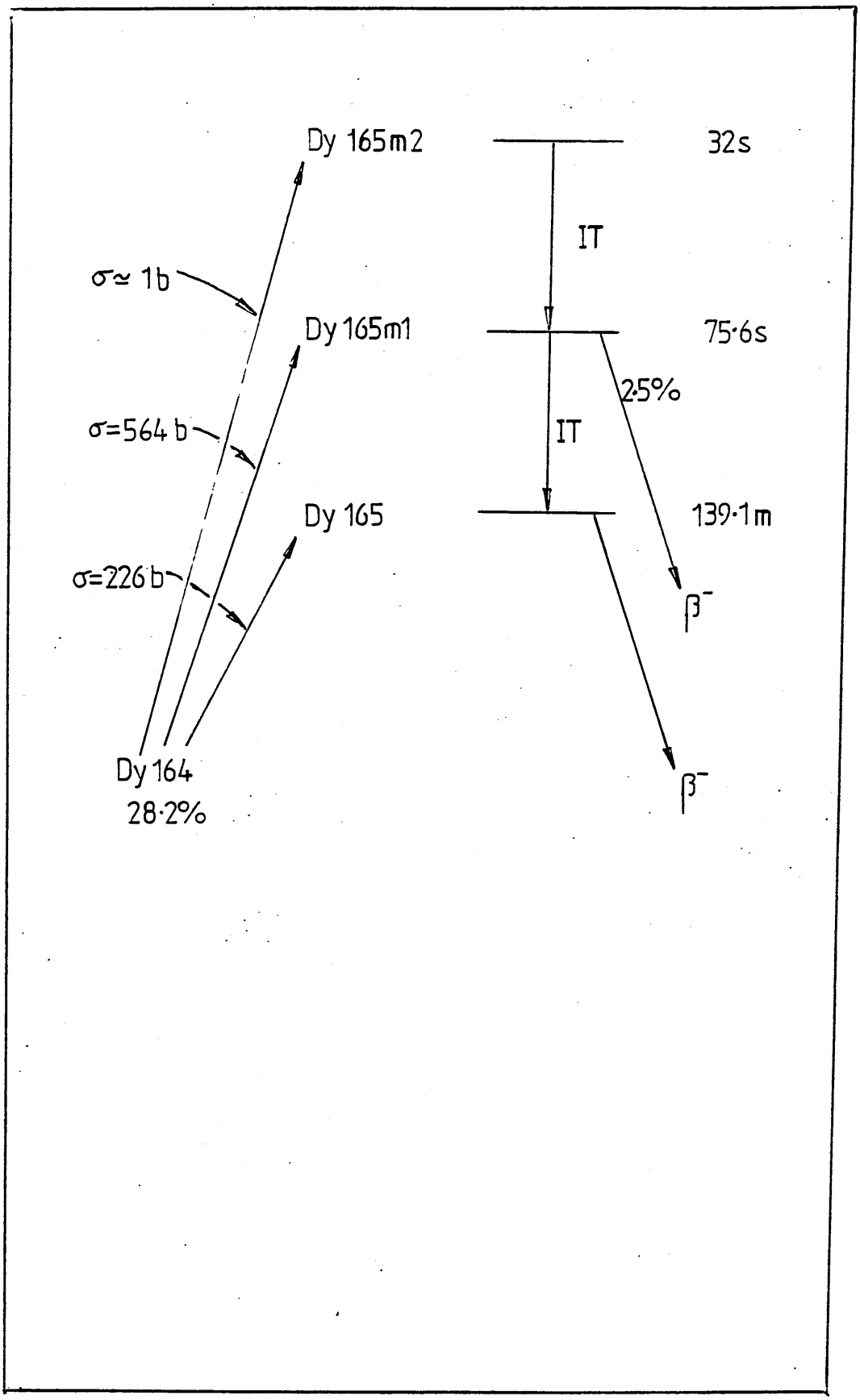

Figure 1.9

Activation and decay schem for ^{165}Dy.

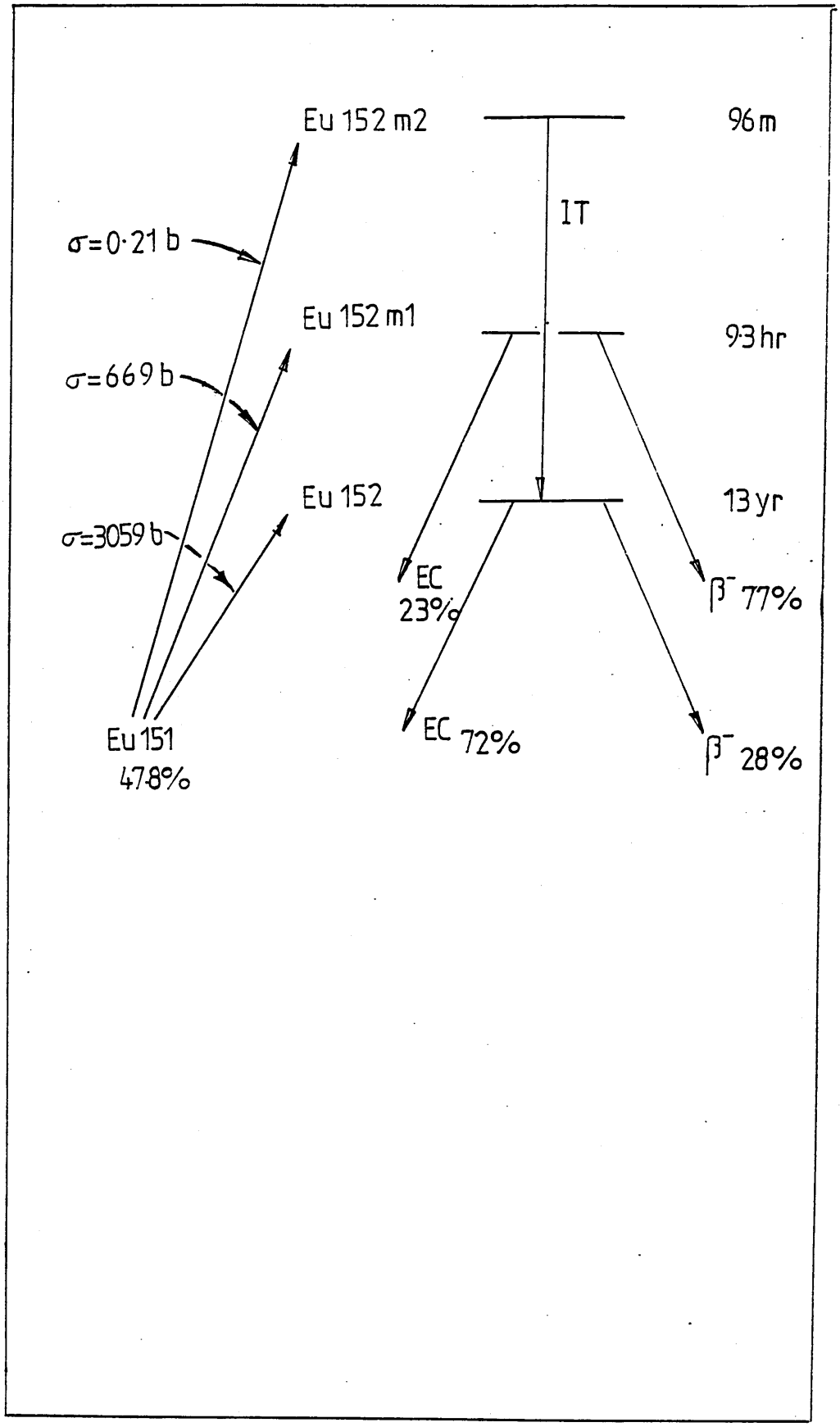

Figure 1.10

Activation and decay scheme for ^{151}Eu.

CHAPTER TWO

Evaluation of numerical parameters

2.1 Fast neutron flux

There is no way of deflecting fast neutrons without transfer of energy, and so enhancement of fast neutron flux can only be achieved by ensuring high geometrical efficiency between source and target. Where weak neutron sources are used, this means that the source and the target should be placed in contact. The flux achieved is then strongly influenced by the configuration of the active material of the source. Assuming that there is no self absorption in the source, the flux is determined by geometrical factors. At small source-to-target distances the source cannot with any accuracy be regarded as a point. It may, however, be thought of as a stack of discs and the total effect determined by a stochastic calculation using the equations derived by Jaffey.[25]

Figure 2.1 represents a neutron source whose active volume is of thickness T, divided into N slices of equal thickness, the first of these being distant from the target by a distance Z. To simplify the calculation it is assumed that the area of each slice is equal to the area of the target.

Jaffey showed that if the activity of each slice is considered as arising from a point source, the geometrical factor (that is, the ratio between the radiation arriving at the target and that emitted isotropically by the source) is given by the expression

$$G_p = \frac{(1 - Z/D)}{2} \qquad \text{.....(2.1)}$$

where G_p in the geometrical factor

Z is the distance between the source and the target

D is distance from the centre of the source to the target

When the activity is uniformly spread over a circle of the same radius as the target, this becomes

$$G_s = G_p\left(1 - \frac{3Z(Z + D)}{8D^4}\right) \qquad \text{.....(2.2)}$$

Although several tabulations of this function have been published these have referred to either off-axis sources [25] or to infinitely thin emitters. [26] A suitable computer program was therefore written to assess the emitted radiation at the surface of such a source; the program is shown in Table 2.1 and the results as Table 2.2 and Figure 2.2. From figure 2.2 it can be seen that the finite thickness of the source has two effects. The maximum flux available is never more than ¼ of the total output; but this figure does not vary so dramatically with the source-to-target distance as would be the case with a thin or point source.

The source used in this work had a total neutron output [27] of 2.2×10^6 n s^{-1}. The planchettes used had an area of 3.8 cm^2 and were placed 0.5 cm from the source.

The flux at this distance was 7.1×10^4 n cm^{-2} s^{-1}.

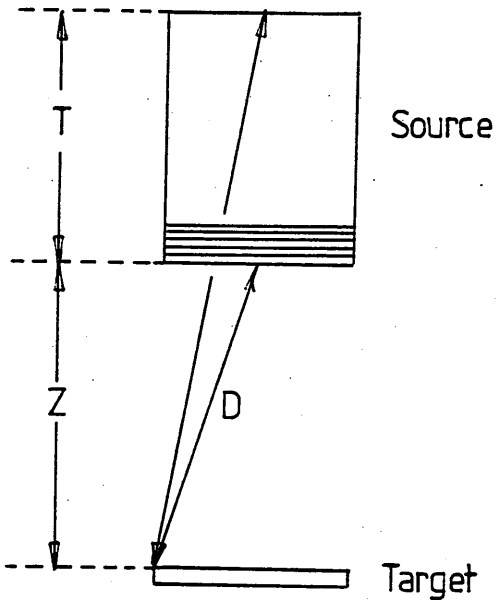

Figure 2.1

Geometrical arrangement of neutron source and target

```
  5  REM:  Copyright M. Taylor 1983
 10  CLS: MODE 1
 15  REM: set print field
 20  @% = &20409
 30  INPUT "STARTING DISTANCE", distance
 40  INPUT "HEIGHT OF SOURCE", height
 50  INPUT "NUMBER OF SLICES", number
 60  FOR X=0 TO 10
 70  distance=distance+0.1
 80  FOR slicenumber=0 TO number
 90  Z=distance+(height*slicenumber/number)
100  PROCcalc
110  Q=Q+GS:  P=Q/number
120  NEXT
130  PRINT P
140  Q=0
150  NEXT
160  END
170  DEF PROCcalc
180  D=((Z↑2)+1)↑0.5
190  GP=0.5*1(1-Z/D)
200  A=(3*Z*(Z+D))/(8*D↑4)
210  GS=GP*(1-A)
220  ENDPROC
```

Table 2.1; computer program used to evaluate equation (2.2). (BBC microBASIC)

Source-target distance cm	G_s
0.1	0.2137
0.2	0.1840
0.3	0.1593
0.4	0.1390
0.5	0.1224
0.6	0.1086
0.7	0.0971
0.8	0.0874
0.9	0.0792
1.0	0.0721

Table 2.2

Evaluation of the geometric factor G_s for a source of active height 1.05 cm considered as 100 slices

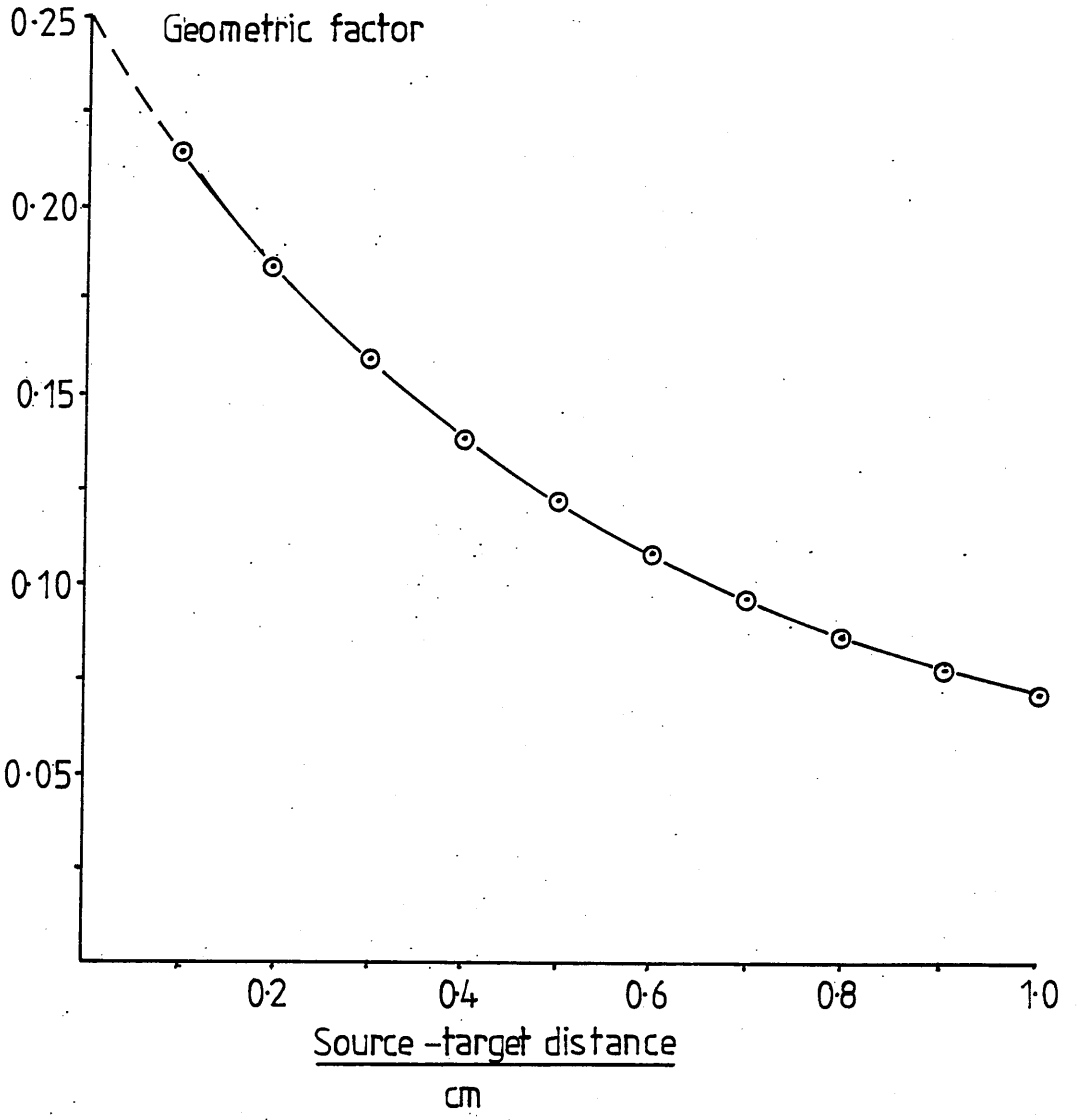

Figure 2.2

Variation of geometric factor G_s with source-target distance for a source of active height 1.05 cm.

2.2 Energy transfer in elastic collisions

Consider an elastic collision between a neutron of initial velocity v_1 and mass m_1, and a stationary nucleus of mass A. (see Figure 1). By conservation of kinetic energy,

$$\tfrac{1}{2}m_1v_1^2 = \tfrac{1}{2}\, m_1v_2^2 + \tfrac{1}{2}\, Av_3^2 \qquad \text{.....(2.3)}$$

and by conservation of linear momentum in the direction of initial motion,

$$m_1v_1 = m_1v_2 \cos\theta + Av_3 \cos\phi \qquad \text{.....(2.4)}$$

similarly, in the direction normal to this,

$$0 = m_1v_2 \sin\theta - Av_3 \sin\phi \qquad \text{.....(2.5)}$$

For the special case of neutrons we may set $= m_1$ 1, whence

$$v_1^2 = v_2^2 + Av_3^2 \qquad \text{.....(2.6)}$$

$$v_1 = v_2 \cos\theta + Av_3 \cos\phi \qquad \text{.....(2.7)}$$

$$v_2 \sin\phi = Av_3 \sin\phi \qquad \text{.....(2.8)}$$

To assess the reduction in energy consequent on various angles of collision, set $v_1 = 1$; then

$$1 = v_2^2 + Av_3^2$$

$$1 = v_2 \cos\theta + Av_3 \cos\phi$$

$$v_2 \sin\phi = Av_3 \sin\phi$$

Solving these equations for v_2 we obtain

$$v_2 = \frac{\cos\theta + \sqrt{\cos^2\theta + A^2 - 1}}{(A + 1)}$$

Maximum energy transfer has taken place when this quantity is at a minimum, which can only be when $\cos\theta = -1$; then,

$$v_2 = \frac{(A - 1)}{(A + 1)} \qquad \text{.....(2.9)}$$

Clearly, then, v_2 (and hence the final kinetic energy of the neutron from this one collision) can only be zero if $A = 1$; i.e., if the target is either a neutron or a proton. Furthermore the magnitude of the energy loss is governed only by the mass of the target nucleus, and not by the energy of the incident particle.

The fraction of the energy transferred may be calculated:

$$\text{Let } K = \frac{v_2^2}{v_1^2} = \frac{(A - 1)^2}{(A + 1)^2} \qquad \text{.....(2.10)}$$

Let E_t be the fraction of the energy transferred. Then

$$E_t = 1 - K$$

$$E_t = 1 - \frac{(A - 1)^2}{(A + 1)^2} = \frac{4A}{(A + 1)^2} \qquad \text{.....(2.11)}$$

Considering the average collision [28] rather than the one in which E_t is a maximum, we may show that if the initial and final energies are E_1 and E_2, then

$$\ln E_1 - \ln E_2 = \left(1 - \frac{K \ln K}{1-K}\right) = x$$

$$\frac{E_2}{E_1} = e^{-x}$$

So the fraction transferred is given by

$$E_t = 1 - e^{-x} \qquad \text{.....(2.12)}$$

The maximum fractional energy loss, the average fractional energy loss, and the number of average collisions needed to reduce a neutron of initial energy 5 MeV to thermal energy (taken as 0.025 eV) are reproduced as Table 2.3.

2.3 Enhancement of thermal neutron flux: the albedo

When a neutron is scattered, it loses energy and changes direction. The angle of scatter in the average collision is given by the formula

$$\cos\theta = \frac{2}{3A}$$

where A is the mass of the scattering particle.

This means that when A = 1, $\theta = 48^{\circ}$ and scatter is principally in the forward direction; but when A = 160, $\cos\theta$ is negligibly small and $\theta = 90^{\circ}$; scatter is then spherically symmetrical.

In either case, after a number of random collisions, a fraction of the incident neutrons will be travelling backwards in the direction from which they entered the scattering medium. If the number of collisions taking place in unit volume is high and the neutrons are not significantly absorbed by the scatterer, then adjacent volumes will repeatedly interchange neutrons, giving greatly reduced neutron mobility and a much enhanced neutron concentration by comparision with that which would obtain in free space.

A	Max Fraction Energy Loss	Average Fraction Energy Loss	Collisions To Thermal
1	1	0.6321	19
2	0.8869	0.5238	26
3	0.75	0.4232	35
4	0.64	0.3528	45
5	0.5556	0.3018	54
6	0.4898	0.2635	64
7	0.4375	0.2337	73
8	0.3951	0.2099	83
9	0.36	0.1905	93
10	0.331	0.1743	102
11	0.3056	0.1607	111
12	0.2840	0.1490	121
20	0.1841	0.0942	197
30	0.1249	0.0645	293
40	0.0952	0.0491	389
50	0.0769	0.0306	484
60	0.0645	0.0332	580
70	0.0555	0.0285	675
80	0.0488	0.025	771
90	0.0435	0.0223	867
100	0.0392	0.0201	962
120	0.0328	0.0168	1153
140	0.0282	0.0144	1344
160	0.0247	0.0127	1535
180	0.0220	0.0113	1726
200	0.0198	0.0101	1917
220	0.018	0.0091	2108
240	0.0165	0.0083	2300
260	0.0153	0.0077	2491
280	0.0142	0.0071	2682
300	0.0132	0.0067	2873

Table 2.3: Evaluation of Maximum fractional energy loss, average fractional energy loss, and number of collisions needed to reduce neutrons from 5 MeV to thermal, with mass of target nucleus.

The effect is influenced by the distance travelled by each neutron, on average, between successive collisions, and the total distance travelled before the neutron is absorbed. If the flux incident on a given plane within the medium in the x direction is ϕ_x and that crossing the plane in the reverse direction is ϕ_{-x}, we may define a quantity β such that

$$\beta = \frac{\phi_{-x}}{\phi_x}$$

This quantity β is called the albedo of the material. It can be shown [29,30] that

$$\beta \simeq 1 - \frac{4}{3}\frac{l_{tr}}{L} \qquad \text{.....(2.13)}$$

where l_{tr} is the mean displacement of the neutron in the direction of motion, i.e. the mean distance between scattering events corrected for the non-sphericity of scatter in any real case.

L is related to the absorption distance l_a (the total path length of the neutron) by the relation

$$L = \left(\frac{l_{tr} \cdot l_a}{3}\right)^{\frac{1}{2}} ;$$

In physical terms, L is the depth from which a neutron can make its way back without being absorbed.

Substituting this in (2.13) we obtain

$$\beta = 1 - 4\left(\frac{l_{tr}}{3l_a}\right)^{\frac{1}{2}} \qquad \text{.....(2.14)}$$

Provided that the medium does not leak (for this to be true its diameter must be at least four times the value of L) then this formula leads to the values of albedo shown in

Table 2.4. High values of albedo are produced if the distance between successive deflections is small, and if the depth of substance from which a neutron can return without absorption is large.

The albedo is not itself used to evaluate the usefulness of a material as a moderating medium; a condensed system composed of atoms of low capture cross section would have high albedo without, necessarily, great moderating power. Instead, the moderation ratio is used. This is the ratio of the moderating power of the medium to its neutron absorbing power. It is given by the expression

$$\text{Moderation ratio} = \frac{\xi\Sigma_s}{\Sigma_a}$$

where ξ is the logarithmic energy decrement

Σ_s is the macroscopic scatter cross section

($\xi\Sigma_s$ is therefore a measure of the moderating power of the medium)

Σ_a is the absorption cross section for thermal neutrons.

Values of these quantities for various media are given in Table 2.5. From the table it is clear that heavy water has an enormous advantage over other media, but it is liquid rather than solid, and it is expensive; furthermore, it has a high value for L, and large volumes are required to ensure that the thermal flux is maximised. Graphite can be obtained in high purity, is solid and easy to machine, but is again needed in large volumes. Paraffin wax and poly(ethene) are both readily available solids, and whilst

their moderating power is not great, they have values of L comparable with that of water and so very much smaller volumes suffice to maximise the thermal flux. For this reason these substances are often used in laboratory installations.

2.4 Electrophoretic behaviour of europium

The computer program (Table 2.6) was written to simulate the electrophoretic behaviour of a mixture of Eu^{2+}(aq) and Eu^{3+}(aq) ions, together with the interchange of one to the other [31,32] which is known to take place in hydrochloric acid solution.

The program creates an electrophoresis paper divided laterally into a number of zones across which the ions will travel. The number of zones is variable. The paper is scanned from the end furthest from the origin, towards the origin. When a zone is encountered which contains ions, a fixed fraction of Eu^{2+} are converted into Eu^{3+} and the same fraction of Eu^{3+} are converted into Eu^{2+}. Each ion is then advanced down the paper by a number of zones proportional to its relative velocity. This completed, the program continues to scan the paper towards the origin until it meets another zone in which ions currently exist. Having reached the origin, the program then returns to the further end of the paper and repeats the process as often as is desired.

When the scans are completed the relative numbers of ions in each zone are printed, together with the total number of

ions in each zone, and the total number of ions in all zones (to check that no ions have washed off the paper).

Despite the elimination of calculation steps when any one zone is empty of ions, the program is slow to execute since it is written in Basic rather than machine code. This means that any attempt to divide the paper into more than 100 zones produces very long computational times. This in its turn means that anything other than crude adjustment of the ratio of velocities between the ions is impracticable.

After some experimentation the program was modified to produce a second version in which all variables except the transfer fraction are fixed in ways which approximate crudely to the conditions expected in the laboratory experiment. The graphs reproduced as Figures 2.3 and 2.4 show how the total amount of europium varies as the paper is traversed for different values of the transfer fraction.

Moderator	l_{tr} cm	L cm	albedo
H_2O	0.49	2.72	0.8
D_2O	2.88	160	0.98
BeO	1.65	29	0.92
C	2.60	54	0.94

Table 2.4

Values of albedo for various moderators.

Moderator	$\xi\Sigma_s$ m^{-1}	$\frac{\xi\Sigma_s}{\Sigma_a}$
Beryllium oxide	12	170
Graphite	6.1	205
Heavy water	18.8	5700
Polythene	161	61
Water	135	61

Table 2.5

Moderating power and moderation ratios for various moderators.

```
>275LIST
    1 REM.....Copyright M.TAYLOR 1982.....
   10 CLS:CLEAR:MODE1
   20 VDU14
   25 REM...Set print field
   26 REM...Set constants
   30 @%=131850
   40 DIMA(120,2)
   50 INPUT"FRACTION",fraction
   60 Vf=2
   70 Vs=1
   80 fastpop = 500
   90 slowpop=1
  100 A(1,1)=fastpop:A(1,2)=slowpop
  110 no_of_levels =50
  120 passes = 20
  125 REM...Run electrophoresis
  130 REPEAT
  140   FOR N = no_of_levels TO 0 STEP -1
  150     PROCmoveions
  160     NEXT
  170   Q=Q+1
  180   UNTIL Q=passes
  190  FOR M= 1 TO no_of_levels
  200   PRINT A(M,1),A(M,2),A(M,1)+A(M,2)
  210    total_number = total_number+A(M,1)+A(M,2)
  220   NEXT
  230  PRINT total_number
  240 VDU15
  245 REM...Enable graph routine
  250 INPUT"ANOTHER RUN",A$
  260 IF LEFT$(A$,1)="Y"THEN 10
  270 IF LEFT$(A$,1)="G"THEN280ELSE350
  275 REM..Plot graph & associated data
  280 CLS:FORM=1 TO no_of_levels
  290   PLOT5,10*M,10*(A(M,1)+A(M,2))
  300   NEXT
  310 PRINT"FRACTION "fraction
  320 PRINTno_of_levels" LEVELS"
  330 PRINTpasses" PASSES"
  340 PRINT"FAST V= "Vf"   SLOW V= "Vs
  350 END
  355 REM..PROCedure for electrophoresis
  360 DEFPROCmoveions
  370 IFA(N,1)=0THEN380ELSE390
  380 IFA(N,2)=0THEN450ELSE390
  390 G=A(N,1)
  400 A(N,1)=A(N,1)*(1-fraction)+A(N,2)*fraction
  410 A(N,2)=A(N,2)*(1-fraction)+G*fraction
  420 A(INT(N+Vf+.5),1)=A(INT(N+Vf+.5),1)+A(N,1)
  430 A(INT(N+Vs+.5),2)=A(INT(N+Vs+.5),2)+A(N,2)
  440 A(N,1)=0:A(N,2)=0
  450 ENDPROC
```

Table 2.6 Program used to simulate electrophoresis of Eu^{2+}/Eu^{3+} mixtures (BBC microBASIC)

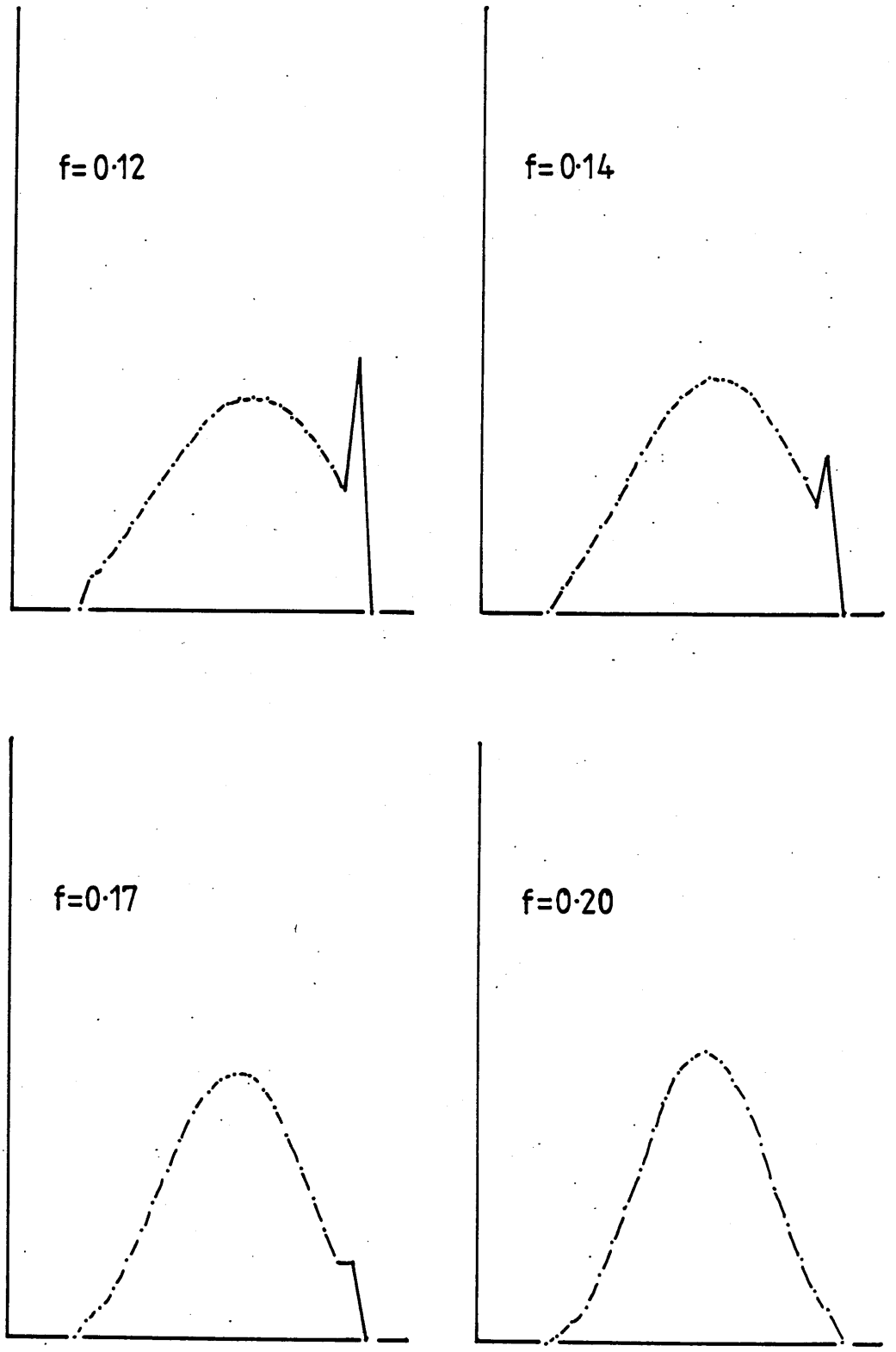

Figure 2.4

Computer generated prediction of europium distribution during electrophoresis with varying extent of $Eu^{2+} \rightleftharpoons Eu^{3+}$ interchange.

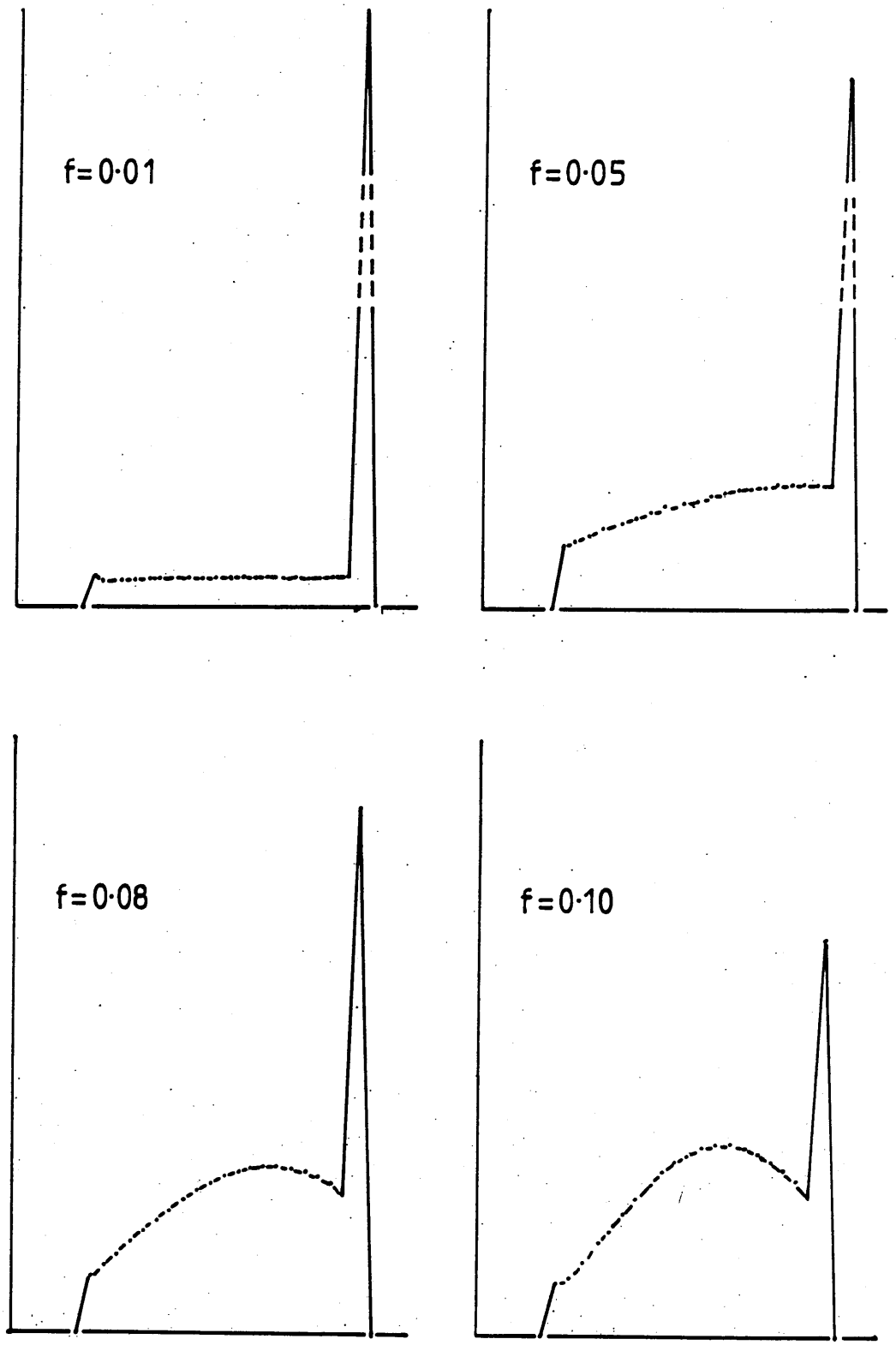

Figure 2.3

Computer generated prediction of europium distribution during electrophoresis with varying extent of $Eu^{2+} \rightleftharpoons Eu^{3+}$ interchange.

CHAPTER THREE

Sequence of experimental work

3.1 The work is described in the following sections:

3.2 Electrophoresis; an attempt to validate a method by which $Eu^{2+}(aq)$ and $Eu^{3+}(aq)$ could be identified in a mixture of the two.

3.3 Adsorption of Eu^{2+} ions, formed by neutron irradiation of europium(III) oxide, on barium sulphate precipitates produced in a hydrochloric acid solution of the oxide.

3.4 Quantitative analysis of Ln^{2+} formed by neutron irradiation of dysprosium and europium trichlorides, by adsorbing the Ln^{2+} from acid solution onto barium sulphate : the method of subsequent precipitations.

3.5 Quantitative analysis of Ln^{2+} formed by neutron irradiation of dysprosium and europium trichlorides, through the reducing action of $Ln^{2+}(aq)$ on methylene blue.

3.6 The effect of the gamma flux accompanying the neutron flux used in sections 3.4 and 3.5.

3.7 Quantitative analyses of the effect of fast neutrons (alone) on dysprosium and europium trichlorides.

3.2 Electrophoresis

It was first necessary to establish a method by which any reduced species, Ln^{2+}, could be identified in the presence of significantly larger quantities of the parent ion, Ln^{3+}. Other workers have found [22,24] that in the case of holmium, this can be done by electrophoresis. There seemed no prima facie reason why this should not be equally effective in the europium and dysprosium systems. Accordingly a paper electrophoresis apparatus was set up in the usual manner and tested by trying to separate $Fe^{2+}(aq)$ and $Fe^{3+}(aq)$ ions dissolved in hydrochloric acid of various strengths. Since the two ions hydrolyse to different extents it was expected that the ratio of their velocities would change with the pH of the carrier.

The efficacy of the apparatus was demonstrated by the results obtained. The ions, made visible by colour reactions, formed clearly defined zones well separated from each other. There was no marked fronting or tailing, though the bands would have been narrower had the papers been blotted before use as was the practice in later experiments. There was no difficulty in estimating the centre of density of each band, and in the least acid solution the dimerised form of iron(III) was clearly differentiated. All this was true whether the ions were applied separately to the paper, or as a mixture.

The distances travelled in each experiment by the two ions are recorded in Table 4.1, and the ratio of the ionic velocities is plotted against the concentration of the carrier in Figure 4.1; details of the apparatus and method are given in Section 7.1.

It was found that the two ions were easily separated from each other. Similar trials were then made with solutions containing $Eu^{2+}(aq)$, $Eu^{3+}(aq)$ and a mixture of the two. It was found that the trivalent ion could most readily be detected by spraying with sodium tungstate solution and viewing in UV light, which produced a vivid red fluorescence, but that under these conditions the divalent ion was revealed by a dark area. The ratio of the velocities of the ions in different concentrations of hydrochloric acid was determined. The values are given in Table 4.3 and shown graphically in Figure 4.2. During the course of an experiment, oxidation of the divalent ion took place, and the dark band was therefore always preceded by a diffuse red front indicative of the Eu^{3+} ion. This was so even when efforts were made to avoid oxidation by using deoxygenated solutions and passing a stream of nitrogen gas across the paper whilst the electrophoresis was in progress. In these experiments, unlike those with iron ions, the trivalent ion travelled more quickly than the divalent ion, presumably suffering less hydrolysis. My inability to prevent oxidation of the divalent species, and the accompanying fronting of the Eu^{2+} band, presented a serious difficulty.

This was accentuated by the behaviour of the ions when applied together to the paper. Despite many trials under various conditions at different times throughout the study, no definite separation of the ions could be achieved. The concentration of the carrier electrolyte was varied from 8M to zero; the temperature of the system was changed from $0^{o}C$ to $20^{o}C$; the wetness of the papers was varied from saturation down to a paper to carrier mass ratio of 1 : 0.7; and papers were run in such a way as to provide reverse diffusion of carrier, opposing the electrophoretic flow. The most common effect observed was a wide, reasonably uniform band which under some conditions contained an intense portion. The (sharp) front edge was observed not to have travelled as far as that from a pure Eu^{3+} sample run under the same conditions and the back edge travelled further than the back edge of a pure Eu^{2+} sample. Edge effects were often marked, although efforts were made to minimise this by placing 'guard strips' on the papers and polishing the glass support sheet with silicone grease prior to each experiment.

Lest the difficulty arose from any failure of the visualising reagent adequately to distinguish regions of high and low concentration, a few milligrams of 'Specpure' europium oxide which had been irradiated in the Risley reactor were dissolved in barely warm hydrochloric acid. From the experiments described in the next section, this sample was believed to contain a measurable concentration of the divalent ion; it was subjected to the electrophoresis. Two such experiments were made; in each case the papers were dried and cut laterally into one centimetre strips,

which were counted in the usual way with a Geiger-Muller counter. The results are tabulated in Table 4.4 and shown graphically in Figure 4.3. In neither case was there a peak corresponding to the divalent ion; but the single large peak which was present occupied in one case more than one third, and in the other, one half, of the electrophoretogram. This was in agreement with observations made using sodium tungstate that the europium became widely spread.

The absence of proper separation of the two ions in the europium system led me to abandon this form of analysis; the reasons for the difference between the europium and iron systems are discussed in Chapter 5.

3.3 Adsorption on barium sulphate

The scavenging action of barium sulphate, precipitated in the presence of small quantities of other divalent ions, is less catholic than that of manganese(IV) oxide or iron(III) hydroxide. Its selectivity is enhanced by the presence of holdback carriers operating on competing ions.

Irradiation of the lanthanide samples was expected to produce reduced species in a matrix of unchanged trivalent ions. However, the flux available was small, and a large percentage of the parent matrix would be unchanged. Under these conditions, if the irradiated sample was dissolved in water and the reduced ions which survived were present, they would be adsorbed onto any barium sulphate precipitated at the same time. Adsorption of active trivalent ions

would be minimised by the large excess of inactive trivalent ions performing the role of holdback carrier.

If the divalent ions arose as a consequence of the (n,γ) reaction, then they would themselves be active and would be revealed (on the precipitate) by a Geiger-Muller counter. If the ions arose as an envelope surrounding an ion suffering a vacancy cascade, then a proportion of them would be activated by the thermal neutron flux and would be similarly revealed.

Before attempting the reaction with the Am/Be neutron source, a small amount of 'Specpure' europium oxide was irradiated in the Universities Research Reactor at Risley. The gamma flux to which the sample was exposed was expected to produce a substantial reduction of Eu^{3+} to Eu^{2+} ion. After storage for one week to allow decay of the short lived isomeric states, milligram amounts of the oxide were dissolved in barely warm hydrochloric acid from which dissolved oxygen had been removed. Also dissolved in the acid was a small concentration of barium ions. When solution of the oxide was complete, deoxygenated dilute sulphuric acid was added. The resulting precipitate was filtered, washed, dried, and counted.

A second barium sulphate precipitate was then formed in the filtrate, filtered, washed, dried, and counted in the same way. This was repeated four times. In two subsequent experiments, samples were treated with bromine water before the formation of the precipitate; the bromine was removed

by boiling prior to the addition of the sulphuric acid. This treatment removed any divalent ions, re-oxidising them to the trivalent state.

The results of these experiments are shown in Table 4.5 and Figure 4.4. Both oxidised samples show no significant difference between the activities of the first and second precipitates. The other four samples each show a higher count on the first precipitate, indicating the presence of divalent ions in the solution. The extent of this excess activity varies from sample to sample; the percentage of total activity apparently in the divalent state is shown in Table 4.21; it varies from 2.9 to 11.0 %. At this stage I did not realise the necessity to age the barium sulphate precipitate for the same time in each experiment.

The unexpectedly large differences between the two precipitates called into question the effectiveness of the holdback carrier. To discover the extent to which the three-valent ion was adsorbed onto the first precipitate, a sample having a substantial total count rate was prepared; the precipitation procedure was carried out repeatedly until six precipitates had been formed each from the filtrate of the one preceding. Care was taken that the amount of barium sulphate was the same in each case, and each precipitate was allowed to remain in contact with the supernatant liquid for the same fixed time before filtering. The results (given as Table 4.6 and Figure 4.5) show that the first precipitate did indeed carry a larger count than the second; thereafter the count on each

precipitate was only a little smaller than that on the one preceding it. The variation after the first precipitate was linear. By extrapolating the linear portion backwards, the contribution made to the count on the first precipitate by the three-valent ion could be estimated.

The activity remaining in the liquid was then determined by measuring its total volume and counting a measured fraction of this in an annular Geiger Muller counter. The efficiency of this counter relative to the solid counter used was found by measuring the activity of a solid sample, dissolving the solid and transferring the solution to the liquid counter, and noting the liquid count. This information was then used to calculate the activity remaining in the liquid as it would have been found by the solid counter used for all other counting. The results are presented in Table 4.7.

3.4 Analysis of irradiated samples by co-precipitation

One reason for the variability of the results obtained from the results so far described was the difficulty of forming a true solution of the oxide, quickly, in the hydrochloric acid. The anhydrous chloride does not have this disadvantage, and so small quantities of anhydrous europium(III) chloride and dysprosium(III) chloride were made and stored over silica gel. Both are free flowing powders, almost white in colour; in the air they very quickly lose their free flowing nature and seem to 'drag' on a microspatula if they are stirred.

Small quantities of the chlorides were placed, separately, in flat bottomed planchettes, which were covered with 'Sellotape' to exclude moisture. It was found that 100 mg was a suitable amount; less than this did not cover the planchette, whilst more became stuck to the Sellotape. Three such planchettes were placed in the wax moderator, their rims touching each other, and the neutron source was placed directly on top of them, as centrally as possible. Normally the source was left in position for about 18 hours. The half life of ^{165}Dy is a little over two hours, and so maximum activity was achieved; $^{m_1152}Eu$ has a half life just over 9 hours and so achieved approximately 75% saturation activity in this time.

After irradiation, the total activity of the sample was found, and the sample was dissolved under nitrogen in deoxygenated hydrochloric acid containing barium ions. Deoxygenated sulphuric acid was added to precipitate barium sulphate in exactly the manner described in the previous section. Either five or six precipitates were made from each sample, in as reproducible a manner as possible. Each filtration was carried out into a nitrogen filled flask with a flow of nitrogen supplied to the chimney filter, so that oxidation by atmospheric oxygen was minimised. Each was counted; the data are presented as Tables 4.8 and 4.9 and shown graphically in Figures 4.6 and 4.7. The same quasi-linear relationship was found in the reduction of the count rate, with an excess count on the first precipitate; the linearity is less obvious, owing to the greater statistical error present in each of

the counts, which are of necessity small. The effect is present in samples of both dysprosium and europium. Blank experiments were done with both elements, by oxidising a sample of the dissolved irradiated chloride with bromine water, prior to the formation of any precipitates. In these experiments, no excess count was found on the first precipitate.

When the results for the two elements are averaged, the amount of the reduced form expressed as a percentage of the total is, for europium, 0.32 ± 0.04 atom %. dysprosium, 0.32 ± 0.08 atom %.

3.5 Analysis of irradiated samples by oxidation

3.5.1 Analyses following irradiation in mixed energy flux

The results recorded in Section 3.4 provide evidence for the existence of Ln^{2+} in the irradiated samples. They do not distinguish between reduced states produced in the (n,γ) reaction and hence present only as radio-active atoms, and reduced states produced by some other means, present amongst all the atoms of the sample, but only revealed in those which have been activated. To distinguish the two, an assessment of the total Ln^{2+} population is needed.

To do this, advantage was taken of a method suggested by Bhattacharya [33], who measured the absorbance of methylene blue at its peak (664 nm) before and after reduction of the dye by $Eu^{2+}(aq)$. A solution of the purified dye was first calibrated against $Sn^{2+}(aq)$ [34] ions; over a substan-

tial range the change in absorbance proved to vary linearly with the quantity of added reductant. The calibrations are shown as Table 4.10 and Figure 4.8.

Various trials were then made to determine the best method for the analysis, and the reasons for the variability of the method noted by Bhattacharya. Once a satisfactory method was discovered, the effect of adding ethanol to the acid solution in which the irradiated salt was dissolved, was investigated. Ethanol is a good scavenger for electrons and for Cl^{o}, which Hacskaylo [13] showed to be present in X-irradiated sodium chloride crystals. Were the same effect present in the irradiated lanthanide chlorides, dissolving them in an alcoholic solvent should minimise electron reduction of the dye. The absorbance of a fixed concentration of the dye was found to vary sharply as the percentage of alcohol in the solution was increased from zero; but between 40 and 100% by volume of alcohol, the change became much less pronounced. The effect is shown in the values of Table 4.11 and in Figure 4.9. Since it was important that the salt should dissolve completely in the solvent, a concentration of 50% ethanol by volume was chosen for subsequent work.

The possibility of the existence of free electrons within the lattice led me to consider whether, even if evidence for reducing species were found this could be ascribed to the existence of Ln^{2+} within the lattice, or to the existence of Ln^{3+}/e^{-} pairs formed at the moment of solution. I prepared crystalline samples of dysprosium chloride,

thinking to irradiate some in the crystalline state and some after fine grinding. If the crystalline samples were handled very delicately, this should have led to a large difference in the number of defects in the irradiated solid and hence a large difference in the number of electron traps.[35] The experiment could not be continued long enough to give meaningful results; although one sample of the crystalline salt was prepared without difficulty, subsequent attempts led only to deep yellow deliquescent crystals which could not readily be handled. Results of such analyses as were done are shown in Table 4.16 and Figure 4.15. A spectrometric analysis of a solution of these crystals in hydrochloric acid of various concentrations suggested that they contained a chloro-complex. The exact structure was not determined and this line of enquiry was abandoned. The spectra of the solution of the salt are shown as Figure 4.10. Once the deep yellow material had appeared, it was impossible to produce the normal form; this may have been due to a temperature change in the laboratory.

The analysis proper was then begun. A number of samples of dysprosium and europium chlorides were irradiated for periods of time ranging from eighteen hours to several days, inside the wax moderator. Each sample was then dissolved in an aliquot of methylene blue. The solution was diluted and its absorbance was found in the absence of oxygen, a minimum of five readings of the absorbance being taken. The solution was then oxidised by vigorous shaking in an atmosphere of oxygen. This oxidation of the dye was

rapid and was complete within a few minutes. The absorbance of the oxidised sample was found and the difference determined.

The results for europium samples are shown in Table 4.13 and as Figure 4.12. For comparison, a number of europium oxide samples were also irradiated and analysed in the same way, though they were very much more difficult to dissolve.

The results for dysprosium samples are shown in Table 4.14 and as Figure 4.13. Both europium and dysprosium results show that the irradiated materials had an appreciable reducing effect on the methylene blue.

At various times during these and subsequent analyses, blank results were obtained by using unirradiated salts. The results thus obtained are shown in Table 4.12 and shown as Figure 4.11; they indicate that the reduction brought about by the irradiated salts is real. The mean blank absorbance difference found was 0.0015 A.U.

When the average values of the reductions obtained, less the contribution attributable to background effects, are converted to show the percentages of the original salts affected, the figures are; for europium, 0.11%; for dysprosium, 0.082% reduction.

3.5.2 Analyses made in other circumstances using mixed flux

In an attempt to stabilise the divalent dysprosium ion in aqueous solution, several analyses were done using a solution of EDTA (disodium salt) to dissolve the irradiated lanthanide. At first this appeared to be very successful, but the change in the measured effect was so large (about an order of magnitude) that other explanations were sought. Although EDTA does not react directly with methylene blue, it was found that the two do react in the presence of light. The reduction was again reversed by saturating the solution with oxygen; the oxidation took place rapidly.

The course of this reaction was followed spectrophotometrically, by introducing EDTA into a sample of the dye, leaving the mixture in the light, and sampling it at intervals of one minute. When the initial rapid reaction had moderated, the sample was saturated with oxygen and sampled at two minute intervals.

The results are shown in Table 4.15 and as Figure 4.14; they confirm that dissolved oxygen quickly restores the methylene blue from its leuco- form, but that the original absorbance is not wholly restored, the final figure being 96% of the original.

A reaction flask was then sprayed on the outside with black paint, taking care to avoid the pinholes often produced when a sprayed coating dries. Four analyses were made using irradiated dysprosium chloride, dissolving it in the

presence of the EDTA. The results (shown in Table 4.16 and Figure 4.15) show that no significant reducing effect could be observed.

3.6 Effect of gamma radiation

Americium-beryllium neutron sources emit only a small gamma flux. It is not vanishingly small; nor is that associated with the neutrons produced in the accelerator used as described in 3.6.3. The dose rate at and near the surface of the source was determined; details are given in Section 7.9. By trial and error, a ^{60}Co source was found which provided an almost identical gamma dose rate. Three dysprosium chloride samples were placed in contact with this source for 24 hours and then analysed. Two dysprosium chloride samples and three europium chloride samples were given one hundred times this dose, delivered in only 10 seconds, using the ^{60}Co irradiation facility in the University of Cambridge Chemical Laboratory. At the time of the experiment this delivered a dose of 7.6×10^2 Gy/hr.

When analysed, the mean value of Δ in the samples exposed to the weak gamma field was 0.0008 ± 0.0007 A.U. The mean value for samples in the stronger field was 0.0025 ± 0.0005 A.U. This is negligible by comparison with neutron-induced effects.

The results are shown in Table 4.17 and Figure 4.16.

3.7 Irradiation by fast neutrons alone

Some of the previous analyses suggested that the increase in the reducing species with time was not controlled by the growth of the (n,γ) reaction product. Accordingly it was decided to make a trial using only fast neutrons, although it was expected that no reaction would be found, since the collision cross section in this energy range is substantially less than for thermal neutrons.

Three separate sets of experiments were performed.

3.7.1 Source neutrons without moderation

From a length of aluminium rod, a number of planchettes were prepared with close fitting lids. The lids fitted inside the planchettes so that powder therein could be compressed and held in position. The design of the planchettes is shown in Figure 7.10.

A number of planchettes were charged with 100 mg samples of anhydrous dysprosium chloride. Three were then placed with their rims in contact with each other on a slab of cadmium metal some 5 mm thick. This in turn rested on a concrete slab. The neutron source was placed centrally on the three samples, and irradiation was continued for various periods of time. Fast neutrons from the source thus passed through the samples, but any scattered and moderated neutrons resulting from collisions in the concrete base were prevented from reaching the planchettes.

The contents of each planchette were analysed in the same manner as before with methylene blue. The results (shown as Table 4.18 and Figure 4.17) show that the irradiation did produce a reducing species, whose amount reached a maximum after about three days. The effect is significantly above the background (blank) results, and amounts to about half the effect so far found when using mixed flux irradiation.

3.7.2 Mixed flux; thermal flux removed

The experiment described in 3.7.1 is open to the objection that it does not duplicate the conditions of previous irradiations, thus making direct comparison difficult. The planchettes used in 3.7.1 were therefore refilled, again with 100 mg samples of dysprosium chloride. A rectangular box was made from 2 mm cadmium sheet, of such a size that it could be inserted into the wax moderator below the removable inner cylinder, but large enough that it could contain three planchettes with their rims in contact. Three planchettes were loaded into the box in this manner; the box was placed in the moderator and the neutron sources was placed in contact with the box, as centrally as possible. The samples were therefore irradiated in the same conditions as when the mixed flux was used, except that practically all the thermal neutrons and almost all the epithermal neutrons were prevented from reaching the planchettes.

The results again show the production of amounts of a reducing species whose quantity increase with the time of

irradiation, approaching a maximum after some days. The extent of the change was greater in these experiments than in those described in 3.7.1, and approached the levels found in the mixed flux irradiations. The results are given in Table 4.19 and shown in Figure 4.18.

3.7.3 Fast neutrons from an alternative source

The results of the last two sets of experiments strongly suggest that fast neutrons are capable of forming significant quantities of reduced species in the lanthanide lattices used. To confirm that the results were indeed the result of neutron bombardment and not some other unsuspected effect, planchettes were again loaded with anhydrous dysprosium chloride, sealed with 'Araldite' to prevent ingress of moisture, and irradiated in the 150 keV generator of the Birmingham Radiation Centre. This produces 15 MeV neutrons. The doses given to the samples were calculated to correspond to irradiation times of 2,3,4,6,8 and 12 days irradiation by the neutron source hitherto used.

When analysed, the samples again showed the presence of a reducing species whose quantity increased with increasing irradiation time. The maximum effect was very similar to the maximum effect observed in the two previous experiments. There is some uncertainty about the true dose given to these samples, due to a failure of the beam monitoring device fitted to the generator; this uncertainty is shown in Figure 4.19, which presents the results obtained. The figures are tabulated in Table 4.24.

The small difference between the reductions produced in the mixed flux and in the fast flux indicate that the majority of the reduction is brought about by reaction with fast neutrons.

Chapter Four

Experimental results

4.1 Electrophoresis

V_1 $Fe^{2+}(aq)$ cm	V_2 $Fe^{3+}(aq)$ cm	$\frac{V_1}{V_2}$	acid conc. mol dm^{-3}	p[HCl]
14.0	12.2	1.15	0.05	1.3
15.0	13.0	1.15	0.05	1.3
12.0	8.5	1.41	0.02	1.69
11.9	7.6	1.57	0.02	1.69
11.6	8.0	1.45	0.02	1.69
22.8	14.5	1.57	0.01	2.0
13.0	8.5	1.53	0.01	2.0
11.0	4.8	2.29	0.006	2.22
10.5	4.8	2.19	0.006	2.22
11.0	4.8	2.29	0.006	2.22
15.0	5.5	2.73	0.003	2.52
14.0	5.0	2.8	0.003	2.52
14.5	4.5	3.2	0.003	2.52
12.5	2.8	4.46	0.001	3.0
14.0	3.8/2.3	3.68/6.09	0.001	3.0
12.0	2.8/2.1	4.29/5.71	0.001	3.0

Table 4.1 Electrophoresis of $Fe^{2+}(aq)$ and $Fe^{3+}(aq)$

$\frac{V_1}{V_2}$	p[HCl]
1.15	1.3
1.48	1.69
1.55	2.0
2.23	2.22
2.91	2.52
4.14/5.9	3.0

Table 4.2 Mean values derived from Table 4.1.

V_1 $Eu^{3+}(aq)$ cm	V_2 $Eu^{2+}(aq)$ cm	$\frac{V_1}{V_2}$	acid conc. mol dm^{-3}	p[HCl]
6.0	3.1	1.94	0.001	3.0
5.5	7.4	1.35	0.002	2.7
4.5	6.6	1.47	0.002	2.7
8.4	7.5	1.12	0.004	2.4
10.3	9.2	1.12	0.006	2.22
10.2	12.2	1.2	0.008	2.1
10.95	11.9	1.09	0.008	2.1
13.9	11.6	1.2	0.02	1.7

Table 4.3 Electrophoresis of $Eu^{3+}(aq)$ and $Eu^{2+}(aq)$

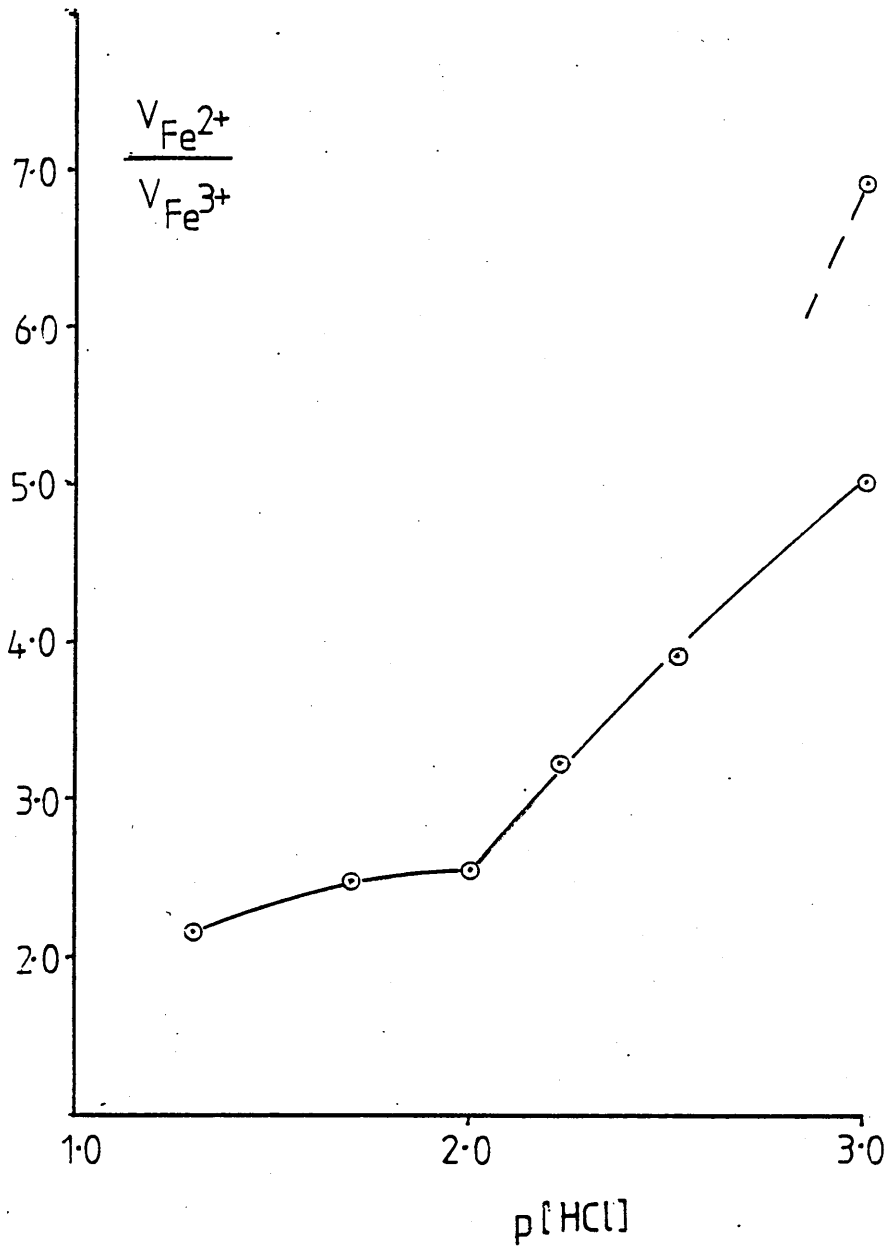

Figure 4.1

Variation in velocity ratio in electrophoresis of Fe^{2+}(aq and Fe^{3+}(aq) against log 1/[HCl]

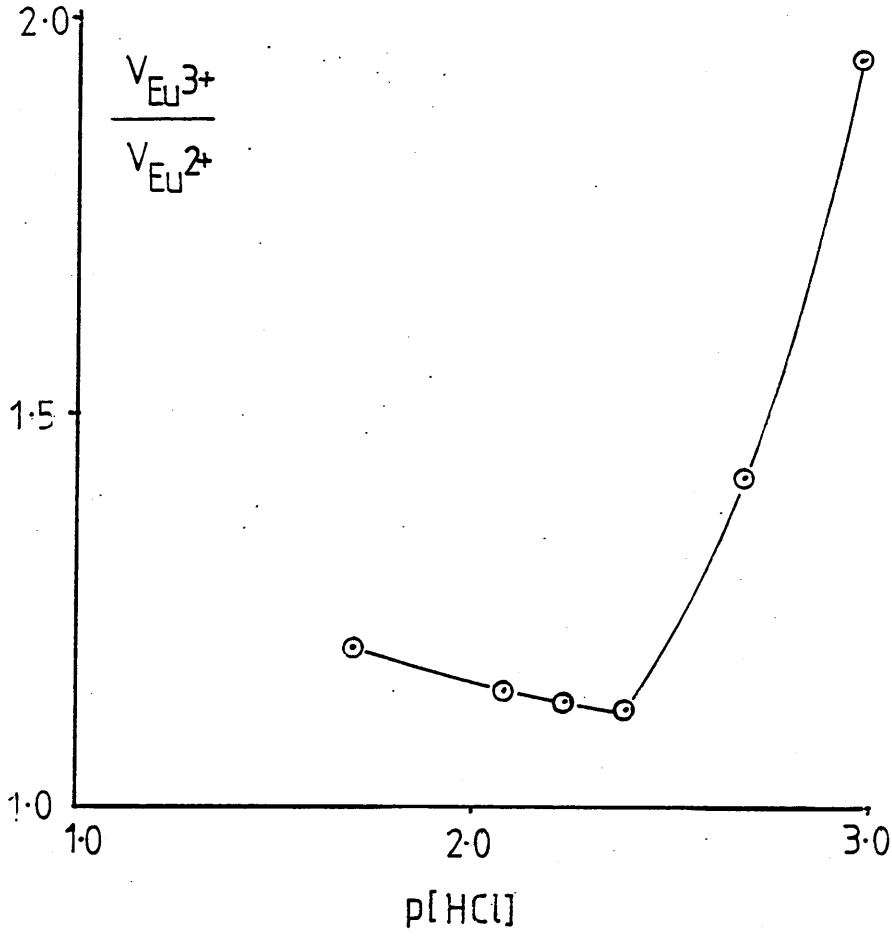

Figure 4.2

Variation in velocity ratio in electrophoresis of $Eu^{2+}(aq)$ and $Eu^{3+}(aq)$ against log 1/[HCl]

PAPER 1		PAPER 2	
Distance from origin cm	Count rate cpm	Distance from origin cm	Count rate cpm
1	33	1	18
2	25	2	27
3	25	3	21
4	25	4	21
5	22	5	20
6	26	6	16
7	23	7	25
8	57	8	58
9	307	9	212
10	290	10	227
11	48	11	116
12	18	12	16

Table 4.4 β^- activity of electrophoresis papers carrying irradiated Eu-151 in hydrochloric acid solution

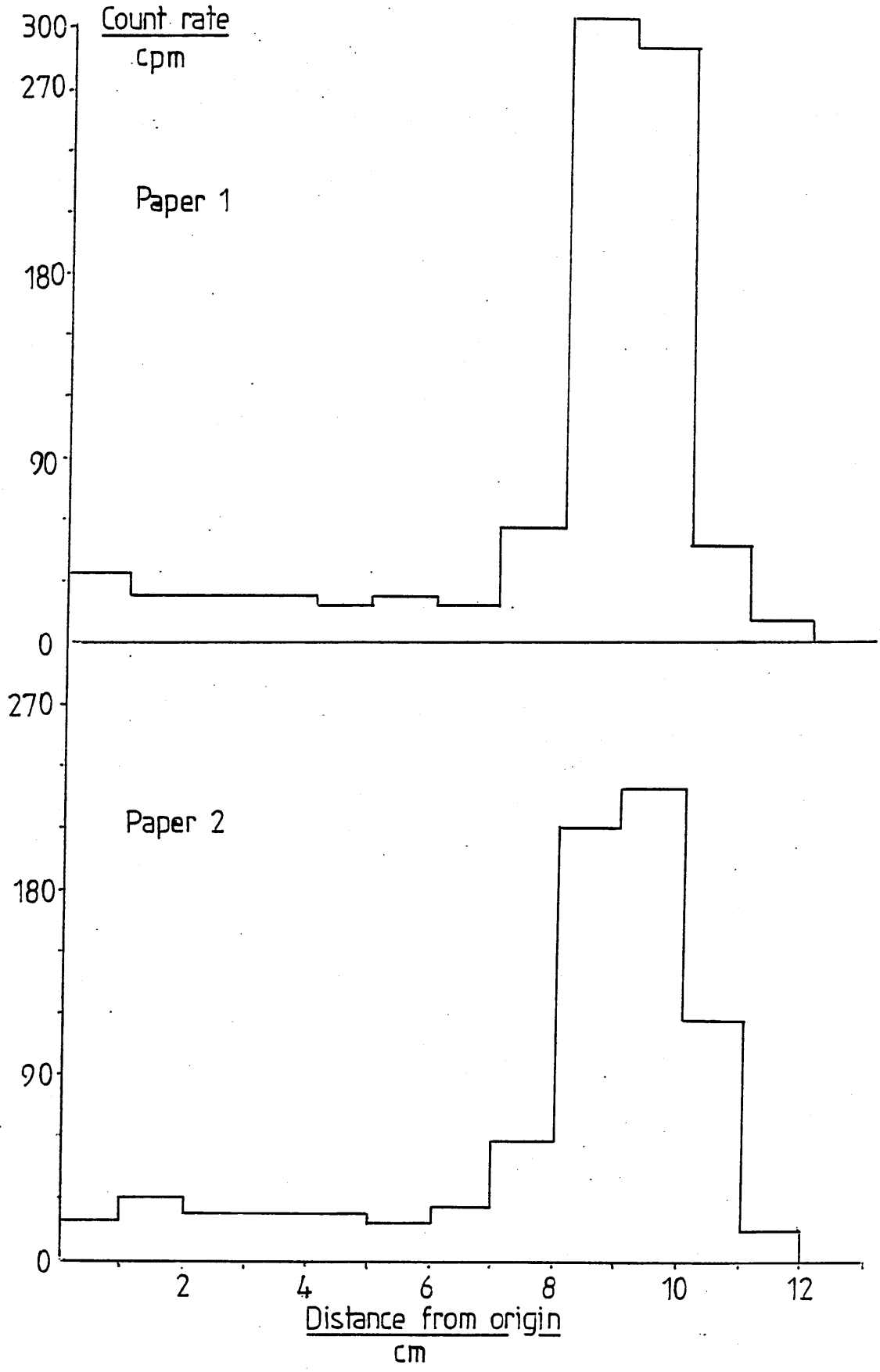

Figure 4.3

Electrophoresis of neutron-irradiated europium oxide dissolved in hydrochloric acid

4.2 Absorption of Ln^{2+} on barium sulphate

	First ppt Count rate c.p.m.	Second ppt Count rate c.p.m.	First ppt Corrected c.p.m.	Second ppt Corrected c.p.m.	Status
1	27513	22214	28838	23078	
2	8000	8020	8108	8218	BLANK
3	27708	19387	29052	20036	
4	34337	21541	36426	22345	
5	35390	36190	37613	38518	BLANK
6	25106	21982	26450	22846	

Table 4.5

Counts obtained from barium sulphate precipitates formed in the presence of irradiated Eu_2O_3 dissolved in dilute hydrochloric acid.

Activation carried out in Universities Research Reactor, Risley.
Corrections have been applied for dead time (100μs) of Geiger counter.

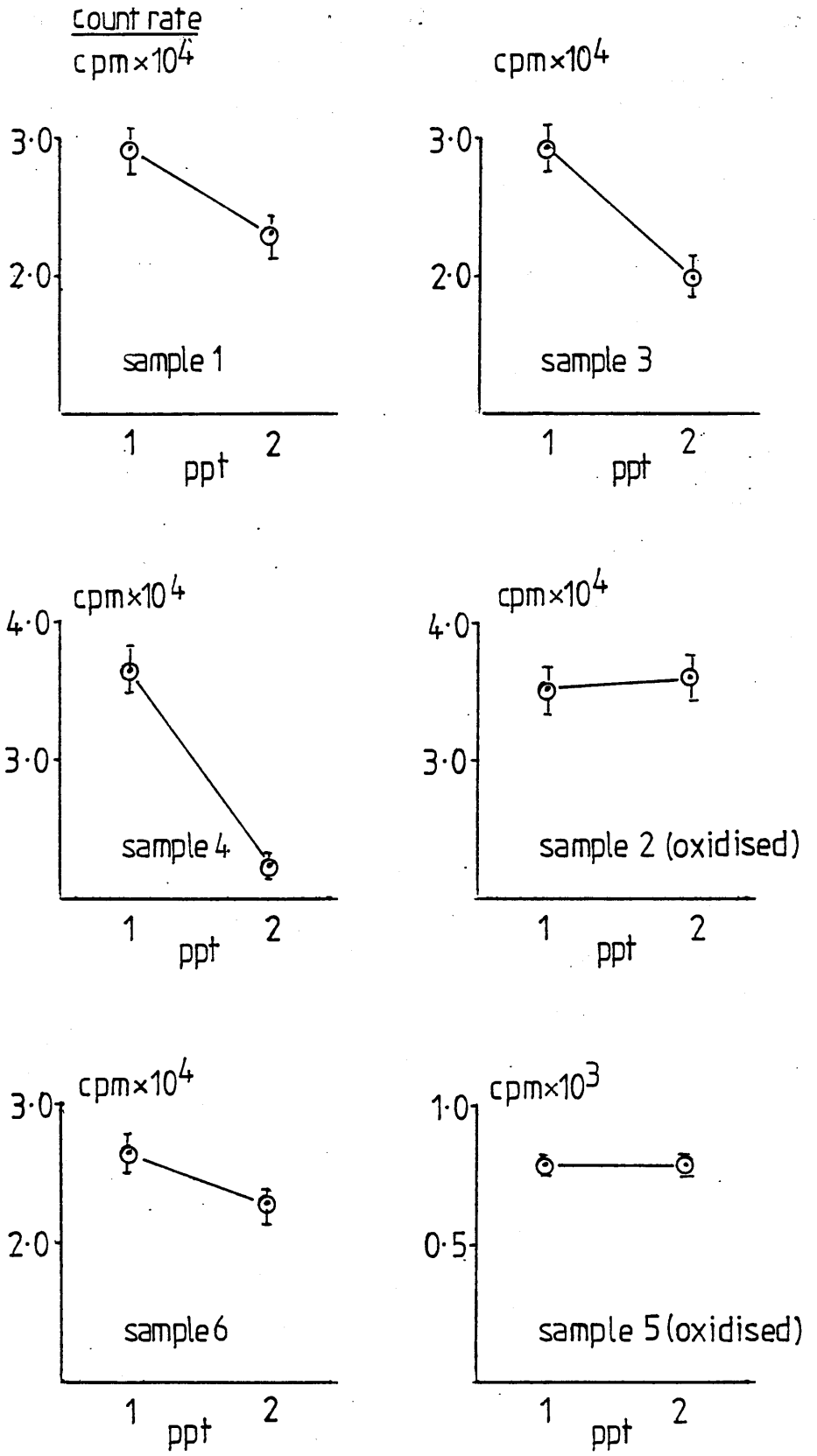

Figure 4.4 (From Table 4.5)

β-activity on barium sulphate precipitates formed in solutions of reactor-irradiated Eu_2O_3

ppt number	activity (cpm)	corrected activity (cpm)
1	44425	47976
2	22910	23817
3	21109	21878
4	17773	18315
5	17533	18061
6	15198	15433

Count measured in 11 cm^3 residual liquid	29560 cpm
Total liquid volume 22 cm^3	
Hence total liquid activity	59120 cpm
Relative efficiency of liquid counter	18.7%
Hence residual activity in liquid as seen by solid counter	316149 cpm

Table 4.6

Activities on barium sulphate precipitates produced in a solution of reactor irradiated Eu_2O_3 dissolved in hydrochloric acid.

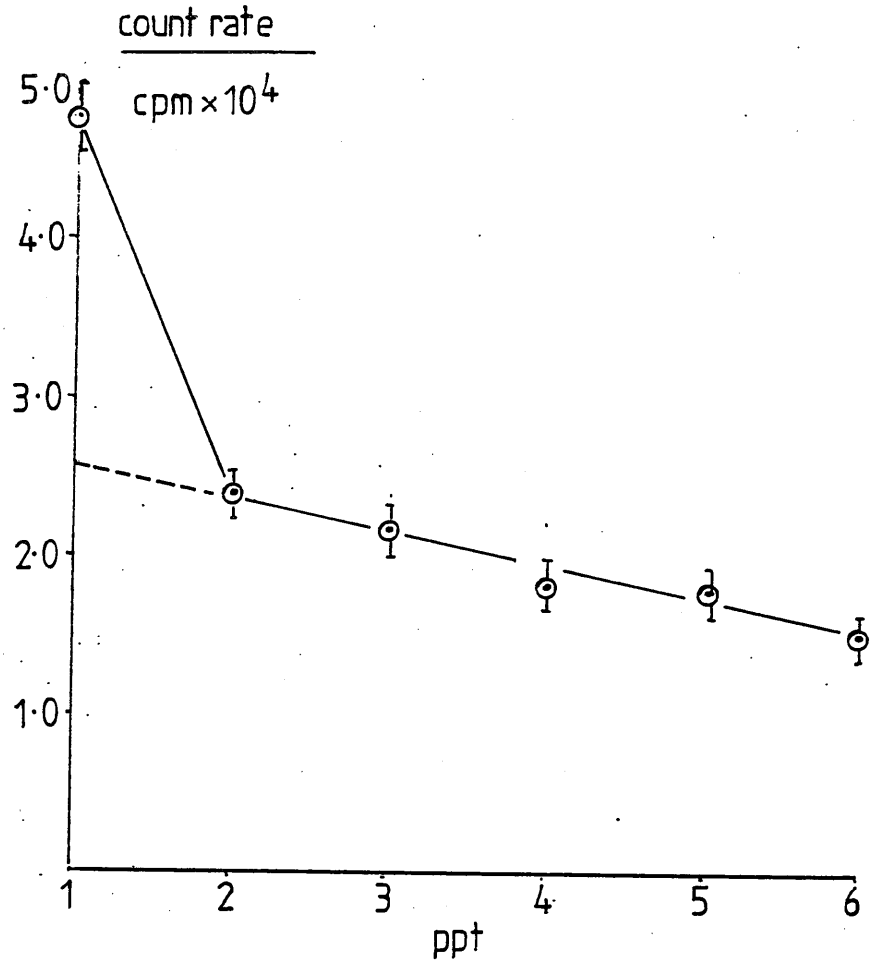

Figure 4.5 (From Table 4.6)

Activities on barium sulphate precipitates produced in a solution of reactor irradiated Eu_2O_3 dissolved in hydrochloric acid

Relative efficiencies of solid and liquid counters

Count on solid sample	4729	cpm
Same material in solution in liquid counter	801	cpm
Solid residue activity	446	cpm
Hence counts extracted to liquid	4283	cpm
Relative efficiency of liquid counter	$\frac{801}{4283}$ x 100	

that is, 18.7%

Table 4.7

Relative efficiencies of solid and liquid counters used to establish the figures of Table 4.6.

Sample	Activity of source cpm	Geiger check cpm	bgd cpm	ppt no	Count observed	length of count min	elapsed time min	corrected count rate cpm
1	10252	4892	22	1	943	11	42	78
				2	631	10	54	54
				3	517	10	65	41
				4	440	10	75	32
				5	368	10	85	23
2	10767	4892	22	1	936	11	45	75
				2	626	10	54	51
				3	438	10	67	29
				4	448	10	78	32
				5	387	10	88	25
				6	369	10	98	23
3	8581	5150	29	1	3474	30	49	125
				2	1609	30	105	47
				3	1422	34	138	29
				4	1133	25	77	28
				5	865	25	167	15
4	11276	4808	23	1	1064	12	37	71
				2	848	13	50	50
				3	528	10	62	37
				4	468	10	72	32
				5	397	10	83	24
				6	329	10	94	15

Table 4.8 (a)

Sample	Activity of source cpm	Geiger check cpm	bgd cpm	ppt no	Count observed	length of count min	elapsed time min	corrected count rate cpm
5	6193	5150	29	1	2999	30	54	146
				2	864	15	139	87
				3	681	15	154	55
				4	1444	30	74	46
				5	1219	30	116	35
6	9565	5036	26	1	1005	12	26	68
				2	607	10	38	44
				3	618	10	49	47
				4	395	10	59	19
				5	439	10	70	26
				6	350	10	80	14
B_1	11441	4982	22	1	670	10	33	47
				2	644	10	51	48
				3	508	10	61	34
				4	488	10	71	33
				5	435	10	81	27
				6	395	10	91	23
B_2	12792	4982	22	1	735	10	33	48
				2	613	10	43	38
				3	554	10	53	34
				4	482	10	65	28
				5	444	10	76	26

Table 4.8 (b)

Activities found on barium sulphate precipitates produced in $DyCl_3$ samples irradiated by the experimental neutron source.

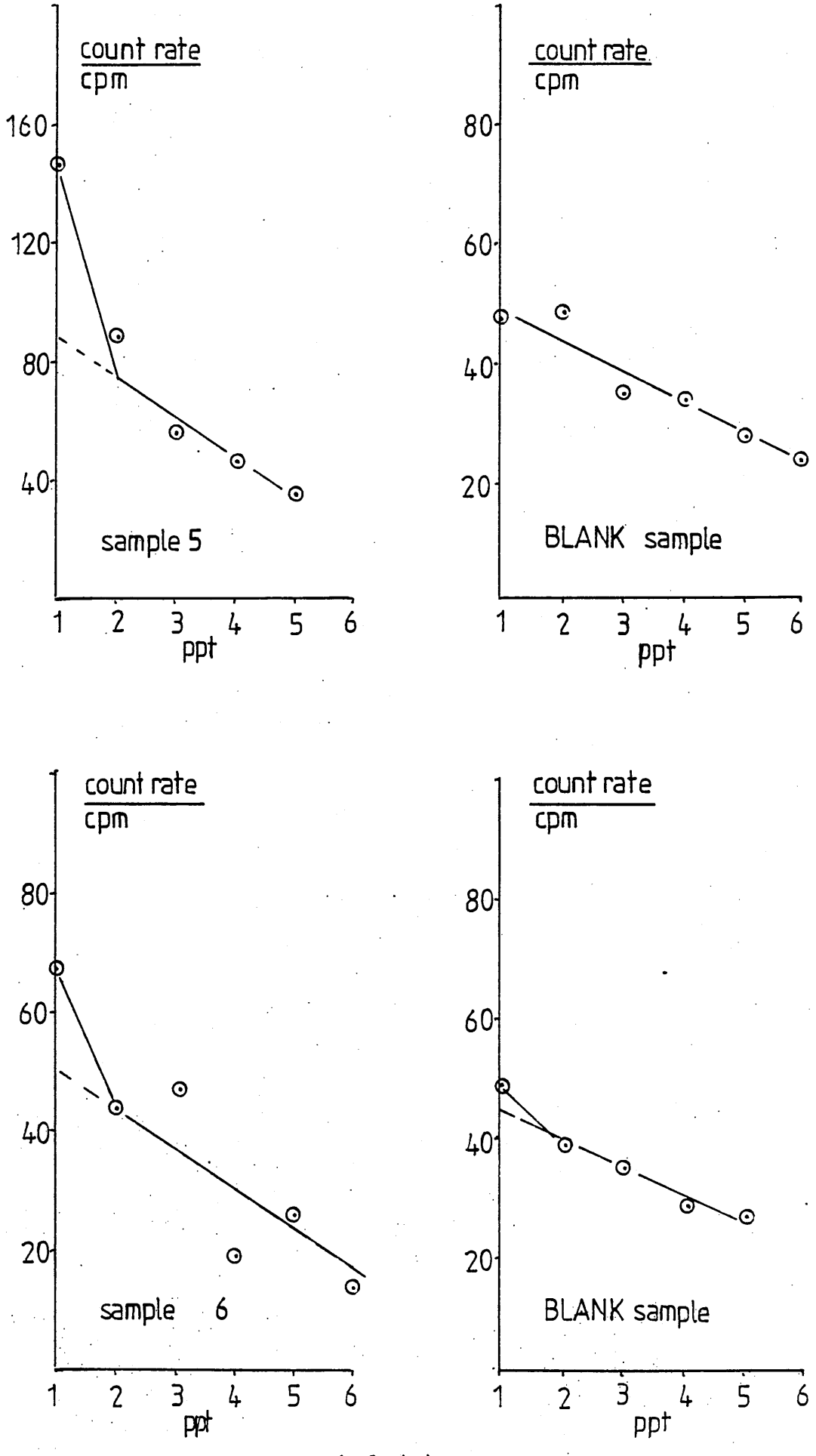
count rate
cpm
160
120
80
40
sample 5
1 2 3 4 5 6
ppt
count rate
cpm
80
60
40
20
BLANK sample
1 2 3 4 5 6
ppt
count rate
cpm
80
60
40
20
sample 6
1 2 3 4 5 6
ppt
count rate
cpm
80
60
40
20
BLANK sample
1 2 3 4 5 6
ppt

Figure 4.6 (a)

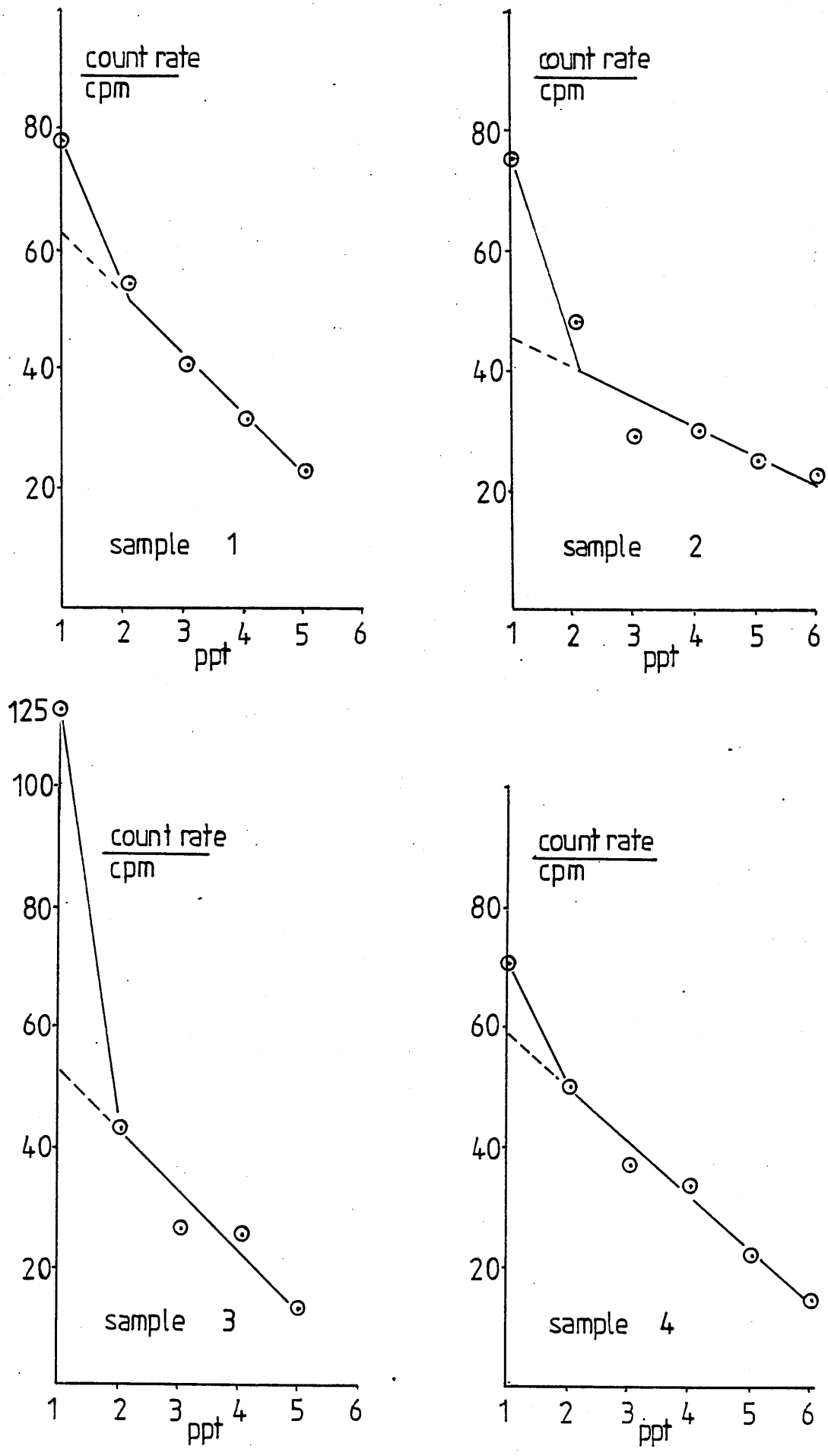

Figure 4.6 (b) (From Table 4.8)

Activities found on barium sulphate precipitates produced in $DyCl_3$ samples irradiated by the experimental neutron resources

Sample	Activity of source cpm	Geiger check cpm	bgd cpm	ppt no	Count observed	length of count min	corrected count rate cpm	$\frac{\sqrt{N}}{T}$
1	6636	4766	28	1	850	10	90	3
				2	618	10	53	2.5
				3	577	10	47	2
				4	539	10	41	2
				5	466	10	29	2
				6	489	10	33	2
2	9519	4746	29	1	1119	10	92	3
				2	760	10	52	3
				3	761	10	52	3
				4	686	10	44	3
				5	573	10	31	2
				6	572	10	31	2
3	7130	4808	23	1	951	10	105	3
				2	881	10	95	3
				3	685	10	66	3
				4	648	11	52	3
				5	530	10	44	2
				6	488	10	38	2
				7	137	3	33	4
4	7892	4697	29	1	861	10	77	3
				2	584	10	48	2
				3	563	10	37	2
				4	529	10	32	2
				5	419	10	17	2
				6	475	10	25	2

Table 4.9 (a)

Continued...

Sample	Activity of source cpm	Geiger check cpm	bgd cpm	ppt no	Count observed	length of count min	corrected count rate cpm	$\frac{\sqrt{N}}{T}$
5	6187	4716	27	1	767	10	85	3
				2	756	10	83	3
				3	594	10	56	2.5
				4	524	10	47	2
				5	512	10	41	2
				6	475	10	35	2
BLANK	8955	4622	28	1	839	10	68	3
				2	833	10	67	3
				3	714	10	52	3
				4	631	10	42	2.5
				5	601	10	39	2
				6	491	10	25	2
7	7203	4964	23	1	761	11	65	3
				2	644	10	58	3
				3	641	10	57	3
				4	494	10	37	2
				5	418	10	26	2
				6	438	10	29	2
				7	199	5	23	3
BLANK	8994	4787	23	1	867	11	65	3
				2	650	10	52	3
				3	662	10	50	3
				4	602	10	43	2.5
				5	541	10	36	2
				6	456	10	26	2

Table 4.9 (b) Activity found on barium sulphate precipitates produced in $EuCl_3$ samples irradiated by the experimental neutron source.

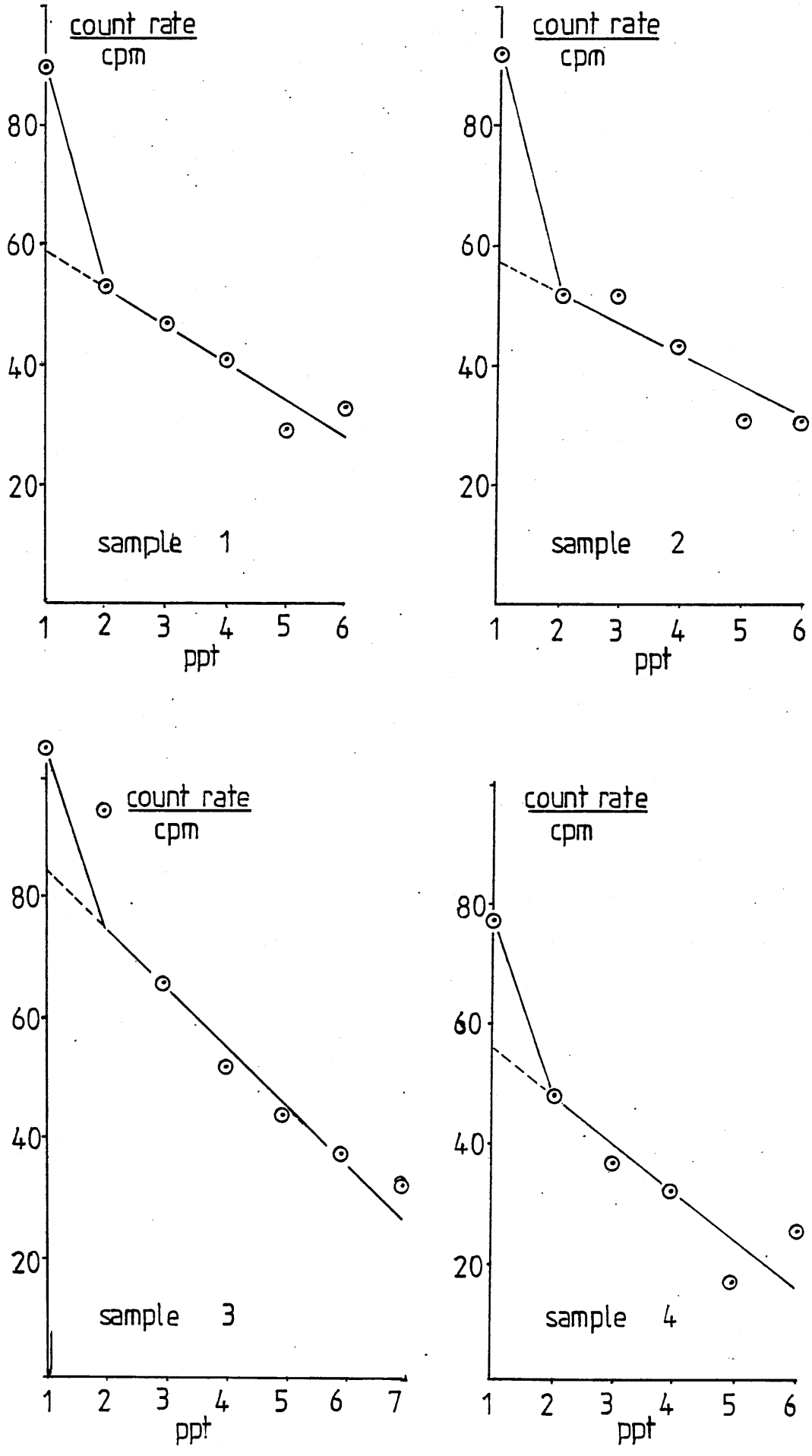
count rate
cpm
80
60
40
20
sample 1
1 2 3 4 5 6
ppt
count rate
cpm
80
60
40
20
sample 2
1 2 3 4 5 6
ppt
count rate
cpm
80
60
40
20
sample 3
1 2 3 4 5 6 7
ppt
count rate
cpm
80
60
40
20
sample 4
1 2 3 4 5 6
ppt

Figure 4.7 (a)

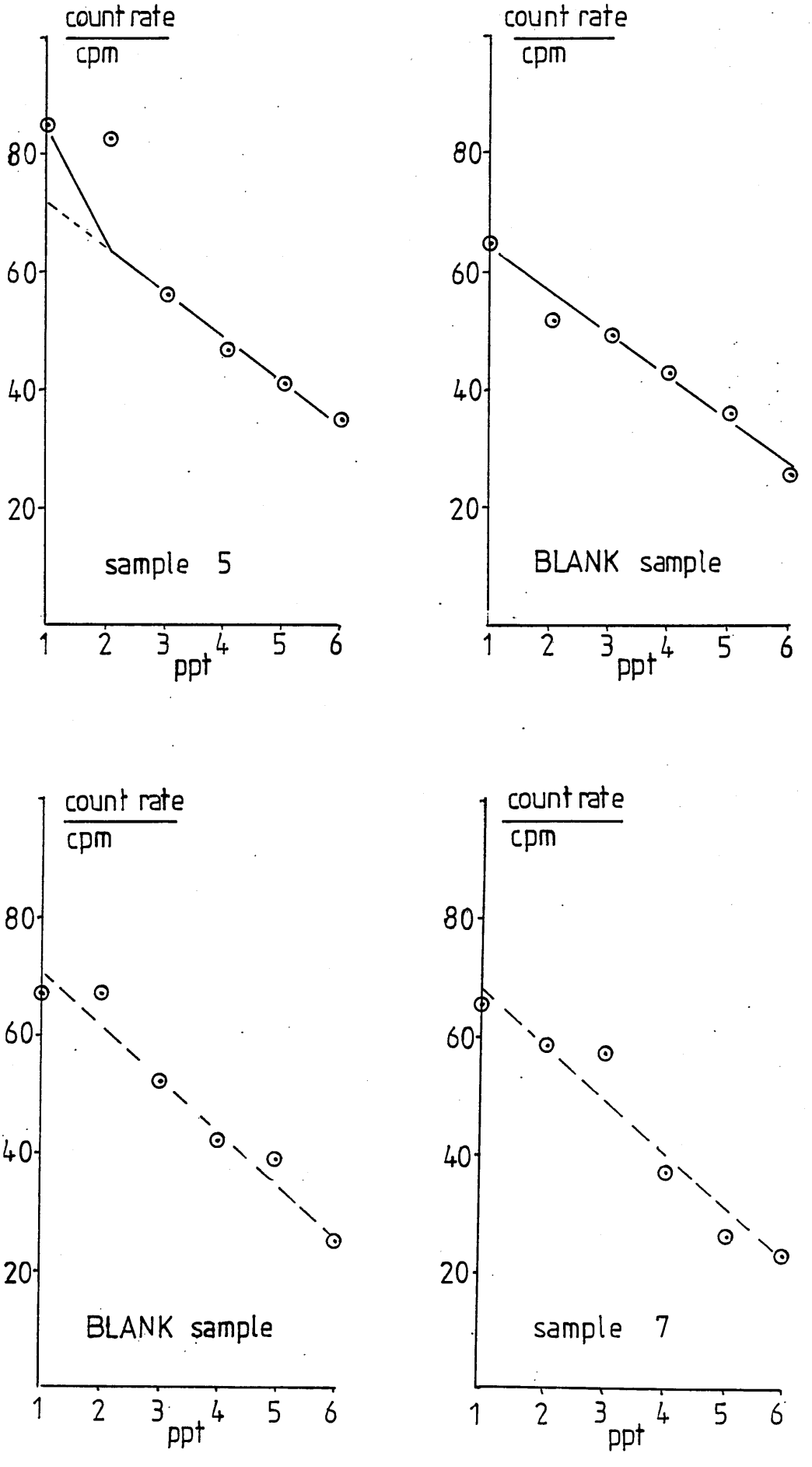

Figure 4.7 (b) (From Table 4.9)

Activities found on barium sulphate precipitates produced in $EuCl_3$ samples irradiated by the experimental neutron resources

4.3 Calibration of methylene blue

Mass of boat - $SnCl_2.2H_2O$	0.6844 g
Mass of boat alone	0.4622 g
Mass of $SnCl_2.2H_2O$	0.2222 g
Volume of solution	1000 cm^3
R.M.M. of $SnCl_2.2H_2O$	225.7
Concentration of solution	$\frac{0.222}{225.7} = 9.845 \times 10^{-4}$ mol dm^{-3}

Volume $Sn^{2+}(aq)$ added /cm^3	0.0	2.0	5.0	10.0	15.0
Absorbance/AU	0.733	0.688	0.519	0.328	0.152

Slope of calibration line $\frac{0.733 - 0.152}{15}$ A.U/cm^3

$= 0.03873$ A.U./cm^3

Hence a change of 1.000 A.U. corresponds to

$\frac{9.845 \times 10^{-4} \times 10^{-3}}{0.03873}$ mol Sn^{2+}

or 2.542×10^{-5} mol Sn^{2+}

Since in the reduction Sn^{2+} is converted to Sn^{4+} but subsequent calculations will assume that the lanthanide reaction is $Ln^{3+} \rightarrow Ln^{2+}$:-

A change of 1.000 A.U. corresponds to 5.084×10^{-5} mol Ln^{2+}

Table 4.10
Calibration and evaluation of methylene blue solution

Figure 4.8

Calibration of methyleneblue solution by $Sn^{2+}(aq)$

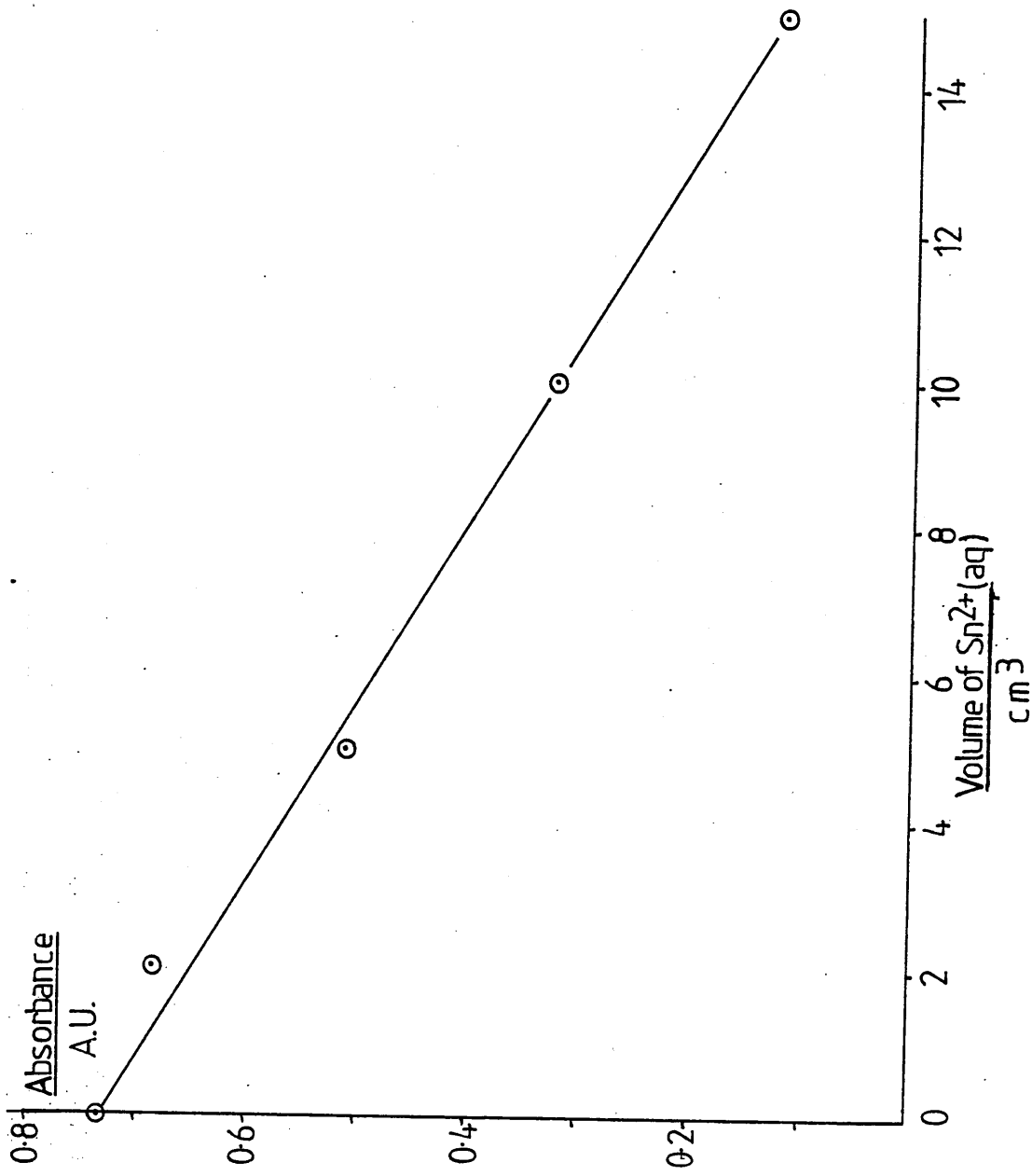

Vol. of alcohol (cm^3)	Vol. of water (cm^3)	% alcohol	A_1	A_2	A_3	A_4	A_5	Mean
			(A.U.)					
0	50	0	0.690	0.690	0.690	0.690	0.690	0.690
5	45	10	0.748	0.749	0.749	0.749		0.749
10	40	20	0.788	0.792	0.791	0.790	0.790	0.790
15	35	30	0.805	0.807	0.808	0.809	0.807	0.807
25	25	50	0.827	0.827	0.829	0.831		0.829
40	10	80	0.834	0.836	0.836	0.837		0.836

Table 4.11

Absorbance of methylene blue at 664 nm in various concentrations of ethanol by volume.

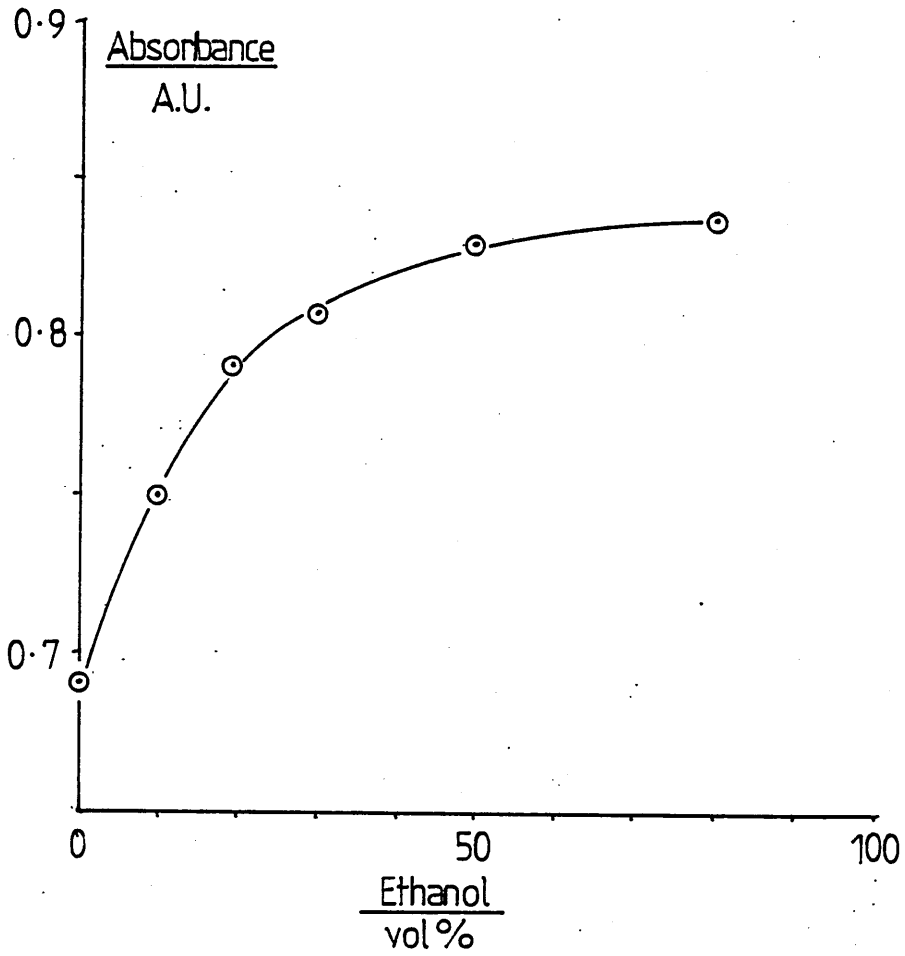

Figure 4.9 (From Table 4.11)

Absorbance of methylene blue at 664 nm in various concentrations of ethanol by volume

4.4 U-V spectra of dysprosium chloride solutions

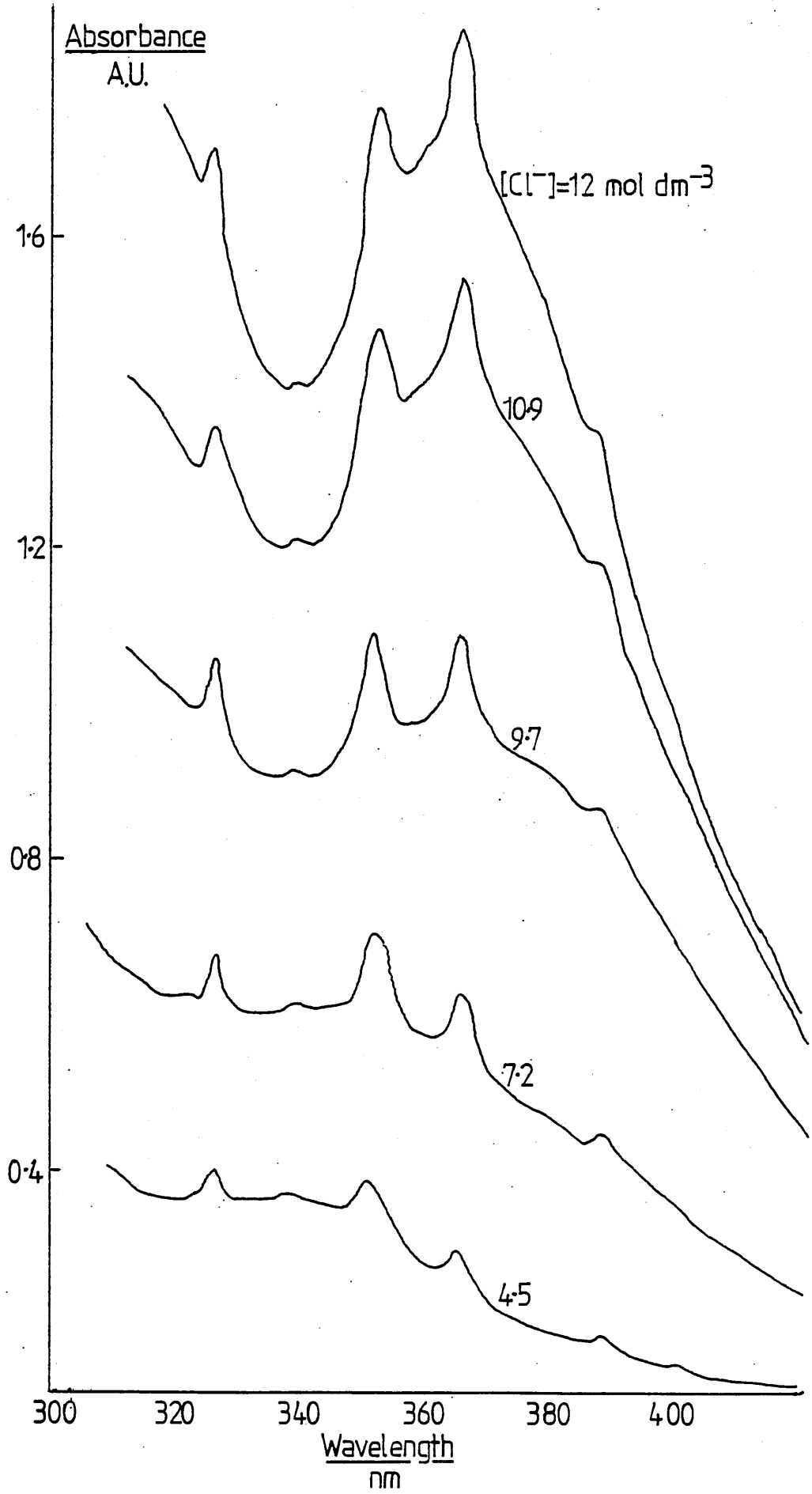

Figure 4.10 Ultraviolet spectra of dysprosium chloride dissolved in various concentrations of hydrochloric acid

4.5 Absorbance changes in methylene blue solution

Absorbance	Mean	Error
Sample (a) $EuCl_3$		
Sample 0.807 0.806 0.804 0.804 0.805		
0.807 0.806	0.805_7	0.0005_7
ox'd 0.808 0.807 0.809 0.808 0.807	0.807_8	0.0003_7
$\Delta = 0.0021 \pm 0.007$		
Sample (b) $EuCl_3$		
Sample 0.805 0.800 0.799 0.799 0.799		
0.801 0.800 0.801	0.801	0.0008_5
ox'd 0.803 0.804 0.803 0.804 0.804	0.803_6	0.0002
$\Delta = 0.0026 \pm 0.0009$		
Sample (c) $DyCl_3$		
Sample 0.641 0.640 0.642 0.641	0.641	0.0003_5
ox'd 0.642 0.642 0.639 0.638	0.640	0.0008_9
$\Delta = 0.001 \pm 0.0009$		
Sample (d) $DyCl_3$		
Sample 0.806 0.807 0.809 0.809 0.809		
0.808	0.808	0.0005_2
ox'd 0.809 0.808 0.808 0.808 0.809	0.808_4	0.0002_4
$\Delta = 0.0004 \pm 0.0006$		
Sample (e) $DyCl_3$		
Sample 0.505 0.504 0.506 0.506 0.505		
0.504	0.504_8	0.0003_7
ox'd 0.508 0.507 0.507 0.506 0.507	0.504_8	0.0003_7
$\Delta = 0.002 \pm 0.0004$		

Table 4.12 (a)

Absorbance	Mean	Error
Sample (f) $DyCl_3$		
Sample 0.500 0.498 0.501 0.499 0.499	0.499_4	0.0005_1
ox'd 0.500 0.501 0.499 0.497		
repeated ox'n 0.500 0.499 0.499 0.499 0.499	0.499_2	0.0002
$\Delta = -0.0002 \pm 0.0002$		
Sample (g) $DyCl_3$		
Sample 0.521 0.522 0.522 0.520 0.520		
0.519	0.520_7	0.0005
ox'd 0.523 0.523 0.522 0.523 0.523	0.522_8	0.0002
$\Delta = 0.002 \pm 0.0006$		
Sample (h) $DyCl_3$		
Sample 0.512 0.508 0.509 0.508 0.509	0.509_2	0.0006
0.509		
ox'd 0.512 0.511 0.511 0.511 0.511	0.511_2	0.0002
$\Delta = 0.002 \pm 0.0006$		

Table 4.12 (b)

Absorbances of BLANK samples of methylene blue before and after oxygenation in the presence of unirradiated $EuCl_3$ or $DyCl_3$.

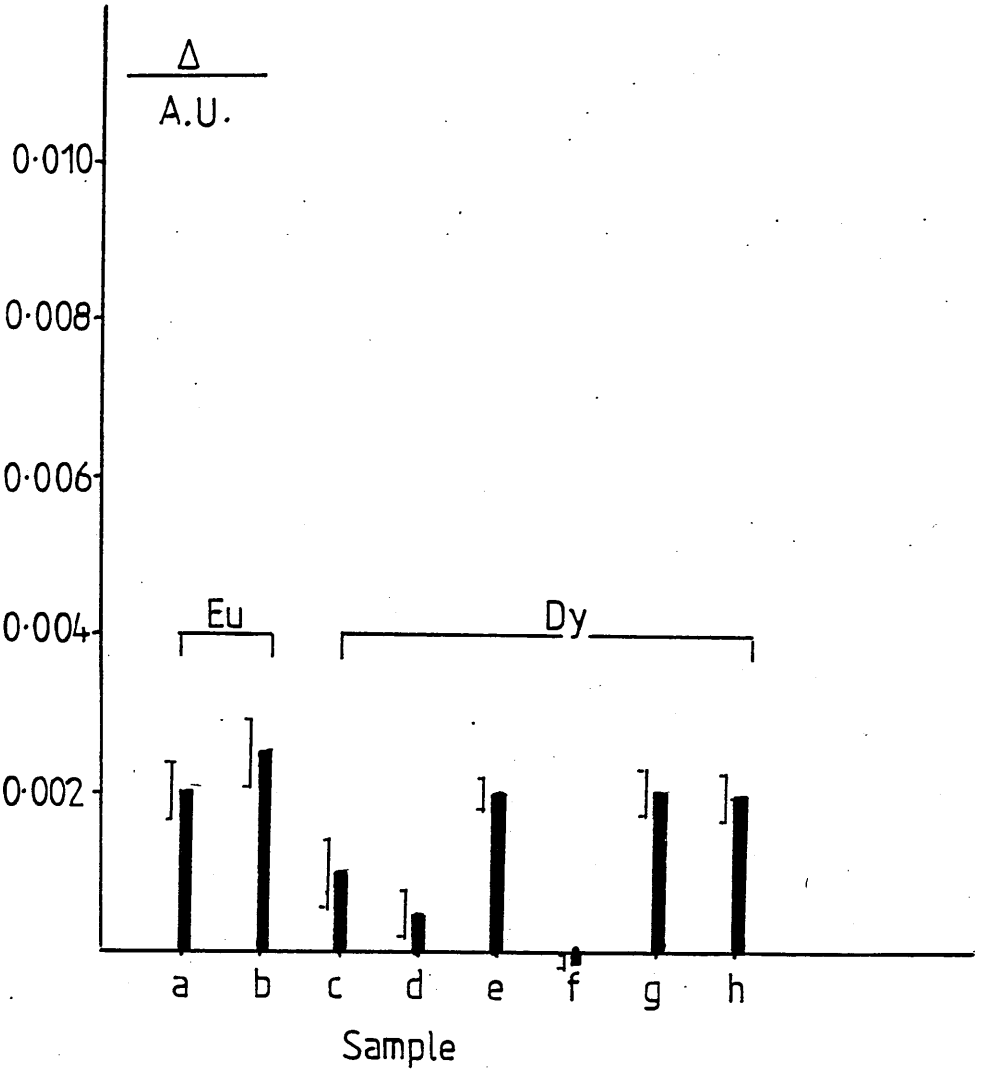

Figure 4.11 (From Table 4.12)

Changes in absorbance produced in blank determinations.

The small bars show the extent of the instrumental uncertainty for each measurement.

Absorbance	Mean	Error
Sample (a) Eu_2O_3		
Sample 0.799 0.801 0.800 0.801 0.803		
0.801	0.800_8	0.0006_1
ox'd 0.806 0.806 0.806 0.805 0.808	0.806_2	0.0004_9
$\Delta = 0.005_4 \pm 0.0008$		
$\Delta_e = 0.004_2$		
Sample (b) Eu_2O_3		
Sample 0.791 0.791 0.793 0.793 0.792	0.792	0.0004_4
ox'd 0.799 0.794 0.795 0.796 0.796		
0.794	0.795_7	0.0007_7
$\Delta = 0.0037 \pm 0.0009$		
$\Delta_c = 0.0027$		
Sample (c) Eu_2O_3		
Sample 0.800 0.802 0.802 0.802 0.802	0.801_6	0.0004
ox'd 0.806 0.805 0.804 0.806 0.806	0.805	0.0004
$\Delta = 0.0034 \pm 0.0006$		
$\Delta_c = 0.0026$		
Sample (d) $EuCl_3$ 28d irradiation		
Sample 0.741 0.739 0.738 0.740 0.741		
0.742	0.740	0.0005_8
ox'd 0.752 0.753 0.754 0.753	0.753	0.0004
$\Delta = 0.013 \pm 0.0007$		
Sample (e) $EuCl_3$ 3½d irradiation		
Sample 0.845 0.846 0.846 0.846	0.845_8	0.0002_5
ox'd 0.858 0.860 0.861 0.862 0.862	0.862_2	0.0007_4
$\Delta = 0.016 \pm 0.0008$		
$\Delta_c = 0.015$		

Absorbance	Mean	Error
Sample (f) $EuCl_3$ 1½ days		
Sample 0.800 0.802 0.803 0.805 0.803	0.802_6	0.0008
ox'd 0.812 0.811 0.809 0.809 0.809	0.810	0.0006_3
Δ = 0.0074 ± 0.001		
Sample (g) $EuCl_3$ 1 day		
Sample 0.809 0.809 0.810 0.812 0.811	0.810_2	0.0005_8
ox'd 0.818 0.820 0.818 0.820 0.819	0.819	0.0008_9
Δ = 0.0088 ± 0.001		
Sample (h) $EuCl_3$ 1 day		
Sample 0.813 0.811 0.814 0.814 0.814	0.813_2	0.0005_8
ox'd 0.821 0.823 0.821 0.823 0.824	0.822_4	0.0006
Δ = 0.0092 ± 0.0008		

Table 4.13 (b)

Absorbance of methylene blue samples treated with irradiated $EuCl_3$, before and after re-oxidation.

Where values Δ_c are quoted the measured change in absorbance has been corrected to that expected for a 100 mg $EuCl_3$ sample. Corrections are pro-rata.

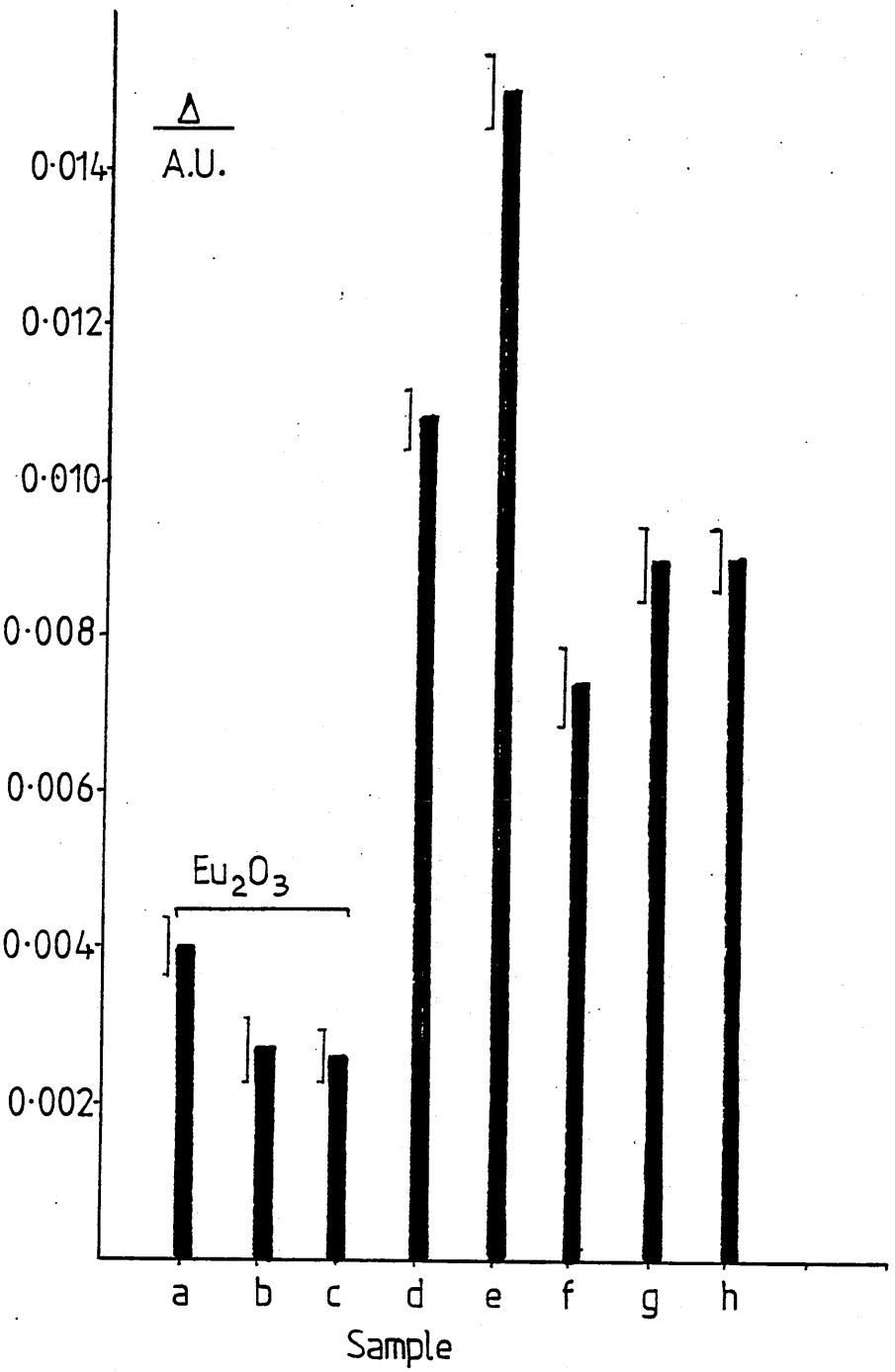

Figure 4.12

Changes in absorbance of methylene blue samples treated with irradiated $EuCl_3$ before and after re-oxidation

Absorbance	Mean	Error
Sample (a) $Dy_2(CO_3)_3$ 3 week irrad.		
Sample 0.777 0.776 0.774 0.775 0.777		
0.773 0.773 0.775	0.755_3	0.0005_6
ox'd 0.782 0.784 0.782 0.783 0.783	0.782_8	0.0003_7
$\Delta = 0.0075 \pm 0.0007$		
$\Delta_c = 0.007$		
Sample (b) $Dy_2(CO_3)_3$ 3 week irrad.		
Sample 0.765 0.767 0.772	0.768	0.002
ox'd 0.782 0.799 0.783 0.781 0.780		
0.781	0.781	0.0005_8
$\Delta = 0.013 \pm 0.002$		
$\Delta_c = 0.012$		
Sample (c) $DyCl_3$ 23h irradiation		
Sample 0.798 0.800 0.799 0.798 0.797	0.798_4	0.0005
ox'd 0.808 0.809 0.813 0.808 0.807	0.809	0.001
$\Delta = 0.0106 \pm 0.001$		
$\Delta_c = 0.01$		
Sample (d) $DyCl_3$ 24h irradiation		
Sample 0.797 0.797 0.799 0.801 0.800	0.798_8	0.0008
ox'd 0.810 0.807 0.808 0.809 0.809	0.808_6	0.0005_1
$\Delta = 0.0098 \pm 0.0009$		
Sample (e) $DyCl_3$ 21h irradiation		
Sample 0.815 0.816 0.817 0.817 0.817	0.816_4	0.0004
ox'd 0.827 0.825 0.827 0.826 0.825	0.826	0.0004_5
$\Delta = 0.0096 \pm 0.0006$		

Table 4.14 (a)

Absorbance	Mean	Error
Sample (f) $DyCl_3$ 23h irradiation		
Sample 0.827 0.826 0.827 0.826 0.825	0.826_2	0.0003_7
ox'd 0.833 0.834 0.832 0.834 0.834	0.833_4	0.0004
Δ = 0.0072 ± 0.0005		
Sample (g) $DyCl_3$ 21h irradiation		
Sample 0.815 0.815 0.816 0.816 0.816	0.815_6	0.0002_4
ox'd 0.828 0.827 0.828 0.828 0.828	0.827_8	0.0002
Δ = 0.0122 ± 0.0003		
Δ_c = 0.011		
Sample (h) $DyCl_3$ 16h irradiation		
Sample 0.768 0.772 0.770 0.770 0.770		
0.771 0.769	0.770	0.0005_1
ox'd 0.776 0.776 0.776 0.776		
Δ = 0.004 ± 0.0005		
Sample (i) $DyCl_3$ 18h irradiation		
Sample 0.731 0.729 0.727 0.727 0.726		
0.726 0.727 0.727	0.727_5	0.0006
ox'd 0.734 0.733 0.732 0.733 0.732		
0.732	0.732_7	0.0003_3
Δ = 0.0052 ± 0.0007		
Sample (j) $DyCl_3$ 20h irradiation		
Sample 0.789 0.791 0.788 0.796 0.790		
0.791 0.792 0.799 0.795 0.791	0.792_2	0.001
ox'd 0.801 0.800 0.801 0.800 0.800		
0.800	0.800_3	0.0002
Δ = 0.0081 ± 0.001		
Δ_c = 0.007_5		

Table 4.14 (b)

Absorbance						Mean	Error
Sample (k) thought to be wrapped in Cd foil but actually encased in Sn							
Sample	0.817	0.816	0.817	0.818	0.818	0.817_2	0.0003_7
ox'd	0.826	0.826	0.825	0.825	0.826	0.825_6	0.0002_4
$\Delta = 0.0084 \pm 0.0004$							
Sample (l) same treatment as (k)							
Sample	0.787	0.787	0.787	0.787	0.787	0.787	
ox'd	0.799	0.800	0.800	0.800	0.799	0.799_6	0.0002_4
$\Delta = 0.0126 \pm 0.0002$							

Table 4.14 (c)

Absorbances of methylene blue samples treated with irradiated $DyCl_3$, before and after re-oxidation.

Where values Δ_c are quoted the measured change in absorbance has been corrected to that expected for a 100 mg $DyCl_3$ sample. Corrections are pro-rata.

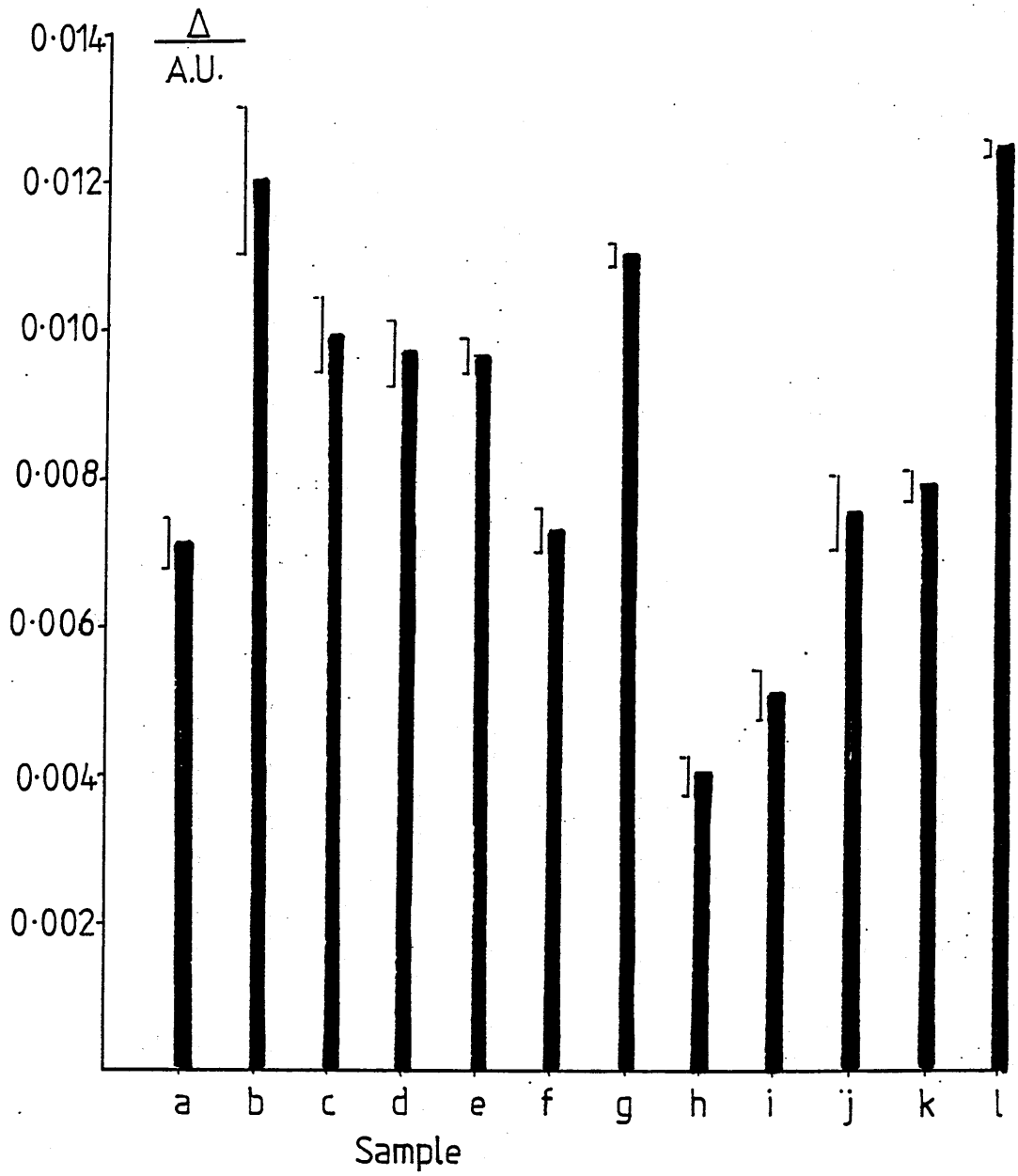

Figure 4.13 (From Table 4.14)

Changes in absorbance of methylene blue samples treated with irradiated $DyCl_3$, before and after re-oxidation

Time	elapsed time min	A A.V.
10.18	0	821
10.19	1	821
10.20	2	824
10.21	3	824
10.22	4	823
10.23	5	824
10.24	6	823
10.25	7	824
10.26	8	814
10.28	10	802
10.30	12	771
10.31	13	749
10.32	14	732
10.33	15	712
10.34	16	697
10.35	17	687
10.36	18	683
10.37	19	686
10.38	20	684
10.39	21	681
10.40	22	679
10.42	24	751
10.44	26	784
10.46	28	789
10.48	30	790
11.08	50	788
11.10	52	788

Table 4.15
Absorbance of methylene blue at 664 nm in the presence of EDTA, in sunlight.

Mixing took place at 8 mins and subsequent treatment with oxygen at 12 minutes from the start.

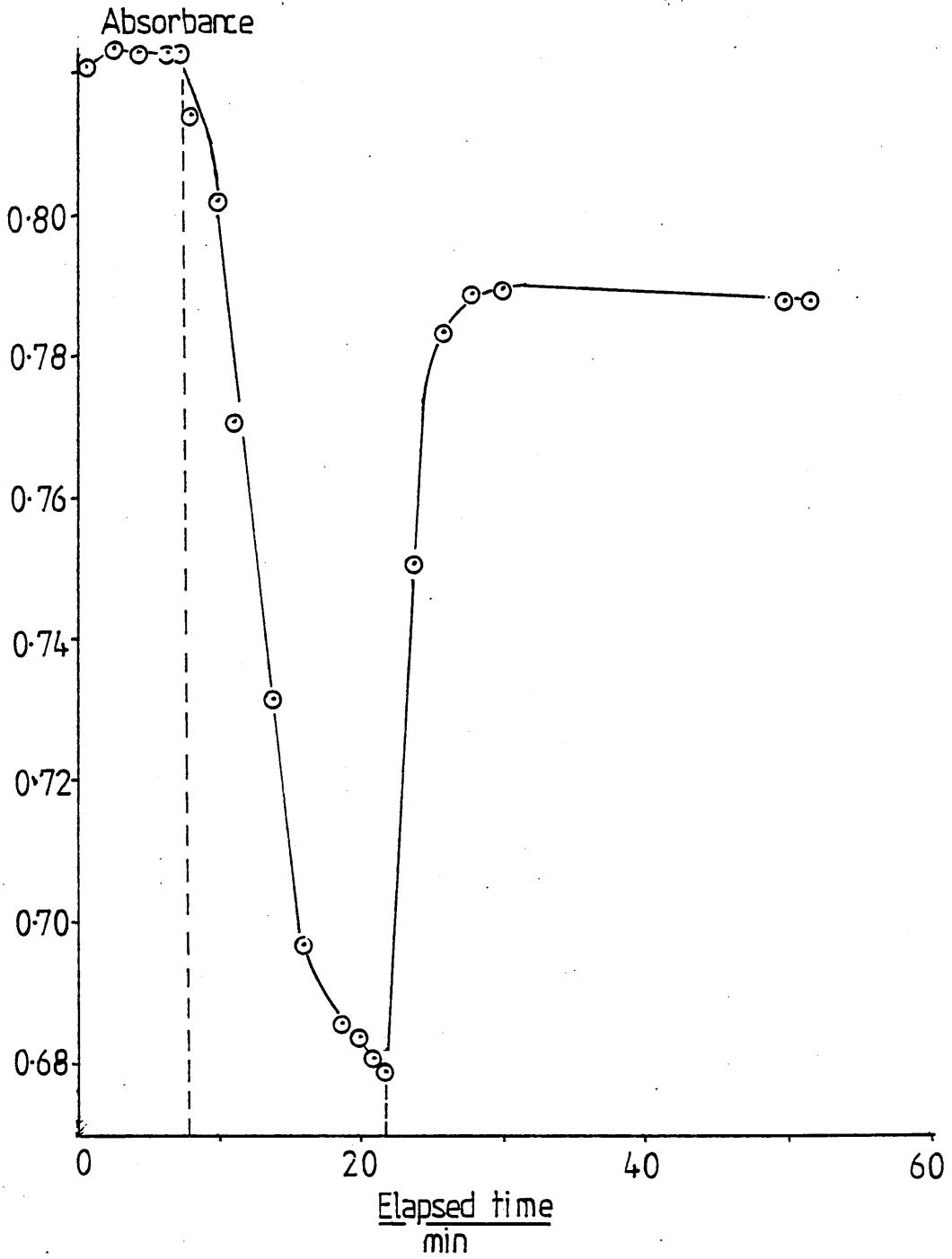

Figure 4.14

Absorbance of a solution of methylene blue at 664 nm in the presence of EDTA, in sunlight.

Absorbance	Mean	Error
Sample (a) $DyCl_3$ dissolved i/p EDTA		
Sample 0.869 0.869 0.867 0.868 0.868	0.868_2	0.0003_7
ox'd 0.868 0.868 0.866 0.867 0.866	0.867	0.0004
$\Delta = 0.0012 \pm 0.0005$		
Sample (b) $DyCl_3$ dissolved i/p EDTA		
Sample 0.864 0.866 0.863 0.866 0.864	0.864_6	0.0006
ox'd 0.865 0.865 0.864 0.866 0.865	0.865	0.0003
$\Delta = 0.0004 \pm 0.003$		
Sample (c) $DyCl_3$ dissolved i/p EDTA		
Sample 0.755 0.755 0.756 0.754 0.754	0.754_8	0.0003
$\Delta = 0.001 \pm 0.0004$		
Sample (d) $DyCl_3$ dissolved i/p EDTA		
Sample 0.731 0.727 0.722 0.721 0.718		
0.712	0.721_8	0.002_8
ox'd 0.720 0.718 0.719 0.724 0.723		
0.723 0.723 0.719 0.720	0.721	0.0007_5
$\Delta = 0.000 \pm 0.002$		
Sample (e) crystalline $DyCl_3$		
Sample 0.797 0.799 0.798 0.799 0.799	0.798_4	0.0004
ox'd 0.800 0.797 0.797 0.797 0.799	0.798	0.0006
$\Delta = -0.0004 \pm 0.0007$		

Table 4.16(a)

Absorbance	Mean	Error
Sample (f) crystalline $DyCl_3$		
Sample 0.783 0.786 0.784 0.783 0.782	0.783_6	0.0006_8
ox'd 0.787 0.787 0.788 0.786 0.786	0.786_8	0.0003_7
$\Delta = 0.003_2 \pm 0.0007$		
$\Delta_c = 0.003_6$		
Sample (g) crystalline $DyCl_3$		
Sample 0.785 0.788 0.785 0.788 0.789		
0.786 0.789 0.787	0.787_1	0.0005_8
ox'd 0.790 0.791 0.790 0.789 0.790		
0.789 0.789	0.789_7	0.0002_9
$\Delta = 0.0002_6 \pm 0.0006$		
$\Delta_c = 0.0003_4$		

Table 4.16 (b)

Absorbances of methylene blue samples tested with irradiated $DyCl_3$ in the conditions stated.

Where values Δ_c are quoted the measured change in absorbance has been corrected to that expected for a 100 mg $DyCl_3$ sample. Corrections are pro-rata.

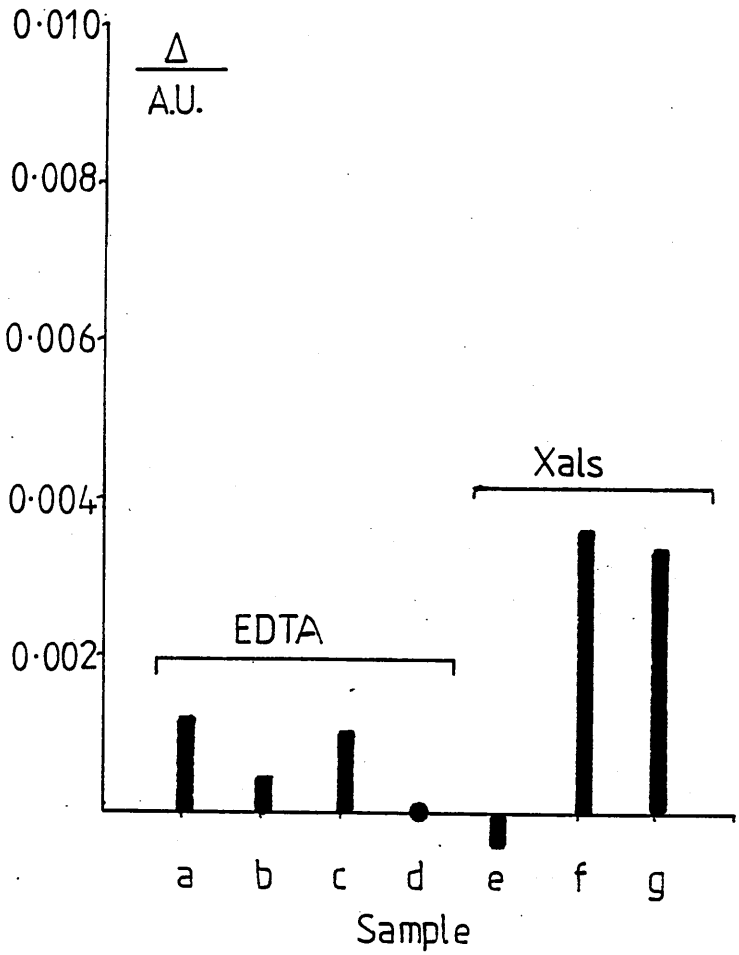

Figure 4.15

Changes in absorbance of a solution of methylene blue at 664 nm, treated with irradiated $DyCl_3$ (in the conditions shown), before and after re-oxidation.

Absorbance	Mean	Error
Sample (a) Eu_2O_3 - dose 91 K Gy		
Sample 0.703 0.701 0.703 0.702 0.701	0.702	0.0004_5
ox'd 0.703 0.703 0.702 0.702	0.702_5	0.0002_5
$\Delta = 0.0005 \pm 0.0005$		
Sample (b) $DyCl_3$		
Sample 0.816 0.818 0.821 0.819 0.820	0.818_8	0.0009
ox'd 0.819 0.819 0.819 0.819 0.818	0.818_8	0.0009
$\Delta = 0.00 \pm 0.0009$		
Sample (c) $DyCl_3$		
Sample 0.796 0.797 0.796 0.798 0.796	0.796_6	0.0004
ox'd 0.798 0.799 0.798 0.798 0.799	0.798_4	0.0002
$\Delta = 0.0018 \pm 0.0005$		
Sample (d) $DyCl_3$		
Sample 0.810 0.811 0.811 0.810 0.811	0.810_6	0.0002
ox'd 0.811 0.812 0.811 0.811 0.811	0.811_2	0.0002
$\Delta = 0.0006 \pm 0.0002$		
Sample (e) $DyCl_3$		
Sample 0.811 0.811 0.814 0.811 0.811	0.811_6	0.0006
ox'd 0.814 0.814 0.813 0.813 0.813	0.813_4	0.0002
$\Delta = 0.001_8 \pm 0.0006$		
Sample (f) $DyCl_3$		
Sample 0.805 0.805 0.806 0.806 0.806	0.805_6	0.0002_4
ox'd 0.808 0.808 0.808 0.809 0.809	0.808_4	0.0002_4
$\Delta = 0.0028 \pm 0.0003$		

Table 4.17 (a)

Absorbance	Mean	Error
Sample (g) $EuCl_3$		
Sample 0.806 0.805 0.807 0.809 0.807		
ox'd 0.807	0.806_8	0.0005_5
ox'd 0.810 0.810 0.810 0.810 0.810		
0.809	0.809_8	0.0001_7
$\Delta = 0.003 \pm 0.0006$		
Sample (h) $EuCl_3$		
Sample 0.813 0.813 0.815 0.814 0.814		
0.813	0.813_7	0.0003_4
ox'd 0.815 0.816 0.815 0.816 0.816	0.815_6	0.0002_4
$\Delta = 0.0019 \pm 0.0004$		
Sample (i) $EuCl_3$		
Sample 0.811 0.809 0.811 0.810 0.810	0.810_2	0.0003
ox'd 0.813 0.813 0.813 0.813 0.813	0.813	
$\Delta = 0.0028 \pm 0.0003$		

Table 4.17 (b)

Absorbances of methylene blue treated with γ-irradiated $DyCl_3$, before and after re-oxidation.

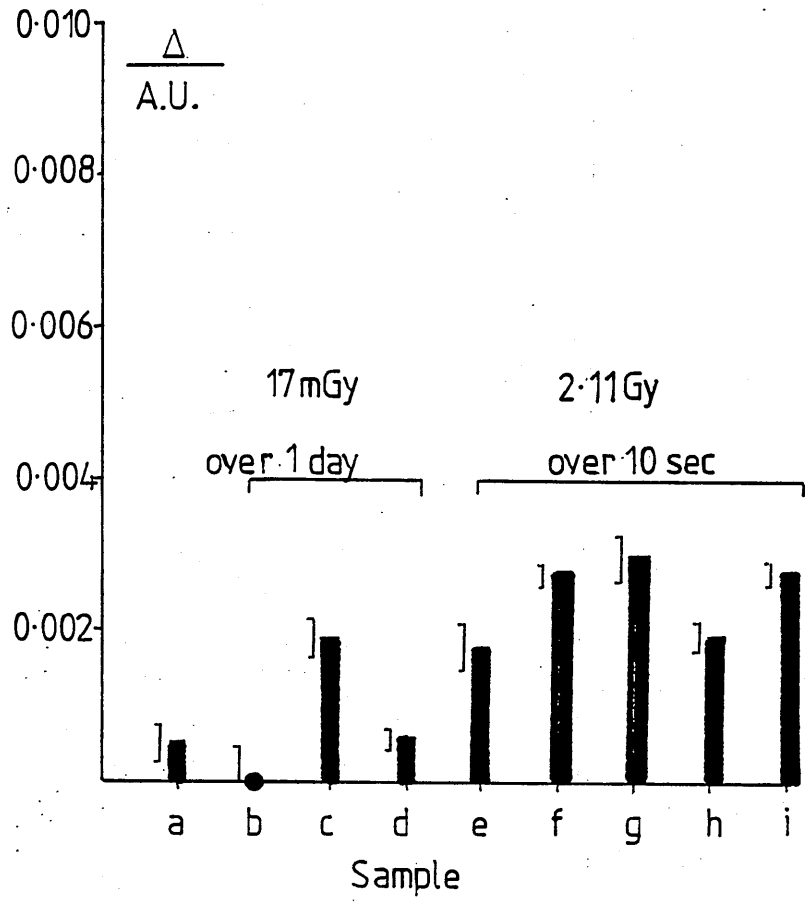

Figure 4.16

Changes in absorbance of methylene blue treated with γ-irradiated $DyCl_3$, before and after re-oxidation.

Absorbance	Mean	Error
1. Irradiation time 1 day		
Sample 0.808 0.808 0.807 0.808 0.806	0.807_4	0.0004
ox'd 0.809 0.808 0.809 0.808 0.809		
0.809	0.808_7	0.0002_1
$\Delta = 0.0013 \pm 0.0005$		
$\Delta_c = 0.0012$		
2. Irradiation time 2 days		
Sample 0.827 0.826 0.825 0.826 0.826	0.826	0.0003
ox'd 0.832 0.831 0.831 0.830 0.831	0.831	0.0003
$\Delta = 0.005 \pm 0.0004$		
$\Delta_c = 0.0049$		
3. Irradiation time 3 days		
Sample 0.808 0.809 0.808 0.809 0.808	0.808_4	0.0002_4
ox'd 0.815 0.814 0.813 0.813 0.814	0.813_8	0.0003_7
$\Delta = 0.0054 \pm 0.0004$		
$\Delta_c = 0.0053$		
4. Irradiation time 6 days		
Sample 0.819 0.818 0.817 0.816 0.818	0.817_6	0.0005
ox'd 0.824 0.821 0.821 0.821 0.822		
0.821	0.821_7	0.0005
$\Delta = 0.0041 \pm 0.0007$		
5. Irradiation time 7 days		
Sample 0.804 0.803 0.804 0.803 0.804	0.803_6	$.0.0002_4$
ox'd 0.809 0.809 0.809 0.809 0.809	0.809	-
$\Delta = 0.0054 \pm 0.0002$		
$\Delta_c = 0.005$		

Table 4.18 (a)

Absorbance	Mean	Error
6. Irradiation time 9 days		
Sample 0.808 0.808 0.809 0.809 0.811		
0.808	0.808_8	0.0004_8
ox'd 0.814 0.814 0.813 0.814 0.813		
0.813	0.813_5	0.0002_2
Δ = 0.0047 ± 0.0005		

Table 4.18 (b)

Absorbances of methylene blue treated with $DyCl_3$ previously irradiated with fast neutrons, before and after re-oxidation.

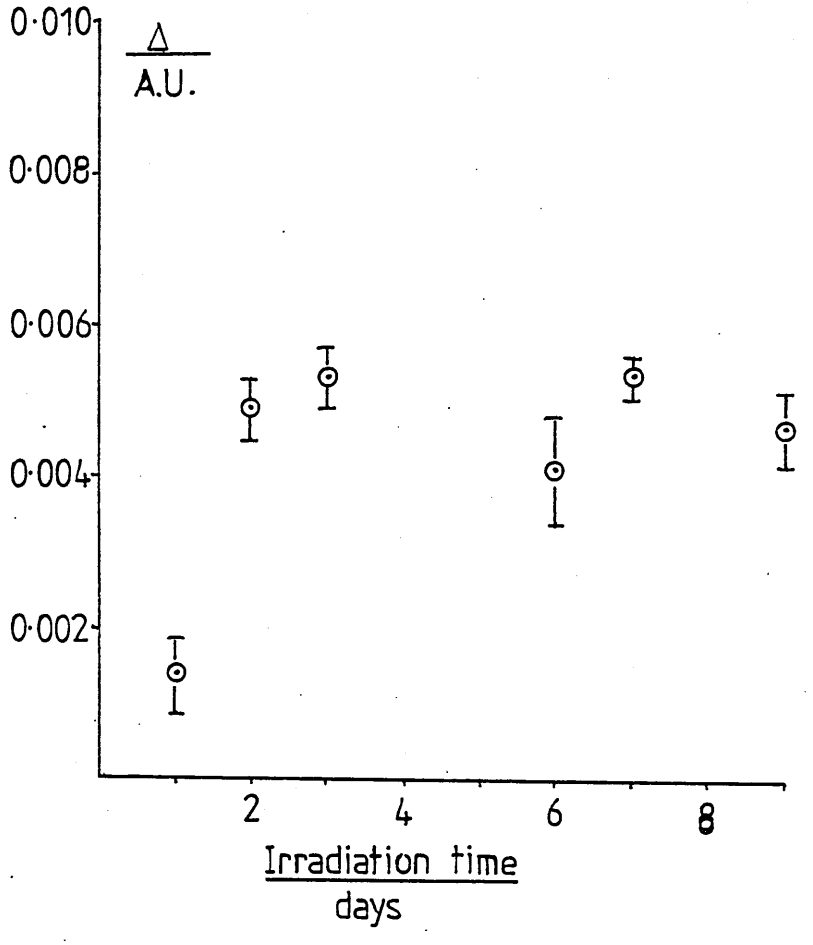

Figure 4.17 Changes in absorbance of methylene blue treated with $DyCl_3$ previously irradiated with fast neutrons, before and after re-oxidation.

Absorbance	Mean	Error
1. Irradiation time 24 hours		
Sample 0.653 0.651 0.649 0.649 0.649		
0.647 0.649	0.649_5	0.0006_9
ox'd 0.650 0.653 0.654 0.653 0.653		
0.652 0.653	0.652_5	0.0004_7
$\Delta = 0.003 \pm 0.0008$		
$\Delta_c = 0.002_5$		
2. Irradiation time 29 hours		
Sample 0.496 0.497 0.497 0.498 0.498	0.497_2	0.0003_7
ox'd 0.503 0.503 0.503 0.503 0.502	0.502_8	0.0002
$\Delta = 0.005_6 \pm 0.0004$		
$\Delta_c = 0.005$		
3. Irradiation time 46 hours		
Sample 0.603 0.601 0.601 0.601 0.602	0.601_6	0.0004
ox'd 0.608 0.607 0.609 0.609 0.608		
0.608 0.608	0.608_1	0.0002_6
$\Delta = 0.006_5 \pm 0.0008$		
$\Delta_c = 0.006_4$		
4. Irradiation time 69 hours		
Sample 0.493 0.493 0.493 0.493 0.493	0.493	0
ox'd 0.500 0.500 0.502 0.501 0.501		
0.500	0.500_6	0.0003
$\Delta = 0.0007_6 \pm 0.0003$		
$\Delta_c = 0.0006_8$		

Table 4.19 (a)

Absorbance	Mean	Error
5. Irradiation time 70 hours		
Sample 0.486 0.486 0.487 0.487 0.487	0.486_7	0.0002_4
ox'd 0.494 0.495 0.494 0.493 0.493	0.493_8	0.0003_7
$\Delta = 0.007_1 \pm 0.0004$		
$\Delta_c = 0.006_8$		
6. Irradiation time 99 hours		
Sample 0.531 0.530 0.529 0.534 0.534	0.531_6	0.001
ox'd 0.545 0.543 0.543 0.544 0.543		
0.545 0.543	0.543_7	0.0003_6
$\Delta = 0.012_1 \pm 0.001$		
$\Delta_c = 0.010_8$		
7. Irradiation time 144 hours		
Sample 0.529 0.529 0.529 0.529 0.530	0.529_2	0.000_2
ox'd 0.540 0.540 0.539 0.539 0.538		
0.539	0.539_2	0.0003_1
$\Delta = 0.010 \pm 0.0004$		
$\Delta_c = 0.009_8$		

Table 4.19 (b)

Absorbances of methylene blue treated with $DyCl_3$ previously irradiated with fast neutrons inside a wax moderator, before and after re-oxidation.

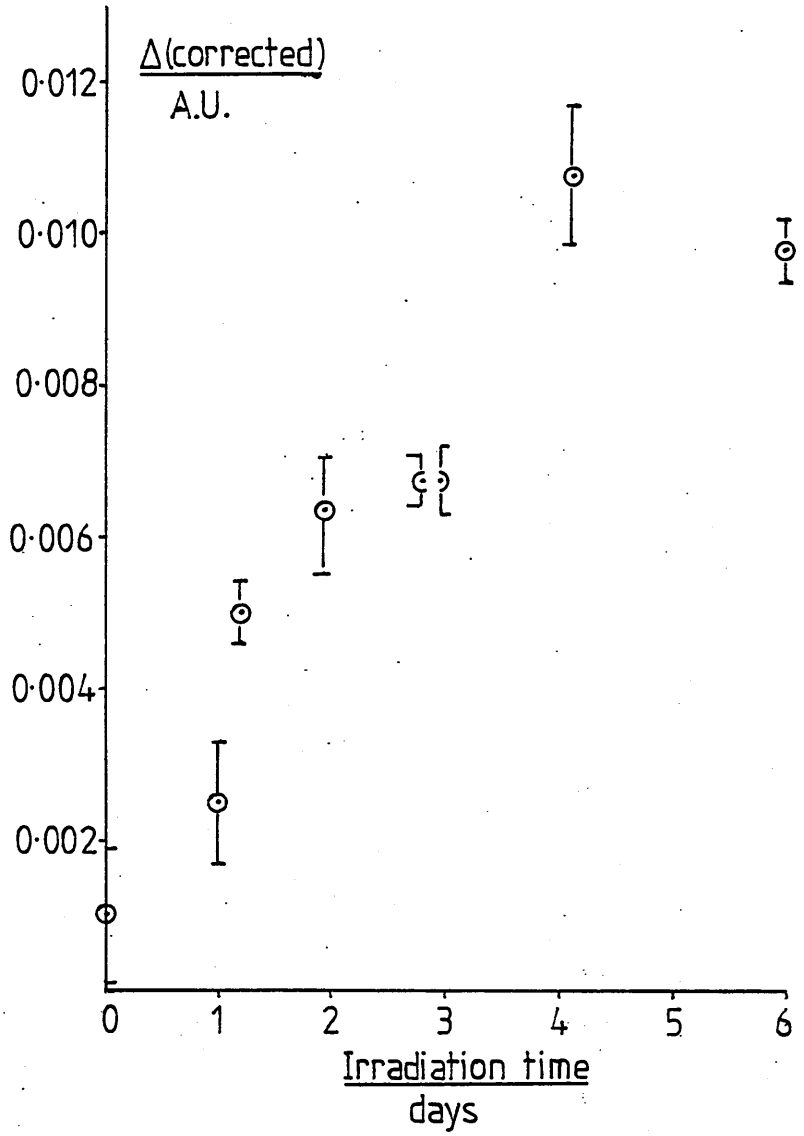

Figure 4.18

Changes in absorbance of methylene blue treated with $DyCl_3$ previously irradiated with fast neutrons inside a wax moderator before and after re-oxidation.

Absorbance	Mean	Error
Sample a $DyCl_3$ n dose (≡2 days)		
Sample 0.722 0.720 0.723 0.722 0.720		
0.722	0.721_5	0.0004_5
ox'd 0.724 0.726 0.726 0.726 0.726		
0.723	0.725_2	0.0004_9
$\Delta = 0.0037$		
$\Delta_c = 0.0041$ 0.0005		
Sample b $DyCl_3$ n dose (≡3 days)		
Sample 0.686 0.683 0.681 0.682 0.681		
0.684	0.682_8	0.0005_8
ox'd 0.690 0.692 0.689 0.688 0.687		
0.688	0.689	0.0006_7
$\Delta = 0.0062$		
$\Delta_c = 0.005_2 \pm 0.0006$		
Sample c $DyCl_3$ n dose (≡4 days)		
Sample 0.694 0.695 0.692 0.693 0.693		
0.694	0.693_5	0.0003_9
ox'd 0.699 0.701 0.699 0.698 0.700		
0.701 0.099	0.699_6	0.0004
$\Delta = 0.0061$		
$\Delta_c = 0.004_2 \pm 0.0004$		
Sample d $DyCl_3$ n dose (≡6 days)		
Sample 0.663 0.663 0.660 0.663 0.665	0.662_8	0.0006_3
ox'd 0.672 0.671 0.671 0.672 0.671	0.671_4	0.0002_4
$\Delta = 0.0086$		
$\Delta_c = 0.005_4$ 0.0005		

Table 4.20 (a)

Absorbance						Mean	Error
Sample e	$DyCl_3$	n dose (≡8 days)					
Sample	0.690	0.690	0.689	0.691	0.689	0.689_8	0.0003_7
ox'd	0.697	0.698	0.697	0.697	0.695		
	0.698					0.697	0.0004_1
			$\Delta = 0.0072$				
			$\Delta_c = 0.0077 \pm 0.0004$				
Sample f	$DyCl_3$	n dose (≡12 days)					
Sample	0.732	0.733	0.731	0.733	0.730	0.731_8	0.0005_5
ox'd	0.742	0.744	0.742	0.741	0.741	0.742	0.0005_5
			$\Delta = 0.011$				
			$\Delta_c = 0.0084 \pm 0.0006$				

Table 4.20 (b)

Absorbances of methylene blue treated with $DyCl_3$ previously irradiated with fast neutrons from a 150 keV generator, before and after re-oxidation.

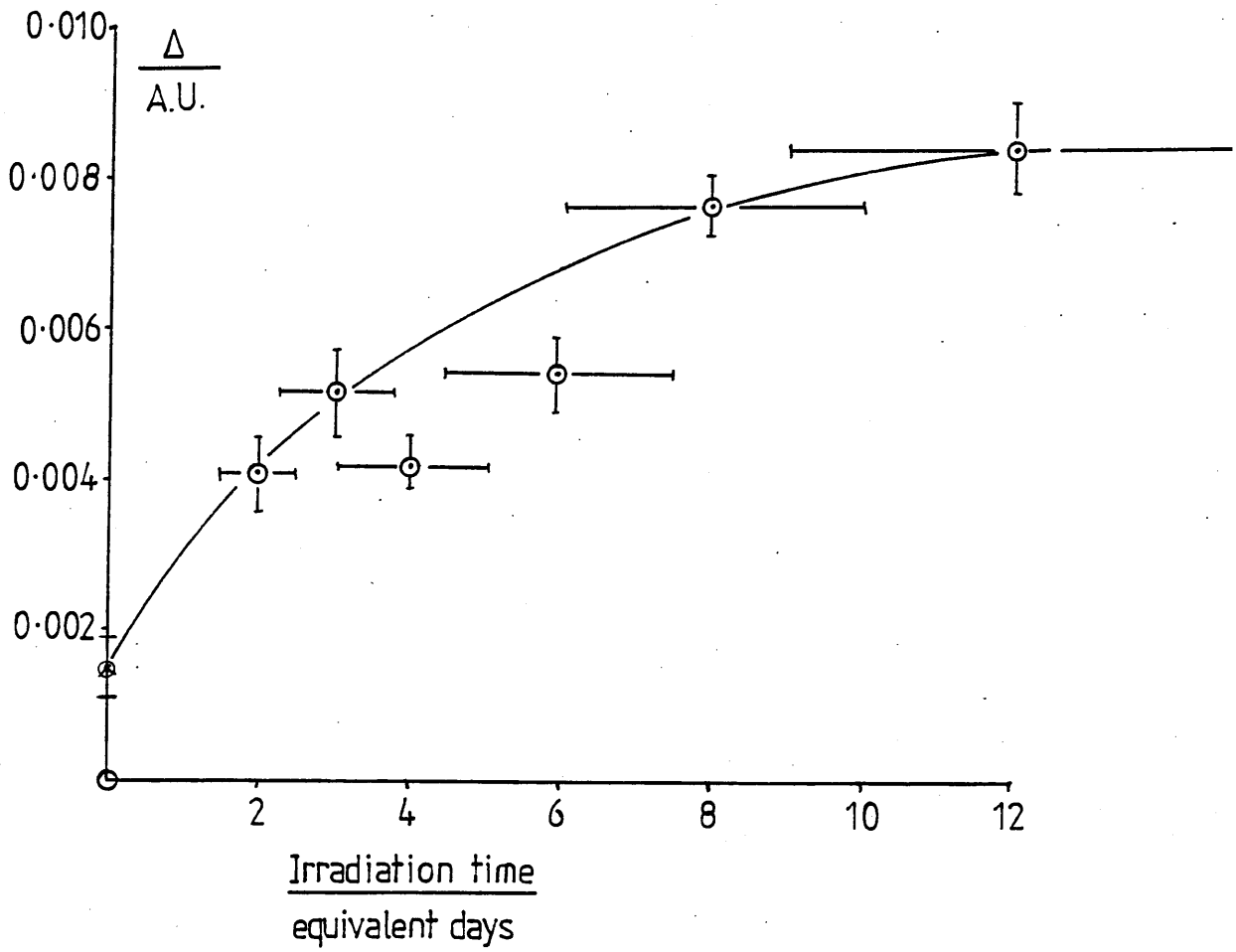

Figure 4.19

Changes in absorption of methylene blue treated with $DyCl_3$ previously irradiated with fast neutrons from a 150 keV generator, before and after re-oxidation.

	Total activity of sample (A) (cpm)	Excess counts as first ppt (E) (cpm)	$\frac{A}{E}$ x 100
1	127 999	5760	4.5
2	97 558	110	0.1
3	109 532	9016	8.2
4	127 933	14081	11.0
5	123 178	-905	-0.7
6	125 812	3604	2.9

Mean value of $\frac{A}{E}$ x 100, samples 1,3,4&6

6.7 ± 2.2%

Mean value of $\frac{A}{E}$ x 100, samples 2&5

(oxidised before analysis)

-0.3 ± 0.3%

Table 4.21

Percentage of total activity precipitated on barium sulphate from solutions of reactor irradiated Eu_2O_3 dissolved in hydrochloric acid

Figures are from Table 4.5

Europium	
Sample	Δ
d	0.013
e	0.015
f	0.0074
g	0.0088
h	0.0092
Total	0.534
Mean Δ	0.0107 ± 0.0014
Dysprosium	
a	0.007
b	0.012
c	0.010
d	0.0098
d	0.0072
e	0.0096
f	0.011
g	0.004
h	0.0052
i	0.0075
j	0.0084
k	0.0126
Total	0.1043
Mean Δ	0.0087 ± 0.0008
Blank	
a	0.0021
b	0.0026
c	0.001
d	0.0004
e	0.002
f	-0.0002
g	0.002
h	0.002
Total	0.0119
Mean Δ	0.00149 ± 0.0003

Table 4.22
Mean absorbance differences from Tables 4.12, 4.13 and 4.14.

Europium chloride			
Sample	Total count cpm	First count excess cpm	$\frac{F}{T}$ x 100
1	6636	30	0.45
2	9519	34	0.36
3	7130	20	0.28
4	7892	21	0.27
5	6187	14	0.23
6	8955	0	0.00 BLANK
7	7203	0	0.00
8	8994	0	0.00 BLANK
Dysprosium chloride			
1	10252	16	0.16
2	10767	30	0.28
3	8581	60	0.7
4	11276	12	0.11
5	6193	29	0.47
6	9565	17	0.18
7	11441	0	0.00 BLANK
8	12792	4	0.03 BLANK

Mean values for % Ln^{2+} found by co-precipitation

Europium chloride	(including 7)	0.27 ± 0.06%
	(excluding 7)	0.32 ± 0.04%
Dysprosium chloride		0.32 ± 0.08%

Table 4.23

Excess counts found on first precipitates of barium sulphate from europium and dysprosium chloride samples. Figures are from tables 4.8 and 4.9.

Calculation of % divalent lanthanide from observed changes in absorbance

1.000 AU 5.084×10^{-5} mol Ln^{2+} (Table 4.10)

RMM $EuCl_3$ 258.5

$DyCl_3$ 269.0

Hence 1.000 AU corresponds to

$EuCl_3$ 13.14 mg

$DyCl_3$ 13.68 mg

However in 50% alcoholic solution the slope of the calibration line is increased by $\frac{0.829}{0.690}$ or 1.2 (Table 4.11)

So in these analyses,

1.000 AU corresponds to the reduction of

$EuCl_3$ 10.95 mg

$DyCl_3$ 11.40 mg

Flux	Δ (mean) A.U. at equilib.	Δ -b mean blank 0.0015 A.U.	Ln^{3+} equivalent mg	atom % Ln^{2+}	
Mixed	0.0107	0.0092	0.10	0.10	europium
Mixed	0.0087	0.0072	0.082	0.082	dysprosium
Fast (i)	0.0053	0.0038	0.043	0.043	dysprosium
Fast (ii)	0.010	0.0085	0.096	0.096	dysprosium
Fast (iii)	0.008	0.0065	0.074	0.074	dysprosium
Fast (MEAN)				0.071 ± 0.013	

Table 4.24

Comparison of mean values of % reduction from Ln^{3+} to Ln^{2+} produced, by various methods of neutron irradiation.

4.6 SUMMARY OF RESULTS

	Element	Neutron flux	Atom % Ln^{2+}
(a)	Eu	Mixed (wax reflector)	0.10
(b)	Dy	Mixed (wax reflector)	0.083
(c)	Dy	Fast (no reflector)	0.043
(d)	Dy	Fast (wax reflector)	0.096
(e)	Dy	Fast (15 MeV generator)	0.074

Table 4.25 Summary of results obtained from methylene blue analyses

CHAPTER FIVE

Discussion

5.1 Electrophoresis

$Eu^{2+}(aq)$ ions are oxidised by a variety of reagents, including molecular oxygen. Although the ion is the most stable of the two-valent lanthanides, Meier and Garner [32] found that despite their careful working in deoxygenated solutions, a significant fraction of their $Eu^{2+}(aq)$ became oxidised even in the course of transfer from one vessel to another. This makes it virtually certain that despite my own efforts to use de-oxygenated solutions and to flood the working volume of the apparatus with nitrogen, the best which could be expected from the analyses would be a significant fronting of each Eu(II) band in the electrophoretograms.

Because the work was carried out in hydrochloric acid solution and using chloride salts, the electron interchange between the two species, known from Meier and Garner's work to be catalysed by chloride ion, is likely to be important. From their kinetic studies we may estimate the half-time of the exchange reaction in the solutions used for electrophoresis; it would be the order of 1 000 minutes. Each analysis was over in less than fifty minutes; the fraction of ions exchanging in any one minute is therefore only small. But any one ion would have a finite chance of changing its charge during this time, which would lead on the one hand to fronting of the Eu(II) band as divalent ions increased their charge and accelerated, and tailing of the Eu(III)

band as trivalent ions lost charge and slowed down. The visualising reagent (sodium tungstate) is highly sensitive to traces of europium and would show the fronted and tailed portions of the bands readily.

To make some assessment of the importance and effect of the interchange, a computer program was written to simulate the course of an electrophoresis. The program is described and listed in Chapter Two and Table 2.6. The modelling employed is crude in two respects; the ratio between the fast moving and slow moving ions is set at 2:1, whereas in practice the ratio would be more nearly 1:1.1; and the number of steps in the stochastic calculation is small. The effect of the former is greatly to exaggerate the separation of the two ionic species; on a 40 cm paper the computer generated separation is 20 cm whereas in practice it would be only 4 cm. To compensate for this in the program, a rather larger fraction of each ionic species is imagined to exchange in any one block of time than is predicted by Meier and Garner's study.

The results of the computer analysis show that with the Eu(III)/Eu(II) ratio biassed heavily towards Eu(III), the first result of interchange is a broadening of the front edge of the Eu(II) band into a generalised low level concentration of europium extending right up to the major (Eu(III)) band, there being no separation between the two. At very much lower values of the exchange probability the Eu(II) band retains its identity above this continuum, but whether to a sufficient extent to be differentiated from it by the tungstate cannot be decided. This would be powerfully

influenced by the degree of oxidation taking place. At improbably high values of the exchange probability, a false intensification of the continuum is seen which would give the appearance of a substantial concentration of Eu(II) where none in fact existed. This, however, could only come about in much more concentrated solutions than were used for the electrophoresis.

This model, however, is grossly oversimplified and cannot explain the observed effects. The model allows for no stochastic broadening of the advancing bands; so that once an ion has travelled to a part of the paper from which the alternate species is absent, no further interchange can occur. From that point, the two species would act independently of each other, which the model does not allow.

My inability to separate the two species is therefore best attributed to oxidation of Eu(II) by the air.

5.2 Adsorption on barium sulphate

5.2.1 General adsorption behaviour of lanthanide ions

The results shown in Figure 4.5 indicate that there is a genuine difference between the first precipitate of barium sulphate created in the presence of irradiated lanthanide ions, and subsequent precipitates, since the activities of the second and subsequent precipitates lie along a quasi-linear graph, whilst the activity of the first precipitate departs markedly from this line.

This makes it possible, by extrapolation, to determine the contribution made to the first activity by the species responsible for the later activity, and hence the activity due to the extra adsorbed ions on the first precipitate.

These are unlikely to be other than Eu^{2+}, since lanthanide ions of lower charge are unknown in aqueous solution. This is confirmed by the behaviour of samples discussed in the next section. However, quantitative investigation shows that the apparently linear graph must (as predicted by the adsorption isotherm) be part of a shallow curve whose gradient gradually decreases. Extrapolation of the 'line' to the X - axis shows that another seven or eight precipitations would be sufficient to remove all activity from the solution, were the same rate of removal maintained. This would correspond to an activity remaining in the solution after the sixth precipitate of about 73 000 counts per minute. In fact, the remaining activity was found to be some 300 000 counts per minute, which would need many more than eight precipitations for its removal.

This notwithstanding, the approximation to linearity is sufficiently good that it may be used to confirm that an excess of counts exists on the first precipitate, and to enumerate the excess. In subsequent experiments, any errors introduced by the use of the linear approximation are small by comparison with those introduced by the random nature of the decay and the experimental uncertainties inherent in the method.

5.2.2 The effect of oxidation prior to adsorption

The experiments in which only the activity on the first and second barium sulphate precipitates was measured demonstrated that under normal circumstances, the activity on the first was in excess of that on the second by an amount greater than the combined uncertainties in the two measurements.

But if the lanthanide solution was treated with aqueous bromine prior to analysis, the activities of the first and second precipitates became equal within fine limits.

This supports the hypothesis that the excess activity on the first precipitate is due to Eu^{2+}, since these ions would readily be oxidised by the bromine solution:-

$$2Eu^{2+} + OBr^{-} + Br^{-} + 2H^{+} \rightarrow 2Br^{-} + H_2O + 2Eu^{3+}$$

The reaction is not instantaneous, since it does not come about by direct electron transfer; but it is complete within a few minutes. Since the hydrochloric acid used to dissolve the europium oxide is in excess, the addition of small quantities of bromide ion is unlikely to affect the course of the subsequent precipitations.

The existence of Eu^{2+} ions in the irradiated europium oxide is not unexpected. Apers (loc.cit.) found that samples of holmium oxide, exposed to gamma radiation either from a ^{60}Co source or as part of a reactor bombardment, can contain up to 5% of Ho^{2+}, analysed in aqueous solution. The Eu_2O_3 lattice may very well react to gamma irradiation in the same way as Ho_2O_3 and the Eu^{2+} so produced would

be more stable in solution and hence easier to detect. The importance of the experiments described above is that they validate a quantitative method of determining the amount of Ln^{2+} present in a mixture of Ln^{2+} and an excess of Ln^{3+}, which is applicable (provided that a suitable excess of inactive Ln^{3+} ion is maintained as a holdback carrier) to a wide range of ionic concentrations.

5.2.3 Irradiation in conditions of very low gamma flux

The results show that in eleven out of twelve cases, samples of europium chloride and dysprosium chloride, irradiated in the mixed flux reactor described in Section 7.8 and analysed by the method of subsequent precipitations, contained a species which was preferentially adsorbed onto the first precipitate. When the samples were oxidised before analysis, no such evidence was found. This is the same behaviour as was found in the europium samples irradiated in the much higher flux of the Universities Research Reactor, and can be ascribed to the same cause - the formation of Eu^{2+} and Dy^{2+} ions, respectively, in the irradiated lattices. The activity produced is as high as the quantity of halide and the intensity of the neutron flux permit.

The effect was thought to be due to a consequence of the (n,γ) reaction and so the time of irradiation was limited to that which produced saturation activity in the samples. In practice this meant an irradiation of some eighteen hours; in the light of later results this is the minimum of time after which any effect might be found.

The measures taken to restrict oxidation of the reducing species by atmospheric oxygen could not be expected to be wholly successful. However, there is no evidence that under these experimental conditions the half-reaction time for this oxidation was so short as to prove a limitation. The possibility does exist that removal of Ln^{2+} by oxidation goes on at such a rate that it compensates the expected asymptotic decay of the adsorption curve producing, fortuitously, the observed linear effect. The activities produced are too low to allow any proper comparison of the europium and dysprosium cases - oxidation would be expected to be more substantial for the latter - but there is sufficient linearity evident in both systems for this hypothesis to be unlikely.

No attempt was made to measure the reaction half-lives of the reduced species.

Although these results encourage the belief that the irradiation of lanthanide halides by neutrons produces reduced species in the crystal lattices, and that these reduced species have at least some stability in deoxygenated water, three objections can be offered.

Firstly, the method of analysis is previously untried. Despite the experiments discussed in Sections 5.2.1 and 5.2.2 which purport to validate the method, it must be viewed with some caution.

Secondly, Apers (on the basis of re-irradiation experiments described in reference 24) showed that in the case of

holmium, the reduction found after reactor irradiation was due to interaction with the gamma flux rather than to the (n,γ) reaction.

Thirdly, if the observation of Ln^{2+} ions is valid, the method offers no distinction between two possibilities. The reduction may be a consequence of recoil subsequent to the absorption of thermal neutrons or it may be a bulk effect taking place throughout the sample independently of the activation step.

It was to resolve the first of these that a second method of analysis for reduced species was sought. As a result of chance observations made during the use of this second method, experiments resolving the second and third difficulties were made.

5.3 Confirmation of the existence of reduced species.

5.3.1 Although a number of precautions were taken to remove the lack of precision from the methylene blue analyses, blank experiments continued to show an uncertainty varying from zero up to 0.002 units of absorbance. The change was always in a negative sense, and the instrument used gave readings to 0.001 units; the blank response is therefore taken to mean that there is an uncertainty in the absorbance of the re-oxidised dye. The maximum value of this uncertainty is 0.002 units. It may be related to the effect found in the presence of EDTA, discussed in Section 3.5.2.

Each of the solutions tested, unless they were deliberately oxidised before analysis, showed a reduction in the

concentration of methylene blue and hence the presence of a reduced species in the irradiated lattices. Oxidised solutions showed a reduction in methylene blue absorbance no larger than that found in the blank experiments. Thus these results qualitatively verify the findings of the previous experiments, that a reduced species is present in the irradiated lattices.

Hacskaylo's observation[13] of free electrons in an irradiated sodium chloride lattice does not affect this suggestion. Free electrons are not adsorbed onto barium sulphate and even if present would not affect a Geiger Muller counter. Thus they cannot account for the results discussed in 5.2.3. Nor can electrons be responsible for the reduction of the methylene blue, since for every free electron which might be produced in the lattice, a free chlorine atom would also exist. The reducing action of the one would be exactly compensated by the oxidising action of the other; the net effect would be zero.

Quantitatively, there is a measure of agreement between the two sets of analyses. The precipitation analyses indicate the presence of 0.3% of Ln^{2+} in each lattice investigated; the methylene blue analyses, a little less than 0.1%. Much of the difference may be ascribed to an experimental error. The water used in the analyses was deoxygenated but saturated with nitrogen. It was assumed that since on mixing this water with alcohol to prepare the diluent for the analyses there was a substantial evolution of dissolved gas, the resulting mixture would contain a negligible concentration of oxygen. It was not until after the completion of the

analyses that investigation of the efficiency of a new type of oxygen sensor called this assumption into question. The solubilities of oxygen and nitrogen in a range of solvents have been determined by Tokunaga [36] who found that at 20 °C in a mixture containing 50% mole fraction of ethanol, Ostwalds's coefficient for oxygen is close to 0.1; calculation shows that in the volume of solvent used this quantity of oxygen would correspond to the reducing action of a further 0.1% of divalent lanthanide. When this is taken into account the correspondence between the two analyses becomes close.

Had the observed reduction been produced by the (n,γ) reaction, the total percentage of material reduced would have been very small, and confined to the active atoms. The substantial effect found indicates that the reduction is a bulk effect, revealed by the precipitation analyses only because the reduced ions in the lattice are of the same nuclear species as their parents and hence are activated in exactly the same way. Therefore these results strongly suggest that the reduction is a consequence of direct collisions between neutrons and ions in the lattice, rather than an inelastic collision process.

5.3.2 Analysis in the presence of EDTA

It was observed by Apers that the reduced form Ho^{2+} appeared more stable in aqueous solution in the presence of EDTA. He ascribed this to 'secondary reactions preventing the re-oxidation of the reduced species'. Certainly the complex formed by Dy^{3+} and EDTA is very

stable, with K of the order of 10^{16}; that formed by Dy^{2+} is unlikely to be less stable by more than a few orders of magnitude. The greater stability of the Dy^{3+} complex would be expected to enhance the oxidation reaction by constraining the Dy^{3+}/Dy^{2+} equilibrium, removing the oxidised form to a greater extent than the reduced form. This notwithstanding, no reducing action could be found in the presence of EDTA which could not be ascribed to the incomplete reoxidation of the dye.

Had the reaction been due to free electrons acting as Dy^{3+}/e pairs, it was felt that some reduction would still have been found in these reactions since it has not been possible to find any reference to the adsorption or reaction of electrons onto EDTA. It is likely that such a reaction (of $e^-(aq)$ with EDTA) would be slower than its oxidation by water.

This therefore suggests that the application of the doctrine of nett effects is valid in this case and that the reduction is not ascribable to free electrons.

5.4 Fast neutron irradiations

If the (n,γ) process has no effect upon the valency state of the Ln^{3+} ions then exposure to a flux devoid of low energy neutrons should produce the same effects as hitherto seen. In the first trial, made by standing the neutron source directly upon the samples irradiated, the effect is still found but its magnitude is reduced somewhat. However, after two or more days irradiation, the reduction of Ln^{3+} to Ln^{2+} is more than three times the 'blank' readings, which confirms

that fast neutrons at least are active in this respect.

This method of activation does not duplicate the conditions in which earlier experiments were performed. In the second series of experiments, with the samples inside the moderator but also inside a shield opaque to thermal and near epithermal neutrons, the fast neutron flux has the same intensity as in the earlier mixed-flux work. This time the magnitude of the observed effect is comparable with that found in mixed-flux experiments. Exact comparison is made difficult by an unexplained uncertainty in the magnitude of the effect in any one observation. The results (shown in Figure 4.18) do not show a smooth variation with time; any one result deviates from the probable curve by up to twice the estimated experimental error. By inspection of the curve, the maximum effect may be estimated to lie between 0.008 and 0.010 absorption units. The mean value for dysprosium chloride samples in the mixed-flux experiments was 0.008 absorbance units. Within the limits of the experimental variation, therefore, the postulate that the effect is due to direct collisions with fast neutrons receives some confirmation.

The difference between the results obtained by irradiation inside and outside the moderator is ascribed to enhancement of the fast neutron flux emitted by the source, by scatter from moderating material lying close to the source. Scatter will take place at the carbon atoms of the wax as well as at the hydrogen atoms; the average angle of scatter even from atoms as light as carbon is nearly 87 ^{o}. Thus a significant flux will be reflected from the moderator which

has not suffered enough collisions to leave the 'fast' range of energies, and the equilibrium level of reduction is accordingly raised.

5.5 Irradiation by neutrons of different origin

The experiments performed using fast neutrons of entirely different origin to those of previous work offers further confirmation of the fast neutron postulate. The total neutron dose to which the samples were subjected was calculated to be near that received in earlier work; the magnitude of the observed effect has the same maximum value (at or near 0.008 units of absorbance) and is achieved over the same range of neutron doses, with samples of equivalent size. Had the effect not appeared in these experiments, had it been of a different magnitude or achieved by using a significantly different neutron dose, then previous conclusions must have been called into question. The correspondence between the different experiments is not a complete proof of the origin of the effect, but constitutes at least a substantial probability that the explanation previously advanced, is valid.

5.6 The effect of associated radiation

In no case was the neutron dose delivered in the total absence of gamma radiation. This is known from Apers' work (loc.cit.) to produce reduction in a lanthanide lattice. However, when subjected to gamma irradiation the samples showed no effect discernable above the 'blank' level unless the dose was delivered in a relatively short time, when the effect could just be noticed. Even in these circumstances

it did not approach the magnitude observed in neutron irradiations.

5.7 The extent of the induced reduction

The extent of the reduction in these experiments with dysprosium and europium is less than was found by Apers & de Block in their work with holmium. Moreover, although the stabilities of the aquated divalent ions are substantially different, lying in the order $Eu^{2+}(aq) > Dy^{2+}(aq) > Ho^{2+}(aq)$, the reduction which I have found has been to all intents and purposes the same, for dysprosium and europium.

The form of the curve obtained when plotting the observed reduction against the time of irradiation (Figures 4.18 and 4.19) suggests that an equilibrium is reached between the production of the reduced form and its decay. In the flux available, this equilibrium was established at about 0.1% reduction after three days.

The reduced form is produced by collisions between neutrons and nuclei in the crystal lattice; if the number of neutrons incident upon the target in one second is ϕ, then the rate of production of Ln^{2+}, $\underset{\rightarrow}{R}$, is given by

$$\underset{\rightarrow}{R} = k\phi$$

If, as seems likely, the oxidative decay is of the first order with respect to Ln^{2+}, then the rate of decay, $\underset{\leftarrow}{R}$, is given by

$$\underset{\leftarrow}{R} = k'(N)$$

where N is the number of Ln^{2+} ions present at any time. At equilibrium these rates are equal, whence

$$\frac{k'}{k} = K = \frac{N}{\phi}$$

Evaluating this expression we obtain

$$K = 9 \times 10^{11}$$

Aper's irradiations were done in the pile; the available flux was therefore, by comparison, very large. Although the equilibrium constant for gamma induced change will not equal that for neutron induced change, his enhanced reduction may be understood.

For a variety of reasons, some of the irradiated samples could not be analysed until several days had elapsed after they were removed from the source. The extent of the reduction does not seem to be affected by the delay, which suggests that the decay process - the annealing - must itself be triggered by exciton interaction and cease when this ceases. No evidence is offered for the mechanism of this radiation annealing, though it has been suggested [37] that it proceeds by a wholly thermal process.

5.8 The efficiency of the reaction

5.8.1 The collision frequency

Consider a flux of n neutrons/sec/cm^2, incident upon a target of effective cross section σ cm^2 per particle. Let the number of moles of target present be m

Then the collision rate between dysprosium atoms in the target and incoming neutrons is given by

Rate $mn\sigma A$

where A is Avogadro's constant.

For the materials under discussion we may take

m as 3.7×10^{-4} mol

σ as 6×10^{-24} cm^2

n as $2.2 \times 10^6 \times 0.1224/3.8$ n s^{-1} cm^{-2}

i.e., 7.09×10^4 n s^{-1} cm^{-2}

(the factor 0.1224 is the geometric factor; the area of the target is 3.8 cm^2)

whence; Rate 94.8 collisions/second

5.8.2 Sources of deposited energy

1 Elastic scatter will occur at both dysprosium and chlorine atoms. The fraction of energy transferred from the incident particle will, on average, be one half of the maximum possible transfer, i.e.,

fraction transferred $\frac{2A}{(A+1)^2}$

where A is the mass number of the target nucleus.

For dysprosium (A=164) this amounts to 0.0121

for chlorine (A=35.5), 0.0533

2 Inelastic scatter will contribute two energy components; one when the neutron enters the target, and one when it leaves. The vectorial addition of the two recoil momenta together produce an effect not greatly different from the elastic scattering case. The actual values differ

with neutron energy and with the nature of the target, but the variations are gradual and available data suggest that in this region inelastic scatter adds roughly 75% the contribution of the elastic scatter.

3 Radiative capture makes only a small contribution to the overall energy balance, the majority of this being the recoil which accompanies the initial absorption of the neutron by the target nucleus. The fraction of energy thus deposited is given by

fraction transferred $1/(A+1)$

where A has the same meaning as previously

For dysprosium this amounts to 0.0061

for chlorine, 0.0274

However, the cross sections for these processes are of the order of millibarns only, thus contributing some ½% to the total number of collisions.

4 Emission of charged particles

Although cross sections for the (n,α) and (n,p) reactions with chlorine nuclei are not precisely defined, they are both likely (for reaction with 5 MeV neutrons) to be about 100 mb. Those for reaction with the much heavier rare earth nuclei may be ignored. For 35.Cl, the reactions are highly exoergic, the (n,α) reaction liberating some 0.94 MeV per event, and the (n,p) reaction 0.62 MeV per event. For 37-Cl the reactions are endoergic, the figures being 1.25 and 3.97 MeV per event; but the isotopic abundance of this nuclide is only 24.5%

More importantly, the range of α-particles and protons in the target is very small, and they will therefore deposit all their kinetic energy within the target lattice. This will equal, to a good approximation, the energy of the original neutron, here assumed to be 5MeV.

5 (n,2n) reaction

If, following inelastic scatter, the nucleus is left with sufficient excitation energy, then a second particle may be emitted. This will usually be (because of the Coulomb barrier) be a neutron. For the reaction to take place the initial neutron energy must be in excess of 8 MeV; relatively few such particles are available in the neutron spectrum of the source and the process may be ignored.

5.8.3 Total energy deposited

1 Elastic and inelastic scatter by dysprosium.

The energy deposited is given by

$$E = nma.\ \sigma\ .fE'$$

where f is the fraction of the incident neutron energy deposited in the target

and E' = 5MeV, the energy of the incident neutron.

The factors may be evaluated:

$mnA.\sigma = 94.8$ events/sec (see 5.8.1)

2/3 of the recoils have f = 0.0121 (elastic scatter)

1/3 of the recoils have f = 0.0121 x ¾ (inelastic scatter)

whence f = 0.0111

$$E = 5.26 \times 10^{6} \text{ eV/sec}$$

$$= 4.55 \times 10^{11} \text{ eV/day}$$

2 Similarly for chlorine, for which $\sigma = 3 \times 10^{-24}$ cm^2

Since the chloride has the formula $DyCl_3$

$mnA\sigma = 142.2$ events/sec

f (similarly calculated) = 0.0489

$E = 3.48 \times 10^7$ eV/sec

$= 3.00 \times 10^{12}$ eV/day

3 From charged particle emission

When reactions with both 35-Cl and 37-Cl are taken into account, the overall reaction may be shown (using the data in 5.8.2.4) to be slightly endoergic; the calculated value for the change is 0.135 MeV/event. The energy deposited is given by

$$E = mnA.\sigma_{cp} .E'$$

where σ_{cp} is the sum of $\sigma_{(n,p)}$ and $\sigma_{(n,\alpha)}$

E' is the energy deposited in one event taking $\sigma_{(n,p)}$ and $\sigma_{(n,\alpha)}$ each to be 100mb and E' to be (5-0.135)MeV

$E = 4.61 \times 10^7$ eV/sec

$= 3.98 \times 10^{12}$ eV/day

The contributions from other processes are small by comparison; the total energy deposited is therefore

$(4.55 \times 10^{11}) + (3.00 \times 10^{12}) + (3.98 \times 10^{12})$ eV/day

$= \underline{7.44 \times 10^{12} \text{ eV/day}}$

In arriving at this figure several assumptions have been made about the magnitude of partial cross sections in the various processes, and no claim to arithmetic precision can be made for the result. Nonetheless it may be regarded as better than an 'order of magnitude' calculation and seems unlikely to be in error by more than 10%.

5.8.4 Efficiency of conversion

From Figure 4.18 we may estimate that over the course of the first day of an irradiation, the extent of the induced reaction is that which produces a value of 0.005 units. This corresponds to a reduction from Ln^{3+} to Ln^{2+} of some 0.07%.

Since the samples were each 3.7×10^{-4} mol, this means that in the one day

$(3.7 \times 10^{-4}) \times (6.022 \times 10^{23}) \times (0.07/100)$ ions were reduce

1.56×10^{17} ions were reduced.

The collision frequency with dysprosium ions, $(94.8 \times 8.64 \times 10^{4})$ collisions per day, is substantially less. The ratio is

$$\frac{1.56 \times 10^{17}}{94.8 \times 8.64 \times 10^{4}}$$

i.e., number ratio - 1.90×10^{10}

If the process involved in the reduction is assumed to be

$$2Ln^{3+} \rightarrow Ln^{2+} + Ln^{4+}$$

then the energy involved in the production of one Ln^{2+} ion would be the difference between the third and fourth ionisation energies of the species involved. For dysprosium, the values are [39,40] I_3 = 23 eV : I_4 = 41 eV. Each conversion would therefore (at worst) involve the absorption of 18 eV. This figure would be lowered by solvation effects within the lattice but could hardly fall below the value of the band-gap, which for these materials is approximately 10 eV.

To produce the observed reduction, taking the latter figure, would need 1.56×10^{18} eV/day. The ratio between this figure and the calculated deposited energy is

$$\frac{1.5 \times 10^{18}}{7.44 \times 10^{12}}$$

i.e. energy ratio - 2.02×10^{5}

The origins of these very high efficiency ratios may lie in a number of causes.

(a) The collision rate between neutrons and lanthanide nuclei may be much higher than postulated.
(b) The energy deposited at each collision may be much greater than postulated.
(c) The energy necessary to disproportionate lanthanide ions in the lattice may be substantially reduced by lattice solvation effects.
(d) Unsuspected secondary processes in the lattice may contribute to the energy balance.
(e) Energy gained through non-elastic processes may not be totally rejected.

I can make no judgement as to which factor is principally involved. The collision rate has been calculated on the assumption that each colliding neutron suffers only the one deflection, and is therefore a minimum value. However, the half thickness in this material is large, and the target was in the form of a thin layer. The chance of a deflected neutron continuing to travel within the target is therefore minimal. It is hard to see how solvation effects could reduce the reaction energies by the required ratio, especially as the majority of the ions are retained at all times within a solid lattice and cannot therefore, except within the miniscule hot zones surrounding each event, adjust their positions. There have been instances [35] in which fission, induced within irradiated lattices, has influenced the degree of retention of crystal defects induced by pile irradiation, but again the magnitude of the

effect did not approach that needed in this case.

Only one piece of evidence is available from this study which may aid discussion. Assuming that the extent of the observed reduction is correct, and adhering to the hypothesis that the annealing decay in the lattice is of the first order, we may say, if N be the number of reduced ions present in a sample at any one time;

$$\frac{-dN}{dT} = \lambda N$$

where λ is the rate constant for the decay process. This may be estimated; the equilibrium was observed to be established in some eight days; the half life for the decay must therefore be about two days. Since

$$t_{\frac{1}{2}} = 0.693/\lambda$$

$$\lambda = 4 \times 10^{-6} \ s^{-1}$$

If at equilibrium the number of reduced ions in a sample was about 0.1% of the total, this amounts to 2.2×10^{17} ions. We may therefore estimate $\frac{-dN}{dT}$;

$$\frac{-dN}{dT} = 4 \times 10^{-6} \times 2.2 \times 10^{17} = \underline{8.8 \times 10^{11} \text{ p.p.s}}$$

At equilibrium however, this must also be the rate of production of the reduced species. The collision rate is calculated to be 196 cps; the ratio between these two figures,

$$\frac{8.8 \times 10^{11}}{196} = \underline{4.5 \times 10^{9}}$$

is within a small amount of the number ratio previously calculated.

The only effect of this evidence is to simplify the problem; either the collision rate estimated is too low, or each collision initiates (in the manner of a chain reaction) a large number of conversions. The solution to this problem remains for the future.

CHAPTER SIX

Conclusions

From these experiments I conclude that:

6.1 Neutrons interact with triply charged ions of dysprosium and europium in a crystal lattice, reducing a significant fraction to the doubly charged state;

6.2 This interaction is largely with fast neutrons, rather than a result of any (n, γ) reaction with thermal neutrons or any subsequent nuclear change;

6.3 Both dysprosium(II) and europium(II) ions have a substantial lifetime in aqueous solution, provided that no fast oxidising species are present;

6.4 The mechanism of the reaction is such that some other lanthanide elements should behave similarly.

CHAPTER SEVEN

Practical details

7.1 Attempted electrophoresis

The apparatus used is shown in exploded section in Figure 7.1. It consisted of a DC power supply capable of delivering 3 kV, continuously adjustable, together with voltage and current meters. The potential difference was supplied through connecting leads terminating in platinum wires, into two perspex troughs. Between these was supported, at a proper height on wooden blocks, a sheet of ¼ inch plate glass 20 x 50 cm in size. The glass was cleaned and dried before each experiment.

Whatman 3MM chromatography paper was used throughout. A strip 2 cm wide and of sufficient length to dip into the troughs was soaked in the desired electrolyte and either drained or (more usually) placed between two sheets of blotting paper and rolled with a photographic roller until the mass of electrolyte held in the paper reached the desired ratio with the mass of the paper itself.[41] The substance for analysis was then streaked onto the previously marked origin in microgram quantities, using a finely drawn out capillary tube.

The prepared paper was then placed in contact with the glass sheet and it was ensured that both ends dipped into the troughs. Sufficient electrolyte was added to each trough to make contact with the paper. The paper was covered with a second glass sheet or, if temperature control was desired,

by a sheet of 12-gauge polythene on which rested a metal tray filled with mushy ice.

The voltage was then applied, adjusted to a suitable value between 20 and 50 volts cm^{-1}. Readings were taken of the voltage, current, and time. The current was maintained manually at a constant value in each run.

After a sufficient time (determined by trial and error) the paper was removed. Papers holding only iron ions were dried in a current of warm air from a hair drier, and sprayed with 10% solutions in water of potassium hexacyanatoferrate(III) to reveal Fe^{2+} and ammonium thiocyanate to reveal Fe^{3+}. Papers holding europium ions were hung for one minute before being dried, in a tall jar containing bromine vapour which served to oxidise Eu^{2+} to Eu^{3+}. Excess bromine was removed in the drying process. The europium was visualised by the method of Alberti and Massucci [42] in which the paper was sprayed with a 15% solution in water of sodium tungstate and viewed in u-v light. In these conditions, europium fluoresces with a vivid red colour, the detection limit being 0.001 γ.

7.2 Preparation of anhydrous lanthanide trichlorides

Suitable quantities of europium or dysprosium oxides were digested with a small excess of 6M hydrochloric acid. The oxides were either 'Specpure' (Johnson, Matthey & Co) or laboratory grade (B.D.H.). After complete solution (which takes several minutes to achieve) the solutions were evaporated gently until crystallisation was just beginning.

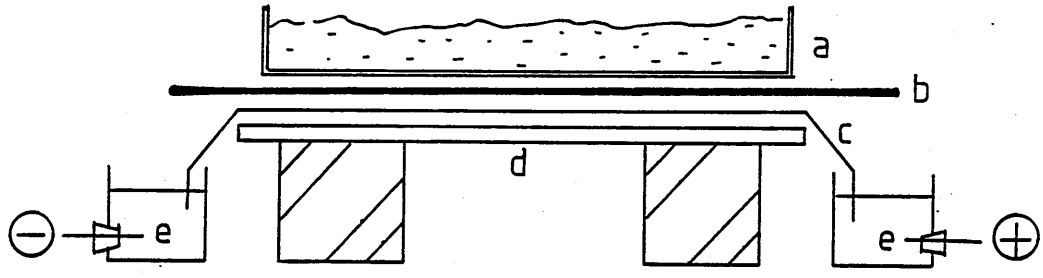

Figure 7.1

Exploded section of electrophoresis apparatus

a - metal tray filled with mushy ice

b - heavy gauge polythene sheet

c - experimental paper

d - plate glass sheet

e - electrolyte reservoir

The hot solutions were then transferred to the apparatus shown in Figure 7.2 and evaporation was continued until solid began to form. At this point sulphuric acid was admitted to the reaction flask, thus liberating hydrogen chloride, which blanketed the sample. Gentle evaporation was continued until all water was removed. The flow of hydrogen chloride was then increased and the solid sample was heated more strongly. At first it dissolved once more in its own water of crystallisation but this was soon removed, leaving an almost white solid. High temperatures were not needed; according to Wendlandt [43] water begins to be evolved at 90 ^{o}C and is virtually complete at 390 ^{o}C, though in the absence of the HCl blanket this latter temperature corresponds to the production of the oxychloride DyOCl. This is avoided in the presence of HCl gas.[44]

The solid mass was, at this stage, very hard. It could be crushed with a glass rod but any attempt to use a metal spatula resulted in contamination of the product. If however it was stored over phosphorus(V) oxide for 24 hours it fell to a powder which was easily ground, white, and free flowing. Each sample was tested by mixing a few milligrams with 1M hydrochloric acid; unless solution was complete and virtually immediate the sample was rejected.

7.3 Preparation of europium dichloride

Europium trichloride, prepared as outlined in Section 7.2, was converted into the dichloride by the method of Marsh. [45,46] A piece of sodium metal was freed from the oil in which it had been stored and about one gram was removed as thin slices. These were added, separately, to

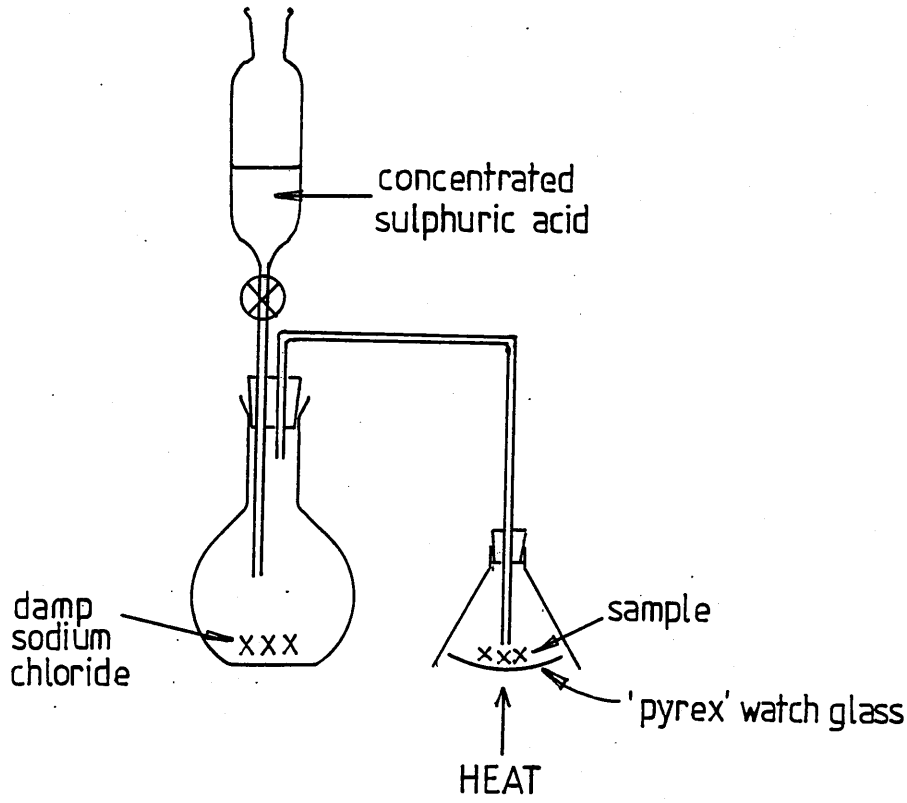

Figure 7.2

Apparatus for the dehydration of lanthanide trichlorides

100 g of mercury in an evaporating dish. The slices dissolved instantly and exothermically; the operation was carried out in the fume chamber. At this concentration, the amalgam remained liquid on cooling.

60 mg of europium trichloride were dissolved in 5 cm^3 of distilled water, and the solution was shaken in a separating funnel with 5 cm^3 of the amalgam, allowing europium to displace sodium from solution in the mercury. Meanwhile 5 cm^3 of concentrated hydrochloric acid were placed in another separating funnel under nitrogen and chilled in melting ice. When the acid became cold, the europium amalgam was run into it and shaken. The europium dichloride was precipitated as a white microcrystalline powder. Stored under nitrogen, it proved to be stable for long periods. If desired dry the powder could be gently warmed in a flow of nitrogen.

Any re-oxidation of the compound could be followed by viewing in UV light; Eu(III) compounds emit a dull red glow, whilst the fresh Eu(II) compound emitted a bright blue fluorescence which appeared to be quenched by moisture or the presence of Eu(III). This fluorescence was not enhanced by spraying with tungstate solution; instead heavy absorption of UV light took place, providing a useful method of distinguishing the two ions.

7.4 Formation of barium sulphate precipitates

This was performed in the absence of oxygen, in the apparatus depicted in Figure 7.3.

The apparatus was first flushed with dry nitrogen. The irradiated sample of lanthanide oxide, carbonate or chloride was quickly introduced into the mixing chamber, which was then replaced on the apparatus. Hydrochloric acid at a concentration of 1 mol dm^{-3} and containing 2.5 mg ml^{-1} of barium chloride was put into the left hand vessel, and sulphuric acid at a concentration of 1 mol dm^{-3} into the right hand chamber.

Taps A and C were opened, and the hydrochloric acid was gently boiled for 30 seconds as nitrogen passed through it. Tap B was then opened and the sulphuric acid was similarly treated. The taps B and C were then balanced so that as the liquids cooled, nitrogen flowed roughly equally through both. Cooling was allowed to go on until the hydrochloric acid was barely above room temperature. In this way it was ensured that both liquids contained very little dissolved oxygen.

Tap A was then closed and the nitrogen supply at a pressure of 4 lb/sq. inch was connected to tap C. By opening taps C and A, 2 cm^3 of hydrochloric acid were forced into the mixing chamber; C and A were then closed and the apparatus was agitated to assist dissolution of the lanthanide compound. Using the oxide it was found that complete solution came about in three minutes if the acid were just warm; but the agitation was continued for a further two minutes to ensure that no active solid remained. The nitrogen supply was transferred to B; taps B and A were opened and 2 cm^3 of sulphuric acid were forced into the mixing chamber.

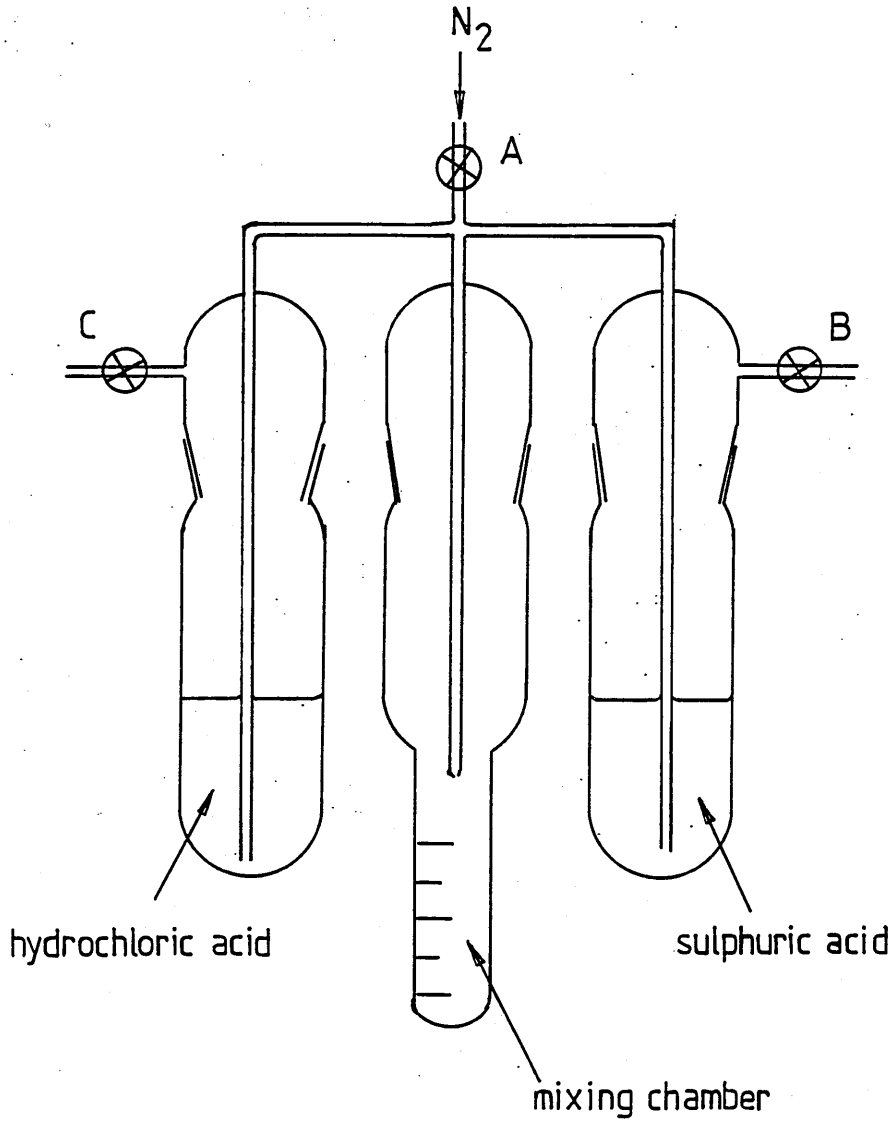

Figure 7.3

Apparatus for produce barium sulphate precipitates in the absence of oxygen.

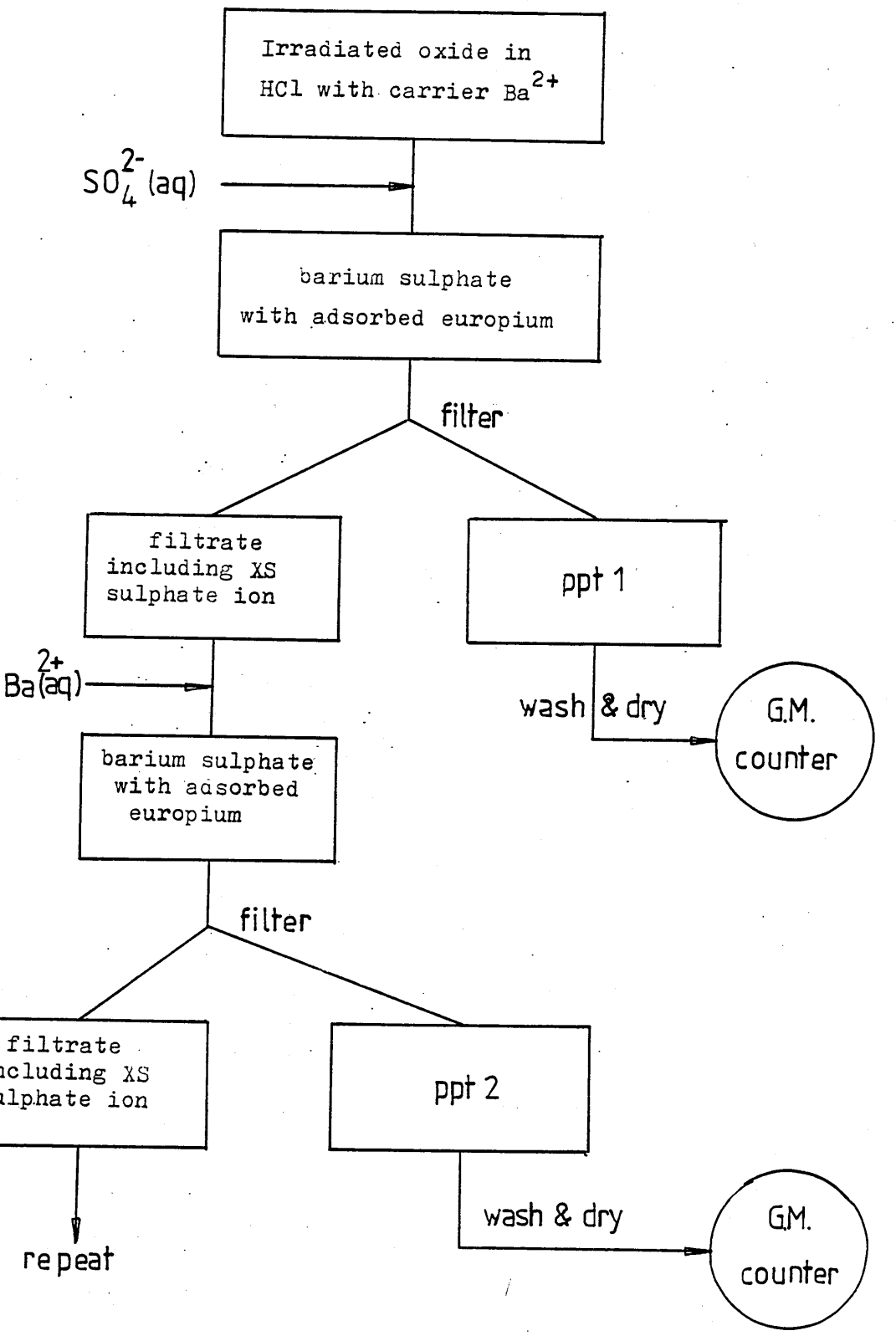

Figure 7.4

Flow diagram illustrating the production of barium sulphate precipitates.

Precipitation was not instantaneous and for reproducible results it was important that a fixed time should elapse between mixing the two solutions and filtering the precipitate. In these experiments the time was ten minutes. After this time the mixing chamber was removed and the suspension was filtered through Whatman GF/C paper in a chimney filter. The filter and receiving flask were previously flushed with nitrogen. Only very gentle suction was needed and a flow of nitrogen could be maintained through the chimney. The filtrate was removed for subsequent analysis, and the precipitate was washed with alcohol and acetone and dried under the lamp before being counted. It was found to be important that no alcohol or acetone be allowed to contaminate the filtrate; any such adulteration produced substantial and erratic changes in the counts obtained from subsequent precipitates.

A further 2 cm^3 of the de-oxygenated acid solution of barium ions was then added to the filtrate and the precipitation, filtration and counting stages were repeated. Up to six precipitates were produced in this way; the process is summarised in Figure 7.4.

7.5 Standardisation of Geiger-Muller counter

A flat bottomed 1" planchette was filled with a dilute solution of polystyrene in toluene, and the toluene was evaporated under the lamp. A weighed quantity of aged uranium oxide was finely ground, suspended in toluene, and added to the planchette. The toluene was again evaporated, leaving the oxide firmly cemented in place.

The planchette was then sealed by cementing an aluminium cover of surface density 28 mg cm^{-2} across the top. The mass of oxide included was 0.0402 g.

An end-window Geiger-Muller tube was connected to an EHT/scaling assembly; the tube was housed in a constant geometry lead castle which had been freshly washed with a dilute solution of EDTA to remove contaminants. The prepared source was placed in the castle in a position approximating to 2π geometry and a series of one minute counts were taken, each at a different operating voltage. The experiment was repeated without the source in place.

Each count was corrected for the dead time of the counter (electronically set at 100 μs) and the corrected values were plotted against the applied EHT. The slope of the curve was greater than expected; the optimum operating voltage was therefore found by calculating, for each value of the voltage, the quantity P, where

$$P = \frac{(s-b)^2}{b}$$

s is the count made with the source in place

b is the background count

The conditions are optimised when P is at a maximum. [47]

Voltage volts	Counts cpm	Corrected cpm	Backgd b cpm	$(s-b)^2/b$ cpm $x10^5$
440	0	0	0	-
450	3436	3455	14	8.46
460	3825	3825	15	9.18
470	4028	4055	16	10.2
490	4259	4289	18	10.1
510	4613	4648	21	10.2
530	4941	4982	21	11.7
550	5107	5150	24	10.9
570	5746	4801	31	10.7
590	6805	6883	46	10.2

Table 7.1

Response of Geiger Muller counter to varying applied voltage.

Uranium oxide source, filtered by 28 mg cm^{-2} aluminium

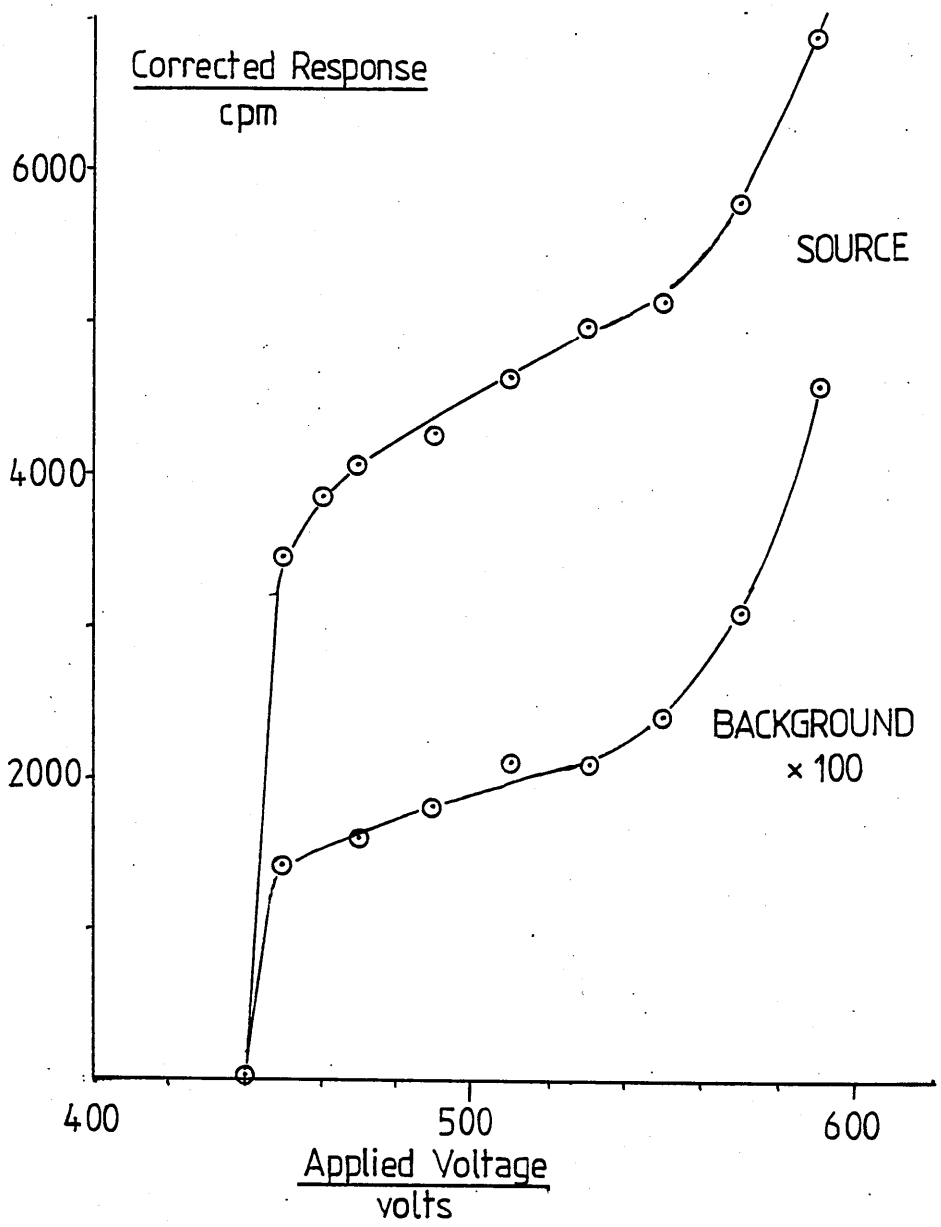

Figure 7.5

Response of Geiger Muller Counter

```
  5   REM--Copyright M. TAYLOR 1982
 10   CLS: MODE 6
 15   REM--Collect data--
 20   INPUT "BACKGROUND", bgd
 30   INPUT "SAMPLE COUNT", sample
 40   INPUT "GEIGER CHECK COUNT", g-m
 50   E = 2.7182818
 60   INPUT "HALF LIFE IN MIN", halflife
 70   INPUT "COUNT MADE", count
 80   INPUT "LENGTH OF COUNT", length
 90   INPUT "DELAY TIME", delay
100   PROCcalc
110   INPUT "ANOTHER", Y$
120   IF LEFT$(Y$,1) = "Y" THEN 70 ELSE 240
130   END
135   REM--Correction procedure--
140   DEF PROCcalc
150   realcount = count - (length*bgd)
160   factor = E↑(-0.693*delay/halflife)
170   original_count = realcount/factor
180   correct_count = original_count*5E7/sample/g-m
190   P.P
200   PRINT "Original was "count
210   P.P
220   PRINT "Corrected value is " INT((correct_count/
      length) + 0.5)
230   ENDPROC
240   END
```

Table 7.2; program used to correct observed radioactivity of 165-dysprosium and 152-europium adsorbed on barium sulphate, for decay, natural background, counter efficiency, and sample size. (BBC microBASIC)

7.6 Measurement of reducing species by means of methylene blue

7.6.1 Previous workers have reported [33] a method for the spectrophotometric determination of reducing species such as Eu(II) using methylene blue, which is converted by reduction into a leuco-form. They commented that the method did not appear to offer the consistent results expected from an analysis of that type.

Methylene blue is commonly contaminated with a substantial concentration of trimethylthionine, and in concentrated solutions dimerises to a significant extent. Both these factors affect the absorbance of the dye.

0.3 grams of methylene blue were freed from trimethylthionine by the method of Bermann and O'Konski. [48] The dye was dissolved in 300 cm^3 of 0.15M ammonia and repeatedly extracted with small portions of toluene until no further pink colouration was extracted. Bergmann and O'Konski used benzene for this purpose; the less carcinogenic toluene appeared to be equally effective. The pH of the extracted aqueous phase was then reduced to near neutral with concentrated hydrochloric acid. The liquid was transferred to a polythene container and purged of dissolved oxygen by passing a brisk stream of nitrogen through it for a minimum of one hour.

A portion of this solution was diluted with deoxygenated distilled water until, when further diluted in the ratio 1:50 with a 50% solution of alcohol in water, its absorbance

was less than 0.8 units. At this dilution the dimerisation of the dyestuff may be considered negligible. The diluted working solution was stored, like the concentrated stock, in a polythene bottle under nitrogen.

7.6.2 Calibration

Despite the relatively high redox potential of the dye ($E^{\ominus}$ = +0.53 v) difficulties are encountered when using it as an oxidising agent, presumably due to the high activation energy of the reactions involved. It has, however, been used in the past to titrate Sn(II) and accordingly this reaction was used to calibrate the stock material.

A solution of tin(II) chloride was prepared in dilute hydrochloric acid, using fresh material so as to avoid difficulty in dissolving the salt due to the presence of the oxide. Various volumes of this solution were added to 1 cm^3 of the purified dye solution, and the absorbance was followed at 664 nm. It was found that oxidation was very slow; calculations made from the first set of readings (Table 7.3) showed that the sensitivity of the method differed from that expected by an order of magnitude.

Accordingly a second solution of tin(II) chloride was made, this time in de-oxygenated water. Various volumes of the new solution were added to aliquots of the dye, and left for six hours under nitrogen. The absorbances of the solutions, at 664 nm., are shown in Table 7.4.

Mass of weighing boat	0.4622 g
Mass of boat + Sn(II)chloride dihydrate	1.0154 g
Hence mass of reactant	0.5532 g
Volume of solution	250 cm^3

Vol added cm^3	Immediate reading Absorbance units	Later reading Absorbance units
2	0.759	0.674
5	0.730	0.617
10	0.686	0.446
20	0.563	0.158
30	0.437	0.080
blank(0)	0.733	0.733

Table 7.3 Results of reaction between methylene blue solution and Sn(II).

Mass of weighing boat	0.4622 g
Mass of boat + Sn(II) chloride dihydrate	0.6844 g
Hence mass of reactant	0.2222 g
Volume of solution	1 000 cm^3
Concentration of solution (0.2222/226)	9.83×10^{-4} M

Volume added cm^3	Absorbance A.U.
0	0.784
2	0.688
5	0.519
10	0.328
15	0.152
20	0.144

Slope of curve $\frac{(0.784 - 0.152)}{15}$ A.U. cm^{-3}

1 cm^3 contains 9.83×10^{-7} moles Sn(II)

Hence a change of 1 A.U. corresponds to $\frac{9.83 \times 10^{-7} \times 15}{(0.784 - 0.152)}$ moles

i.e., 2.33×10^{-5} moles

This in turn means that a change of 1 A.U. corresponds to

4.66×10^{-5} moles Ln(II)

i.e. 12.0 mg $EuCl_3$

12.6 mg $DyCl_3$

Table 7.4 Results of calibration of methylene blue

From these results it was calculated that a change in absorbance under these conditions of 1.0 units corresponds to the presence of 4.66×10^{-5} moles Ln(II).

7.6.3 Method of Ln(II) analysis

For these analyses the apparatus shown in Figure 7.6 was used. It was first flushed with nitrogen; the planchette containing the irradiated lanthanide was opened; the flask was quickly freed from the separating funnel; the powder was tipped from the planchette into the flask; and the funnel was replaced. Since the powder was dry, no difficulty was encountered in transferring it into the flask.

25 cm^3 of deoxygenated water were transferred into a 100 cm^3 measuring cylinder flushed with nitrogen, and 25 cm^3 of ethanol were added and mixed. There was a small rise in temperature and dissolved gases were expelled from the mixture. The air space above the mixture was flushed with nitrogen.

1 cm^3 of the working solution of dye was then pipetted into the separating funnel, and the whole apparatus was flushed with nitrogen. The dye was admitted to the flask, and the water-alcohol mixture was poured into the separating funnel, which was restoppered. After shaking the flask to assist reaction of the dye with the dissolving solid, the water-alcohol mixture was admitted to the flask and shaken until all the powder had dissolved. This did not take more than a few seconds; the liquid, in passing from funnel to flask, also had the effect of rinsing any remaining dye through the neck of the funnel.

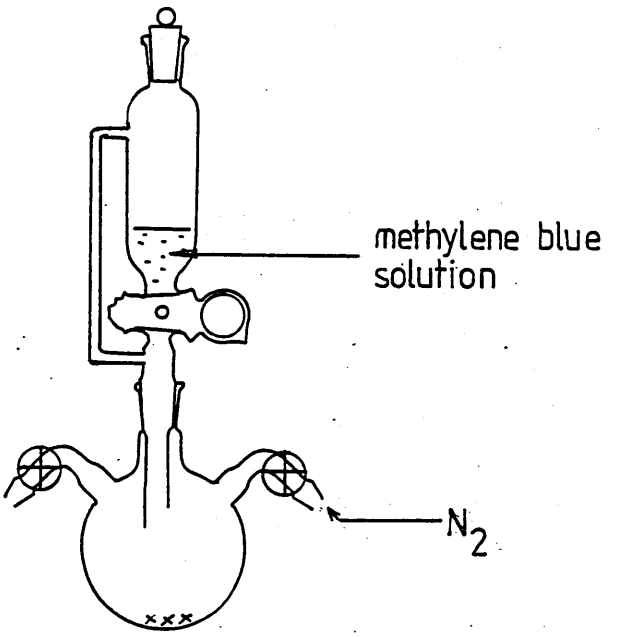

Figure 7.6

Apparatus for reaction of irradiated lanthanide trichloride with methylene blue solution

The spectrometer (Pye-Unicam SP8-400) having been set to read absorbances at 664 nm, the reading was set to zero with distilled water in both sample and reference cells. The sample cell was removed and the reading was noted; this reading was re-checked each time the sample cell was removed. Any change indicated a drift in the zero reading.

The sample cell was flushed with nitrogen and filled with the reduced dye solution. The absorbance was measured. The sample was tipped away, the cell was reflushed, refilled with dye, and returned to the spectrometer. This was repeated until five readings of the absorbance were available; if the absorbance changed unduly during this sequence, further readings were taken until a satisfactory reproducibility was obtained.

The sample flask was then flushed thoroughly with oxygen and shaken for about 30 seconds. The flask was then allowed to stand until all bubbles had risen from the solution. The absorbance of the dye was measured, and the oxygenation was repeated. A further determination of the absorbance was made; if as was usually the case it did not differ from that found after the first oxygenation by more than a very small amount it was assumed that re-oxidation was complete and five readings of the absorbance were taken in the same way as before, but in an atmosphere of air rather than nitrogen.

For the readings to be consistent it was found necessary:

(a) to rinse the cell with the solution whose absorbance was to be measured, and discard the rinsings, before

taking any readings. This was ascribed to the habit of the dye to be absorbed onto glass surfaces;

(b) to allow a fixed time after shaking the flask to elapse, before making any measurements. Even when oxidation of the dye appeared to be complete and all visible bubbles in the solution had risen to the surface of the liquid, the absorbance continued to change for a little time afterwards.

7.7 Preparation of oxygen-free water

A 15 litre flask was 2/3 filled with laboratory distilled water and supported over a gas-ring. The neck of the flask was loosely stoppered in a delivery tube, attached to the nitrogen cylinder, reached to the bottom of the flask. The water was boiled briskly for five minutes whilst a stream of nitrogen was passed through it; the heating was then stopped but the nitrogen flow was continued until the water was again at room temperature. The flask was then tightly stoppered.

When required, this water was transferred into the apparatus shown in Figure 7.7, which had a capacity of 1 litre. The water was reboiled under nitrogen and allowed to cool. By closing the pressure release valve and admitting nitrogen to the flask, the water was discharged through the delivery jet.

7.8 Neutron irradiation

7.8.1 Irradiations were carried out in four separate facilities: the initial work in this study was done using an Am/Be source type AMN 16, made by the Radiochemical Centre

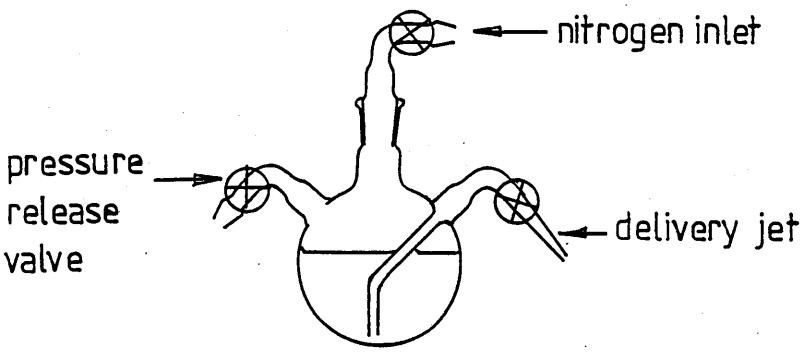

Figure 7.7

Apparatus for storage and delivery of de-oxygenated water

and housed at Worcester College of Higher Education. The output from this source (6.6×10^4 n s^{-1}) proved too small for any meaningful results to be obtained.

The majority of the irradiations were done with a larger Am/Be source, type AMN 22, at the University of Cambridge Chemical Laboratory. The output from this source was 2.2×10^6 n s^{-1}; details of the source are given in Table 7.5 and the emission spectrum on Figure 7.8.

To provide some material of higher activity for my investigation of the adsorption of Eu(II) and Eu(III) ions on barium sulphate, a small quantity of 'Specpure' europium oxide was sealed in quartz and irradiated for 30 minutes in an estimated flux of 3×10^{12} n cm^{-2} s^{-1}, in the Universities' Research Reactor, Risley.

To assess the effect of delivering the neutron dose in a very much shorter time than was possible with the Cambridge source, several 100 mg samples of dysprosium(III) chloride were irradiated in the 150 keV generator at the Birmingham Radiation Centre, which produces 15 MeV neutrons.

7.8.2 Mixed flux reactor

Where a mixed flux of fast and slow neutrons was wanted, this was produced by placing the samples (held in aluminium planchettes and sealed with 'Sellotape') directly in contact with the source, and surrounding sample and source with a large cube of wax to act as a moderator and reflector. The apparatus is shown in Figure 7.9. The cube had 60 cm sides and could therefore be regarded as effectively infinite so

far as the albedo effect was concerned. In use, the inner wax cylinder and the neutron source were removed; three samples were placed symmetrically in the centre of the well in the wax; the inner cylinder (encased in a thin aluminium casing) was replaced, and then the neutron source was introduced, taking care that it was placed as centrally as possible over the samples. This was done by eye and thus (together with the necessarily uneven distribution of material in the planchettes) introduced an uncertainty into the neutron dose received by each sample.

The fast neutron dose was calculated by noting the time for which the irradiation took place, and the geometric factor evaluated in Chapter two. The slow neutron dose was obtained from the peak thermal flux quoted in the source specification[27], assuming that this was the flux obtained in the wax moderator.

Fast neutron doses (in the absence of slow neutrons) were delivered firstly by standing the samples, in aluminium planchettes with closely fitting aluminium covers, on a 5mm thick slab of cadmium 10 cm square, which in turn rested on a substantial concrete block. The neutron source was placed directly on top of the samples. Secondly, in separate experiments, the samples were placed inside a box made from 2mm cadmium sheet, which is substantially opaque to thermal neutrons. This was placed in the wax cube beneath the wax cylinder, and the neutron source was introduced in exactly the same manner as when carrying out mixed flux irradiations. In this way, only the energy distribution of the flux incident on the samples differed from the mixed-flux irradiations.

Americium/Beryllium Neutron Source

Manufacturer	The Radiochemical Centre
Type	AMN 22
Output	2.2×10^6 n s^{-1}
Casing	Stainless steel
Mean energy	
(a) low energy	400 keV
(b) high energy	4 - 5 MeV
Peak thermal flux in infinite H_2O	5×10^3 n cm^{-2} s^{-1}
Dimensions	
(a) depth	31 mm
(b) radius	11.2 mm
Packing material	Americium oxide compacted with beryllium metal powder
Emission geometry	Isotropic [49]
Gamma exposure rate one metre from source	1 mR hr^{-1} (approximately) per 10^6 n

Table 7.5 Properties of neutron source

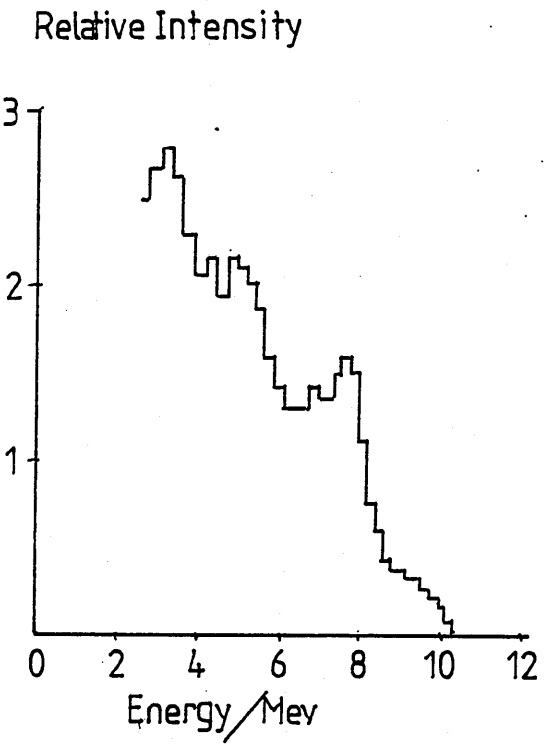

Figure 7.8

Emission spectrum of neutron source type AMN 22

(Ref. 50)

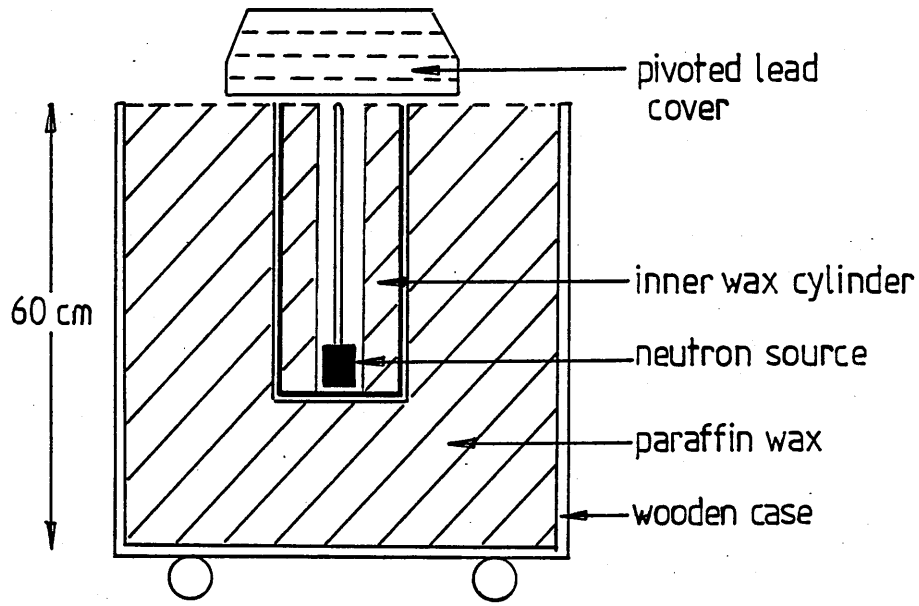

Figure 7.9

Experimental arrangement of low gamma neutron-irradiation facility

Fast neutron emission from source	2.2×10^{6} n s^{-1}
Geometrical factor (at 5 mm)	0.1224
Neutrons striking target	2.7×10^{5} n s^{-1}
Target area	3.8 cm^{2}
Flux	7.1×10^{4} n s^{-1} cm^{-2}
γ Flux at 5 mm	0.065 Gy/hr

Flux per day is therefore:-

Days	Fast neutron flux n/cm^2	Total fast neutrons	Associated gamma dose/Gy
1	6.12×10^{9}	2.33×10^{10}	1.56
2	1.22×10^{10}	4.64×10^{10}	3.12
3	1.84	7.0	4.68
4	2.44	9.27	6.24
5	3.06	1.16×10^{11}	7.80
6	3.67	1.39	9.36
7	4.29	1.63	10.92
8	4.9	1.86	12.84
10	6.12	2.32	15.60
12	7.34	2.79	18.72

Table 7.6

Fast neutron dose received by samples

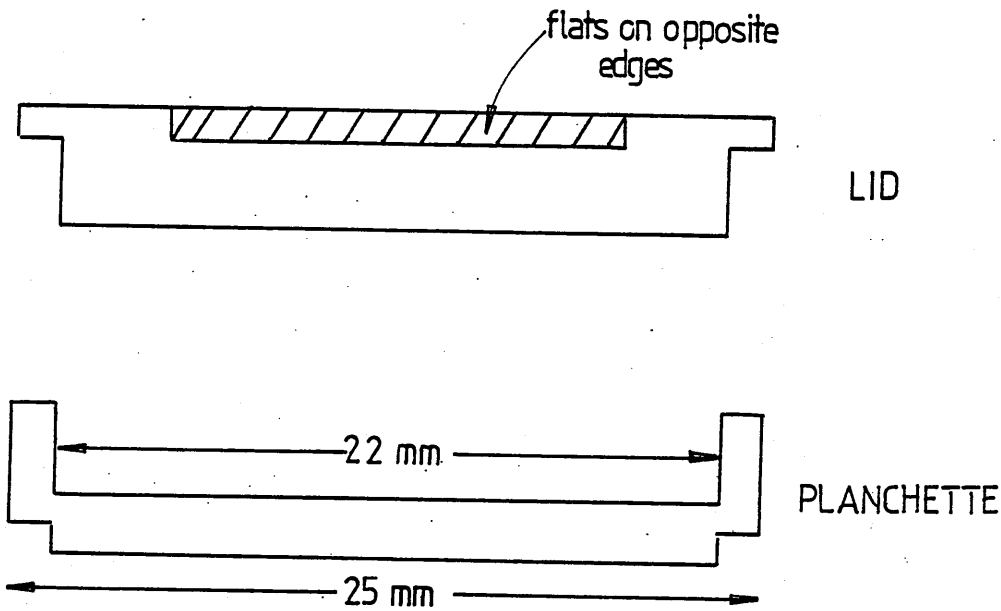

Figure 7.10

Details of irradiation planchettes

Material	Aluminium
Cross section	Circular
Scale	x 4

7.9 Measurement of gamma flux

At a distance of one metre from the source, the expected gamma dose rate is approximately 2.2 mR hr^{-1}. At this distance the source approximates to a point source and so the dose rate at the working distance from its centre (some 15mm) would be given by

$$\text{Expected D.R.} \quad 2.2 \times 10^{-3} \times \frac{1000^2}{15} \text{ R hr}^{-1}$$

$$\text{i.e.} \quad 9.8 \text{ R hr}^{-1} = 0.098 \text{ Gy hr}^{-1}$$

To assess the reliability of this estimate, measurements of the gamma dose rate were made at a variety of distances from the face of the source, using a BERTHOLD LB 1200 gamma dose rate meter. The results were plotted against distance from the source face and the curve was extrapolated to contact distance.

The distance of target material, in the planchettes used, from the source face, was estimated to be 5mm. At this distance the measured dose rate was 6.5 R hr^{-1}, which is in close agreement with the anticipated value.

When selecting a ^{60}Co source to deliver the same gamma dose rate as the neutron source, the same meter was used to ensure that, even if the measurements made were in error, the same error would occur in both.

The measurements made on the gamma field are listed in Table 7.7 and shown graphically in Figure 7.10.

Distance source face to counter (cm)	Dose rate (R/hr)
0.5	6.5
1	6.0
2	5.4
3	4.9
4	4.5
5	4.2
6	3.8
7	3.5
8	3.2
9	2.9
10	2.5

Table 7.7

γ-Dose received by target at varying distances from neutron source; measured using BERTHOLD LB 1200 γ-dose rate meter, calibrated in rad/hr.

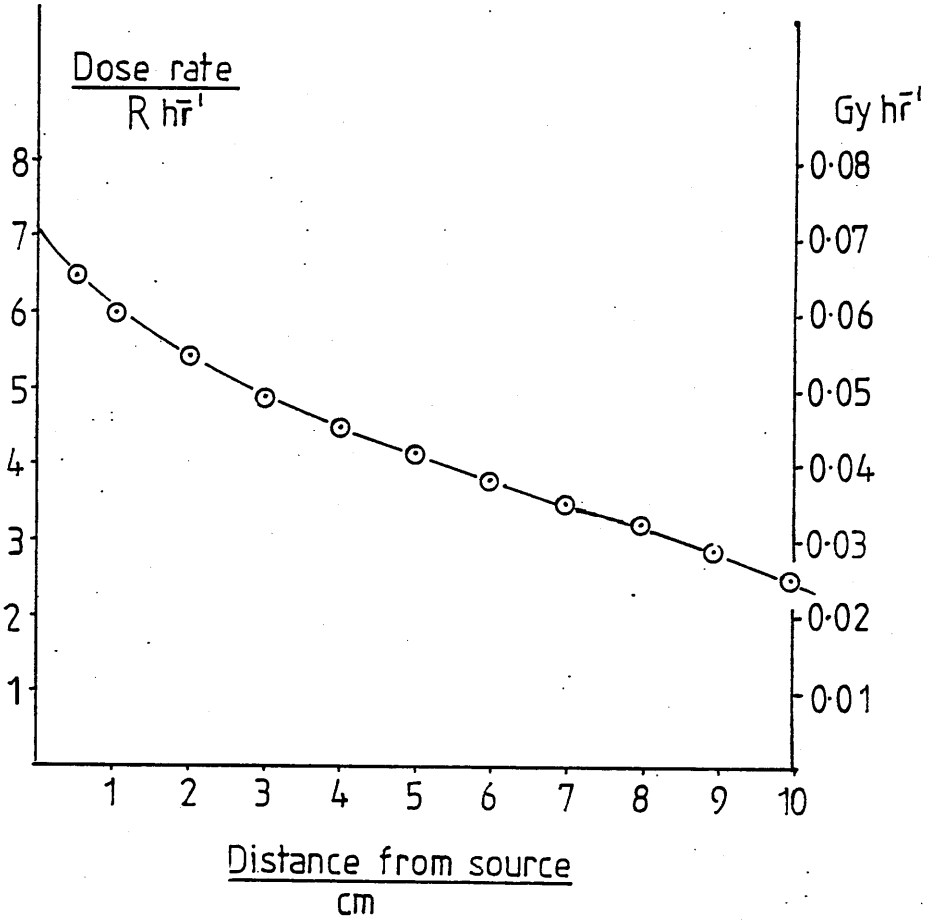

Figure 7.11

γ-dose rate at various distances from neutron source, in air

Bibliography

1 Chadwick, J., Proc. Roy. Soc., A136, 692, (1932)

2 Pleasanton, F. & Snell, A.H., Proc. Roy Soc., A241, 141 (1957)

3 Tate, J.T. & Smith, P.T., Phys. Rev., 46, 773 (1954)

4 Thomson, J.J. 'Conduction of Electricity through Gases' 1, 273 (C.U.P., 1928)

5 Murray, R.L. 'Nuclear Energy', 48 (Pergamon, 1980)

6 Friedlander, G. et al., 'Nuclear & Radiochemistry' 437, (Wiley, 1981)

7 Open University, 'Data Book' (O.U.Press, 1976)

8 Brooks, H., Nature, 70, 270, (1904)

9 Szilard, L. & Chalmers, Nature, 134, 462, (1934)

10 McKay, H.A.C., 'Principles of Radiochemistry' 27, (Butterworth, 1971)

11 Carlson, T.A., ORNL - 3268, 65 (1962)

12 Stratton, J.A., 'Electromagnetic Theory', 15 (McGraw-Hill, 1941)

13 Hacskaylo, M. et al., J. Chem. Phys., 21, 1434 (1953)

14 Johnson, D.A., 'Advances in Inorganic & Radiochemistry' 20, 89-105 (1977)

15 Johnson, D.A., J. Chem. Ed., 57, 475 (1980)

16 Matignon, C.A., & Cazes, E., Ann. Chem. Phys., 8, 417, (1906)

17 Urbain, G., & Bourion, F., C.R. Hebd. Seances. Acad. Sci., 153, 1155 (1911)

18 Klemm, W., & Schuth, W.Z., Z. Anorg. Allg. Chem., 184, 352 (1929)

19 Drudig, L.F., & Corbett, J.D., J. Am. Chem. Soc., 81, 5512 (1959)

20 Corbett, J.D., & McCollum, B.C., Inorg. Chem., 5, 938 (1966)

21 Asprey, L.B., & Kruse, F.H., J. Inorg. Nucl. Chem., 13, 32 (1960)

22 de Block, R., Ph.D. Thesis, U. Catholique de Louvain (1971)

23 Latimer, W.M., 'Oxidation States of the Elements and their Potentials in Aqueous Solution' 2nd Ed. 42ff., (Prentice-Hall, 1952)

24 Apers, D.J., de Block, R. & Capron, P.C., J. Inorg. Nucl. Chem., 36, 1441 (1974)

25 Jaffey, A.H., Rev. Sci. Inst., 25, 349 (1954)

26 Wiernik, M., Rchem. Acta., 23, 46 (1976)

27 Radiochemical Centre, Technical Bulletin 76/7

28 Klimov, A., 'Nuclear Physics & Nuclear Reactions' Ch.5 (Mir, Moscow, 1975)

29 Klimov, A., loc. cit.

30 Glasstone, S., 'Elements of Nuclear Reactor Theory' (1952)

31 Meier, D.J., & Garner, C.S. J. Amer.Chem. Soc., 73, 1894 (1951)

32 Meier, D.J., & Garner, C.S. J. Phys. Chem., 56, 853, (1952)

33 Bhattacharya, S., Lyle, S.J., & Maghzian, R., Talanta, 27, 59 (1979)

34 Leutwein, F, Z. Anal. Chemie., 120 233-42 (1940)

35 Maddock, A.G., & Vargas, I., Nature, 184, 1931(1959)

36 Tokunaga, J., J. Chem. Ed. Data., 20, 1 (1975)

37 Maddock, A.G., & Müller, H., Trans. Faraday Soc., 56, 509ff (1959)

38 Kellie, J.D., et al., J. Phys. A: Math., Nucl., Gen. 7, 14 ,1758 (1974)

39 Johnson, D.A., 'Recent Advances in the Chemistry of the Less Common Oxidation States of the Lanthanide Elements' (Academic Press, 1977)

40 Bratsch, S. & Silber, H.B., Inorg. Chem. Acta., 65 L53 (1982)

41 Heftmann, E., (Ed) 'Fundamentals of Chromatography' 209ff., (Reinhold, 1961)

42 Alberti, G., & Massuchi, M.A., J. Chromatog. 11, 394 (1963)

43 Wendlandt, W.W., J. Inorg. Nucl. Chem. 9, 136 (1959)

44 Taylor, M.D., & Carter, C.P. J. Inorg. Nucl. Chem., 24, 387 (1962)

45 Marsh, J., J. Chem. Soc., 398 (1942)

46 Marsh, J., J. Chem. Soc., 531 (1943)

47 Loevinger, R., & Berman, M., Nucleonics, 9 1, 26f(1951)

48 Bergmann, K., & O'Konski, C.T., J.Phys.Chem., 67, 2169 (1963)

49 Bishop, M., Private communication

50 Lorch, E.A., Int. J. App. Rad. Isotopes, 24, 588 (1973)